Autonomous Reorientation of a Maneuver-Limited Spacecraft Under Simple Pointing Constraints

Thesis by

Charles A. Vanelli

In Partial Fulfillment of the Requirements
for the Degree of
Mechanical Engineer

California Institute of Technology
Pasadena, California

1997
(Submitted May 30 1997)

Acknowledgments

Ralph Goddard

Richard Murray

Joel Burdick

Erik Antonsson

James Vanelli

Willem Sluis

Fred Serricchio

Slawomir Zaremba

Nancy Winfree

Howie Choset

Martin Lo

Roberto Zenit

Philippe Adam

Bon Calayag, and

The National Science Foundation, under grant CMS-9502224

Abstract

This report presents techniques for using discrete finite rotations to reorient a spacecraft from a given initial attitude to a final attitude which satisfies a specified aiming objective. The objective may be a fully specified final orientation or it may require that the spacecraft direct an instrument along a certain direction. Constraints are also imposed on the allowable intermediate orientations that the spacecraft may assume during the course of the maneuver, representing the operational requirements of onboard instrumentation. The algorithms presented consider solutions that will achieve the desired objective with only one or two slew maneuvers, although they may be easily extended to consider more complicated solutions requiring additional maneuvers.

Contents

List of Figures

List of Tables

List of Symbols

$\mathcal{F}_A$	frame	generic reference frame A in $\mathbb{R}^3$.
$\vec{v}$	vector	generic vector in $\mathbb{R}^3$.
$\mathbf{v}$	column vector	3×1 matrix representation of $\vec{v}$ with respect to a frame $\mathcal{F}_A$.
$\vec{v}'$	stereographic projection	stereographic projection of $\vec{v}$ onto a plane P.
$\mathbf{v}'$	stereographic projection	2×1 matrix representation of $\vec{v}'$ in P.
$\hat{\mathbf{v}}$	skew matrix	skew symmetric *matrix* formed from the elements of the *unit* column vector $\mathbf{v}$.
$\mathcal{C}$	configuration space	space of all possible spacecraft configurations, SO(3).
q	spacecraft attitude	position of spacecraft in $\mathcal{C}$.
$\mathcal{F}_S$	spacecraft body frame	3-axis body frame in $\mathbb{R}^3$ representing spacecraft orientation.
$\vec{e}$	aimsight	spacecraft body vector to be aimed.
$\vec{e}_f$	target-vector	direction along which to aim the aimsight $\vec{e}$.
$\mathcal{A}(\vec{e}_f)$	aimset	collection of spacecraft frames sharing a common axis $\vec{e}_f$.
$Q(\vec{e}_f)$	aimset-curve	closed curve in $\mathcal{C}$ representing $\mathcal{A}(\vec{e}_f)$.
$\vec{b}_k$	instrument vector	spacecraft body vector indicating direction of k^{th} instrument boresight.
$\vec{t}_k$	threat source vector	*absolute* vector indicating direction of threat source for the k^{th} spacecraft instrument.
α_k	sensitivity angle	sensitivity angle of k^{th} instrument.
$\vec{\omega}$	rotation axis	unit rotation axis during slew maneuvers.
θ	angular displacement	angular displacement about $\vec{\omega}$.
$M(\vec{\omega}, \theta)$	slew maneuver	spacecraft slew *trajectory* in $\mathcal{C}$ resulting from rotation about body axis $\vec{\omega}$ through angular displacement θ.
σ	composite slew path	composite spacecraft trajectory in $\mathcal{C}$ resulting from a sequence of sequential slew maneuvers M.

Chapter 1

Introduction

During the course of its lifetime, a satellite or interplanetary space probe must often reorient itself to aim the main engine for a subsequent firing or simply for the retargeting of onboard instrumentation. Often there exist constraints against the intermediate orientations that the spacecraft may assume while meeting its retargeting objective, such as not directing light-sensitive payloads along the Sun vector [1, 2]. The planning, execution, and monitoring of these maneuvers by ground-controllers is extremely costly and time-consuming. This report is devoted to the problem of *autonomous* motion planning in the space of orientations, SO(3), with particular application to the problem of spacecraft reorientation maneuvers. Figure 1.1 provides an illustration of these reorientation maneuvers, known as *attitude transfers* [11] or *slew maneuvers* [14]. We shall refer to the planning of such maneuvers as *attitude motion planning.*

1.1 Motivation

Autonomous spacecraft reorientation is desirable for a number of reasons. At the present time, instructions for reorientation maneuvers are developed on the ground through a long process involving maneuver design, testing, and subsequent transmission to the spacecraft [5]. The received instructions are then confirmed by the spacecraft, and finally executed [5, 12]. The process is often tedious, especially under the long communications lags endured by interplanetary space probes. Consequently, spacecraft maneuvers are not performed in real-time and therefore are quite inflexible to changes in operating conditions [5, 13, 14]. Additionally, there is a risk that the inherently long response times in the procedure will reduce the lifetime of the spacecraft: a threat to the spacecraft might force it to expend precious consumables (such as fuel) while waiting to receive instructions from the ground, or communications delays might lead to additional spacecraft damage.

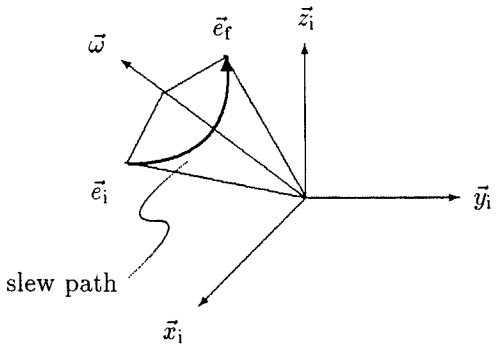

Figure 1.1: Illustration of slew maneuver $M(\vec{\omega}, \theta)$. The spacecraft has a reference frame $\mathcal{F}_{S_i} = (\vec{x}_i, \vec{y}_i, \vec{z}_i)$ as shown, with given body vector $\vec{e}$. Under counter-clockwise rotation about $\vec{\omega}$, the body vector slews from its initial position $\vec{e}_i$ to the final position $\vec{e}_f$ (shown with respect to the *original* frame $\mathcal{F}_{S_i}$).

Long communications delays can be particularly dangerous for interplanetary missions: the nature of the threat may have changed by the time instructions from ground control are received. Further complicating interplanetary missions are periods of communications blackout, when ground control is unable to monitor the spacecraft. Should a calamity befall the spacecraft during these blackouts, such as an equipment malfunction, intelligent maneuver planning is critical [2, 12, 13]. Finally, the maintenance of a large panel of specialists on ground control teams is costly in terms of personnel and equipment [13, 14]. Autonomous onboard systems, with their potential for timely and intelligent action, offer the promise of alleviating or at least reducing many of these concerns [13].

Further increasing the difficulty of attitude motion planning are the orientation requirements of spacecraft payloads. As previously mentioned, light-sensitive instrumentation must never be directed towards or near a bright body, such as the Sun or the bright side of the Earth [1, 2, 12, 14]. This is an example of an *avoidance constraint.* Other constraints might include keeping solar cells in an attitude for optimum power generation, maintaining a proper communications link with ground control, and properly targeting special payloads (such as cameras and telescopes) to meet mission objectives [2, 12]. These requirements are examples of *aiming constraints.* An additional class of constraint might limit the use of expendables, such as fuel. In that case we impose a *usage limit* on the motion planning process [2].

An attitude motion planning algorithm, capable of designing reorientation maneuvers in real-time and installed onboard the spacecraft, could alleviate much of the above difficulty. Additionally, it could conceivably be designed with a failsafe, so that the spacecraft attempts to maintain a communications link with ground control in the event of a major malfunction requiring a change in

mission objectives [12, 13].

1.2 Attitude Motion Planning Requirements

In designing an autonomous attitude motion planner, we strive to provide four main features:

1. **Admissibility**. First, we require that the motion planner always consider the constraints on the allowable spacecraft orientations. Only those slew maneuvers which always satisfy the constraints can be considered as candidate solutions to the motion planning task.
2. **Completeness**. Next, we desire that the planning algorithm be *complete* [7]. Not only should the algorithm be intelligent enough to find any solution that will meet the reorientation objective, it should also recognize when no solution exists [7]. The latter requirement is typically the most difficult. Note also that any motion planning problem generally has multiple solutions.
3. **Optimality**. The motion planner should have the ability to discriminate among superior and inferior solutions, applying some notion of cost or optimality to rank the solutions accordingly. The final solution chosen is the one that best satisfies the constraints. As we shall see, conflicting constraints require some sort of trade-off in the optimization process, with mixed results depending on the particular optimization employed.
4. **Autonomy**. Lastly, our motion planner must enable the spacecraft to perform maneuvers in an independent fashion, without intervention and detailed direction from ground controllers [4]. Ground control should merely specify *what* should be done, rather than *how* to do it [9]. Only in the case where no admissible maneuver can be found should the motion planner consider instructions for ignoring some of the constraints or request assistance from ground control.

Of the four points just mentioned, only the first and the last are strictly required for any practical autonomous motion planner. Completeness testing and optimality, while extremely desirable, are not strictly necessary. The special peculiarities of SO(3) play a significant role in the development of an attitude motion planner, being helpful in some respects (such as multiplicity of solutions) while being a hindrance in others (testing for completeness).

1.3 Previous Work

Considerable literature in the field of robot motion planning and autonomous navigation has been devoted to the task of computing a sequence of maneuvers that will take a specified vehicle from a

given position and orientation to a final position and orientation [7, 9, 10, 16]. The constraints that are applied to the vehicle in question typically limit its motions to certain kinds of maneuvers (e.g., no sideways translation for a car) or require that the vehicle avoid collision with a set of obstacles in $\mathbb{R}^3$. The obstacles primarily impose a constraint on the *position* of the vehicle. The orientation of the vehicle is often unconstrained or is considered less important. However, there are applications in which this situation is reversed: certain vehicle orientations are constrained, while vehicle position is left unconstrained. One of these applications is that of spacecraft reorientation.

Compared to traditional Cartesian motion planning, there is relatively little work published in the area of attitude motion planning, especially as regards spacecraft and spacecraft orientation constraints. McInnes describes a system for autonomous threat avoidance using potential functions [14]. Other published works in the area of spacecraft attitude motion planning focus mainly on time-optimal maneuvering [17, 20] and fuel-optimal maneuvering [18], choosing to neglect constraints on spacecraft orientation.

1.4 Results

In this report we present an algorithm for attitude motion planning in the presence of constraints of the form mentioned above. The algorithm accepts as inputs an initial orientation, an aiming criterion, and a set of constraints to be satisfied at all times. The algorithm returns the set of trajectories composed of discrete, finite slew maneuvers in SO(3) that meets the given constraints while achieving the aiming objective. These trajectories are optimized according to defined preferences, so that a single trajectory is presented as the best course for reorienting the spacecraft. The algorithm first tries a single slew maneuver, advancing to more complex solutions consisting of multiple reorientations in sequence only if no single slew maneuver can solve the problem. For simplicity, a limit of two slew maneuvers has been artificially imposed, based on the experience of spacecraft operators at NASA's Jet Propulsion Laboratory and to crudely simulate limited maneuvering fuel [2]. The algorithm we present here can be extended to consider other forms of orientation constraints, or even to allow for the temporary violation of those constraints and the removal of limits on the number of slew maneuvers to be executed.

1.5 Notation

The following notations and conventions are used throughout this report. The notational style is a mixture between the styles of Hughes [6], Latombe [9], and Shuster [19].

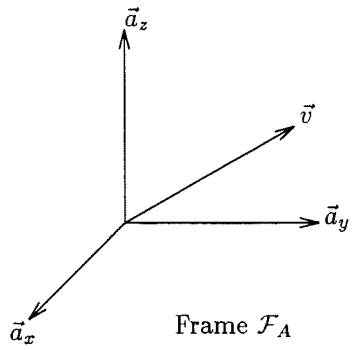

Figure 1.2: A vector $\vec{v}$ and a reference frame $\mathcal{F}_{\mathrm{a}}$.

1. At any given moment, the orientation (attitude) of the spacecraft is represented by a point q in SO(3).

2. The spacecraft configuration space is denoted $\mathcal{C}$ to represent the set of all possible spacecraft configurations. In the context of this report, a configuration is an attitude q; the configuration space is therefore identical with SO(3).

3. The hazardspace $\mathcal{H}^*$ is a collection of hazardous configurations. It is *not* a submanifold of $\mathcal{C}$.

4. A Cartesian frame is represented by $\mathcal{F}$. All frames are taken with reference to an absolute inertial reference frame $\mathcal{F}_{\mathrm{abs}}$, unless some other reference is specifically given. Figure 1.2 illustrates a frame $\mathcal{F}_{\mathrm{a}}$ with basis vectors $\vec{a}_{\mathrm{x}}$, $\vec{a}_{\mathrm{y}}$, $\vec{a}_{\mathrm{z}}$. Note that any frame $\mathcal{F}$, when viewed as an orientation only, is a point in SO(3).

5. Frames can be represented as a orthonormal 3×3 matrix $\mathbf{F}$, whose elements f_{ij} are the projections of the frame basis vectors onto the coordinate system of an assumed reference frame. Since orthonormal matrices can represent rotations, the frame matrix $\mathbf{F}$ is also called a relative rotation matrix.

6. Frames are generally used to indicate spacecraft attitudes, unless specifically indicated otherwise.

7. For every spacecraft attitude q in $\mathcal{C}$ there is a corresponding spacecraft frame $\mathcal{F}_{\mathrm{S}}(q)$ attached at the spacecraft center of mass and defined with respect to the absolute reference frame $\mathcal{F}_{\mathrm{abs}}$. The spacecraft attitude q_{abs} corresponds to the reference frame $\mathcal{F}_{\mathrm{abs}}$.

8. A finite rotation of the spacecraft about a fixed axis $\vec{\omega}$ through a counter-clockwise angular displacement θ is called a *slew maneuver*. For convenience, we define a function M that accepts

these two slew maneuver parameters and returns a *trajectory* in $\mathcal{C}$,

$$M = M(\vec{\omega},\, \theta)\,.$$

The axis $\vec{\omega}$ must be specified with respect to some reference frame, such as the spacecraft body frame $\mathcal{F}_S$.

9. The slew trajectory function M is a 2-to-1 mapping of slew maneuvers; that is, $M(\vec{\omega},\, \theta)$ and $M(-\vec{\omega},\, -\theta)$ return the same trajectory in $\mathcal{C}$.

10. Although the slews $M_1 = M(\vec{\omega},\, \theta)$ and $M_2 = M(\vec{\omega},\, \theta - 2\pi)$ achieve the same final spacecraft attitude q, the path in $\mathcal{C}$ is different for each slew. Therefore, while the *final* orientation achieved by a slew maneuver can be represented with a relative rotation matrix $\mathbf{M}$, the *path* taken along the slew itself cannot.

11. An ordered sequence of discrete slew maneuvers $M_1, M_2, \ldots$ defines a *piecewise* path σ in the configuration space $\mathcal{C}$,

$$\sigma = (M_1, M_2, \ldots).$$

12. Roman numeral subscripts indicate values at the commencement of each slew in a composite path. Thus, q_{i} is the initial attitude, q_{ii} is the attitude at the beginning of the second slew, and so on. The letter 'f' denotes the final value at the end of all maneuvering, as in q_{f}.

13. Sets are denoted with calligraphic text, such as $\mathcal{M}$, representing a particular set of slew maneuvers M. (The symbol $\mathcal{F}$, however, always represents a frame.) The null-set is denoted $\emptyset$.

14. A vector in $\mathbb{R}^N$ is denoted by an over-arrow, as in $\vec{v}$. The modulus is $\|\vec{v}\|$. The inner product between two vectors $\vec{v}_1$ and $\vec{v}_2$ is denoted by $(\vec{v}_1 \cdot \vec{v}_2)$. The angle between the same two vectors is denoted by $\angle(\vec{v}_1, \vec{v}_2)$.

15. A vector $\vec{v}$ can be represented by a 3×1 column matrix $\mathbf{v}$, whose elements v_i are the projections of the vector $\vec{v}$ onto the coordinate axes of an assumed reference frame.

16. Unless otherwise indicated, all Euclidean vectors in $\mathbb{R}^3$ are unit vectors. (Vectors in $\mathbb{R}^2$, however, are not unit vectors unless specifically indicated.) The set of all unit vectors describes a sphere in $\mathbb{R}^3$, commonly called the celestial sphere $\mathcal{S}$. Because unit vectors primarily convey directional information, the term *direction vector* is used interchangeably.

1.5.1 Vectors, Column Vectors, Frames, and Matrices

In this report, we often use vector quantities from several different reference frames. When reading an equation that uses those vector quantities, we shall assume that all vectors are *first converted to a standard frame of reference* before applying the equation.

We also make a distinction between the abstract vector $\vec{v}$, meant to convey both magnitude and direction, and its "column vector" representation $\mathbf{v}$, which requires an assumed reference frame. When converting vectors from one frame to another, we employ the frame matrix $\mathbf{F}_{\mathrm{a}}^{\mathrm{ref}}$ whose components represent the frame $\mathcal{F}_{\mathrm{a}}$ as seen with respect to a known reference frame $\mathcal{F}_{\mathrm{ref}}$. The matrix $\mathbf{F}_{\mathrm{a}}^{\mathrm{ref}}$ can be viewed as a rotation matrix that converts the components of $\vec{v}$ in the "a" frame to corresponding components in a universal "ref" frame, that is

$$\mathbf{v}_{\mathrm{ref}} = \mathbf{F}_{\mathrm{a}}^{\mathrm{ref}} \cdot \mathbf{v}_{\mathbf{a}}.$$

This notation is adapted from Hughes [6] and Shuster [19].

1.5.2 Aimset Notation

A set of frames defined around a common axis is called an *aimset*. Aimsets are convenient for denoting the set of frames that meet a particular pointing (or aiming) requirement, e.g., that a telescope be directed along a given direction $\vec{e}$. Aimsets are denoted with the calligraphic symbol $\mathcal{A}$ and a parameter indicating the common aiming vector: for example, $\mathcal{A}(\vec{e})$ denotes the set of frames that share a common axis $\vec{e}$. The axis vector must be specified with respect to some known frame; therefore, aimsets too are specified with respect to a known frame.

Observe that in SO(3), the aimset $\mathcal{A}(\vec{e}_{\mathrm{f}})$ maps to a closed curve $Q(\vec{e}_{\mathrm{f}})$.

1.5.3 Common Definitions

Fundamental interval. The fundamental interval used in the context of angular displacements is the interval $[0 \ldots 2\pi]$.

Coaxial vectors. Coaxial vectors are vectors which lie in the same line, along either the same or opposite direction. Two vectors $\vec{a}$ and $\vec{b}$ are coaxial if $||\vec{a} \times \vec{b}|| = 0$.

Chapter 2

Spacecraft Model and Problem Statements

Reasons for planned spacecraft reorientations generally fall into two categories: reorientation into a new desired attitude (*attitude transfer* [11]), and reorientation in order to point an instrument or device in a particular direction (*aiming*). Attitude transfers are typically performed to preserve spacecraft stability and to periodically correct for attitude drift due to disturbance torques, while aiming is usually performed to properly sight telescopes, fire the main engine, and align communications equipment [3, 6, 22]. Reorientation maneuvers with and without constraints are described in the sections that follow.

2.1 Spacecraft Model

Before considering problems of spacecraft reorientation, we must first define a model of the spacecraft under consideration.

Let $\mathcal{F}_S$ denote the spacecraft body frame of reference, attached at the spacecraft center of mass. All spacecraft components *and* maneuvers are defined against this reference frame, unless otherwise stated. The spacecraft is considered to be rigid and very small with respect to the environment (e.g., the planets or the solar system), so that all onboard instrumentation is considered to be located at the spacecraft center of mass [22]. We thus need only consider the "viewing direction" (or *boresight*) of each instrument, denoted with a direction vector $\vec{b}$, rather than also considering the position of the instrument relative to the mass center of the spacecraft. Effectively, this reduces the spacecraft to a point in space.

Additionally, we assume that all spacecraft reorientation maneuvers are performed quickly with

regard to the time-scale of the spacecraft's translation in $\mathbb{R}^3$ during the maneuver, so that upon completion of the reorientation maneuver, the spacecraft's Cartesian position in $\mathbb{R}^3$ is essentially unchanged from its position at the commencement of the maneuver. We employ this assumption to stipulate that all constraints imposed on the spacecraft as static and unchanging during the course of the maneuver.

Reducing the spacecraft to a single point in $\mathbb{R}^3$ allows us to consider only the orientation of the spacecraft without having to worry about the translation of various spacecraft components. This is reminiscent of the configuration space approach to Cartesian motion planning, in which the position of a robot in its workspace is reduced to a point in the robot's configuration space [9].

Since we are concerned only with spacecraft orientation, we define the configuration space $\mathcal{C}$ of the spacecraft to be the space of orientations, SO(3). That is,

$$\mathcal{C} := \mathrm{SO}(3). \tag{2.1}$$

The orientation of the spacecraft at any instant is represented by a single point q in $\mathcal{C}$. As the spacecraft changes orientations, this point traces a path in $\mathcal{C}$. We can equivalently represent changes in spacecraft orientation by following the motion of the spacecraft body frame $\mathcal{F}_\mathrm{S}$. Naturally, an arbitrary reference must be chosen in both paradigms. Without loss of generality, we shall always take the absolute reference frame to be the initial spacecraft frame at the commencement of any sequence of reorientation maneuvers, so that

$$\mathcal{F}_\mathrm{abs} := \mathcal{F}_{\mathrm{S_i}} \Longleftrightarrow q_\mathrm{abs} := q_\mathrm{i}. \tag{2.2}$$

In this manner, we use the notion of an oriented frame $\mathcal{F}_\mathrm{S}$ to represent spacecraft configuration.

2.2 Classes of Unconstrained Reorientation Problems

In the simplest case, there are no constraints on spacecraft attitudes or the maneuvers that may be executed to change those attitudes. While the case of such a freely maneuverable spacecraft may seem trivial, examination of the unconstrained reorientation problems provides insight into the problem of constrained reorientation maneuvering.

2.2.1 Unconstrained Attitude Transfer Problem

The simplest reorientation objective is to completely reorient the spacecraft into a new attitude, known as the *attitude transfer problem* [11]. Simply put, we require the spacecraft to maneuver from its current attitude to a given final attitude using a sequence of slew maneuvers. In general, there are no limitations imposed on the number of slew maneuvers allowed.

Problem 2.1. ***Unconstrained Attitude Transfer.*** Let the initial orientation of a rigid spacecraft be given by a body frame $\mathcal{F}_{S_i}$ taken with respect to a reference frame $\mathcal{F}_{abs}$.

Given a desired goal orientation $\mathcal{F}_{S_f}$, construct a path σ in $\mathcal{C}$ that specifies a *discrete* sequence of slew maneuvers $(M_1, M_2, \ldots)$, starting at the initial orientation $\mathcal{F}_{S_i}$ and ending at the final orientation $\mathcal{F}_{S_f}$.

Without any constraints on the intermediate attitudes assumed by the spacecraft, the problem is a simple rigid body displacement. Chasles' theorem [16] shows that only one slew maneuver is necessary to achieve the desired reorientation. Determining the axis $\vec{\omega}$ and corresponding angular displacement θ of that maneuver constitutes the solution to the unconstrained attitude transfer problem. The solution procedure is given in [16] and is repeated in Appendix C.

As a practical matter, the desired final attitude $\mathcal{F}_{S_f}$ can be specified by choosing any two *non-coaxial* body vectors on the spacecraft and specifying the desired final directions that these body vectors should take at the conclusion of the slew maneuvers. The selected body vectors are termed *aimsights* while the desired final direction vectors are termed *target-vectors.* Maneuvering the spacecraft until both aimsights are aligned with their corresponding target-vectors is sufficient to complete the desired attitude transfer. Note that the directions of the target-vectors must be specified in some inertial (i.e., non-rotating) frame.

The definitions of aimsight and target-vector are sufficiently important that they deserve special emphasis. An aimsight vector and its target-vector together form a *pointing requirement.* Note that two simultaneous pointing requirements are required to define a desired final orientation for the attitude transfer problem.

Definition 2.1. ***Pointing Requirement*:** A spacecraft pointing requirement is defined by a given spacecraft body vector $\vec{e}$ (the aimsight) which is to be aligned along a given target-vector $\vec{e}_f$.

With constraints placed on the intermediate attitudes that the spacecraft may assume during a slew maneuver, it may not be possible to move directly from the initial attitude to the desired final attitude with a single slew. As will be shown, the use of multiple slewing maneuvers significantly complicates the attitude transfer problem, mainly due to the fact that finite rotations in SO(3) do not obey the normal laws of algebraic addition.

2.2.2 Unconstrained Aiming Problem

The next simplest reorientation demand is a relaxation of the attitude transfer problem. The *unconstrained aiming problem* specifies only one pointing requirement: a single aimsight and its corre-

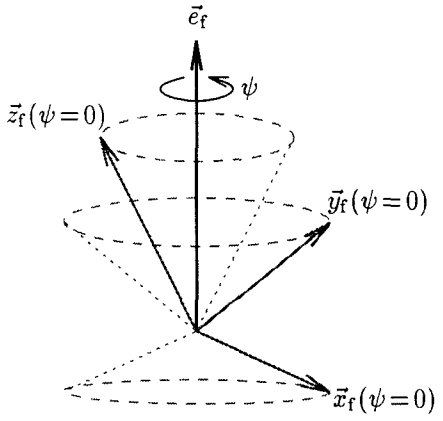

Figure 2.1: Illustration of an aimset $\mathcal{A}(\vec{e}_f)$, created by starting with any spacecraft attitude $\mathcal{F}_{S_f}$ that meets the aiming requirement and rotating the corresponding spacecraft body frame $(\vec{x}_f, \vec{y}_f, \vec{z}_f)$ about the target-vector. The tips of the frame vectors describe cones about $\vec{e}_f$. A particular member of the aimset $\mathcal{A}$ can be selected by rotating $\mathcal{F}_{S_f}$ about $\vec{e}_f$ through an angle ψ.

sponding target-vector. We require the spacecraft to reorient so that the aimsight is aligned along the target-vector, much like aiming a gun at a target.

By removing one of the pointing requirements from the reorientation demand, we gain an extra degree of freedom in the acceptable final attitudes. There are now many final attitudes that satisfy the aiming requirement. It is easily seen that all acceptable final attitudes can be generated by rotating any one acceptable attitude about the given target-vector: valid final attitudes are unique to within a rotation about the target-vector. We refer to a set of acceptable final orientations generated in this manner as an *aimset.*

> **Definition 2.2.** ***Aimset:*** An aimset $\mathcal{A} = \mathcal{A}(\vec{e}, \vec{e}_f, \mathcal{F}_{ref})$ is the set of all spacecraft orientations (frames $\mathcal{F}_S$) for which the spacecraft body vector $\vec{e}$ points along the vector $\vec{e}_f$. The aimsight vector $\vec{e}$ is specified with respect to the spacecraft frame, while the target-vector $\vec{e}_f$ is specified with respect to some reference frame $\mathcal{F}_{ref}$.

The universal reference frame $\mathcal{F}_{ref}$ is required to define the direction of $\vec{e}_f$. Note that for each member frame of $\mathcal{A}$, the direction cosines of $\vec{e}_f$ are the same. For convenience, we simplify the notation to $\mathcal{A}(\vec{e}_f)$ by assuming a universal reference frame and a description of the spacecraft. Figure 2.1 illustrates an aimset as a collection of rotated frames. In the configuration space paradigm, the set of attitudes $\mathcal{A}(\vec{e}_f)$ describes a closed curve $Q(\vec{e}_f)$ in $\mathcal{C}$.

Using the concept of aimsets, we state the unconstrained aiming problem as follows:

> **Problem 2.2.** ***Unconstrained Aiming.*** Let the initial orientation of a rigid spacecraft be given by a body frame $\mathcal{F}_{S_i}$ taken with respect to a reference frame $\mathcal{F}_{abs}$. Let the initial

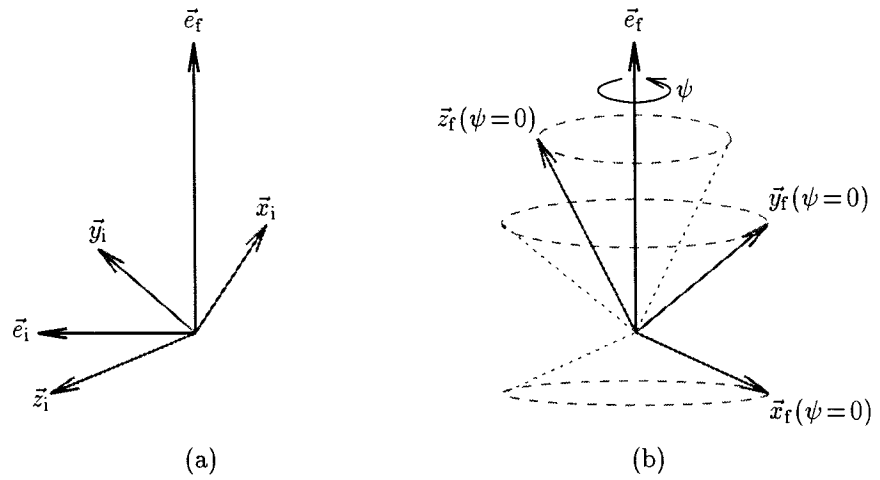

Figure 2.2: (a) Given information for the unconstrained aiming problem. The initial frame is $\mathcal{F}_{S_i} = (\vec{x}_i, \vec{y}_i, \vec{z}_i)$, with initial and final aimsights $\vec{e}_i$ and $\vec{e}_f$ as shown. (b) The aimset $\mathcal{A}(\vec{e}_f)$ of spacecraft attitudes that satisfy the aiming problem. Frame $\mathcal{F}_{S_f} = (\vec{x}_f, \vec{y}_f, \vec{z}_f)$ is any frame that satisfies the problem, used to construct the aimset as in Figure 2.1.

direction of the spacecraft aimsight be given by $\vec{e}_i$, and its desired goal direction given by $\vec{e}_f$.

Construct a path σ in $\mathcal{C}$ specifying a *discrete* sequence of slew maneuvers $(M_1, M_2, \ldots)$ that starts at the initial orientation $\mathcal{F}_{S_i}$ and ends at any final orientation $\mathcal{F}_{S_f} \in \mathcal{A}(\vec{e}_f)$.

Figure 2.2 illustrates the given information for the unconstrained aiming problem.

A common example of the aiming problem is reorienting the spacecraft to fire the main engine along a desired thrust axis. The aimsight is the main engine thrust axis, and the target-vector is the desired final direction for the engine. The problem is solved when the spacecraft achieves *any* orientation that aligns the engine thrust axis along the desired target thrust axis. Another practical example is that of aiming a telescope at a target.

Again, for a spacecraft without any pointing constraints, Chasles' theorem indicates that only a single slew maneuver is necessary to solve the aiming problem. In fact, as will be shown in detail in Chapter 3, there is an entire set of single slew maneuvers that will directly solve the unconstrained aiming problem.

One such solution to the aiming problem deserves special mention: The rotation axis that minimizes the slewed angular displacement of the aimsight is called the *eigenaxis* [20]. The minimum displacement slew maneuver about the eigenaxis is called the *eigenslew.*

Definition 2.3. ***Eigenslew*:** An eigenslew is the slew maneuver $M_{eig} = M(\vec{\omega}_{eig}, \theta_{eig})$

that minimizes the angular displacement traversed by the aimsight from its initial position $\vec{e}_i$ to its target $\vec{e}_f$.

The parameters for the eigenslew maneuver are

$$\left.\begin{aligned} \vec{\omega}_{eig} &= \frac{\vec{e}_i \times \vec{e}_f}{\|\vec{e}_i \times \vec{e}_f\|}, \\ \theta_{eig} &= \angle(\vec{e}_i, \vec{e}_f). \end{aligned}\right\} \tag{2.3}$$

2.3 Constraint Models

As described above, the unconstrained forms of the attitude transfer problem and the aiming problem are simple to solve and relatively rare in practice. A spacecraft typically is restricted from being in certain attitudes due to the *pointing constraints* of onboard instrumentation. For example, star-trackers must never be directed towards bright objects like the Sun, while communications equipment must often be tightly locked onto the Earth. These requirements can result in severe limitations on allowable spacecraft attitudes.

An additional constraint that we consider is the *usage limit,* i.e., a limitation on the consumption of some valued resource, such as thruster fuel. We later discuss one such usage limit, called the *maneuver limit.*

2.3.1 Simple Pointing Constraints

Pointing constraints on spacecraft attitude arise from the orientation, mounting, and sensitivities of onboard instrumentation. There are two classes of pointing constraints: avoidance constraints and aiming constraints. An avoidance constraint is defined from a set of directions along which a spacecraft instrument must not be aligned—in other words, the instrument must avoid a set of restricted directions. Conversely, an aiming constraint requires that the instrument's pointing direction always remain in a set of allowed directions. Note that the aiming constraint and the avoidance constraint are duals: for every aiming constraint there exists an avoidance constraint that accomplishes the same task, and vice versa.

We consider only "simple" pointing constraints. For simple constraints, we assume that the instrument is axis-symmetric and the set of hazardous (or desired) directions forms a cone.

Simple Avoidance Constraints

An avoidance constraint requires that the vector to a hazardous object never fall within the region of sensitivity of an instrument sensitive to that object. For example, the Sun should never lie within the field of view of any low-level light-sensitive devices like star-trackers.

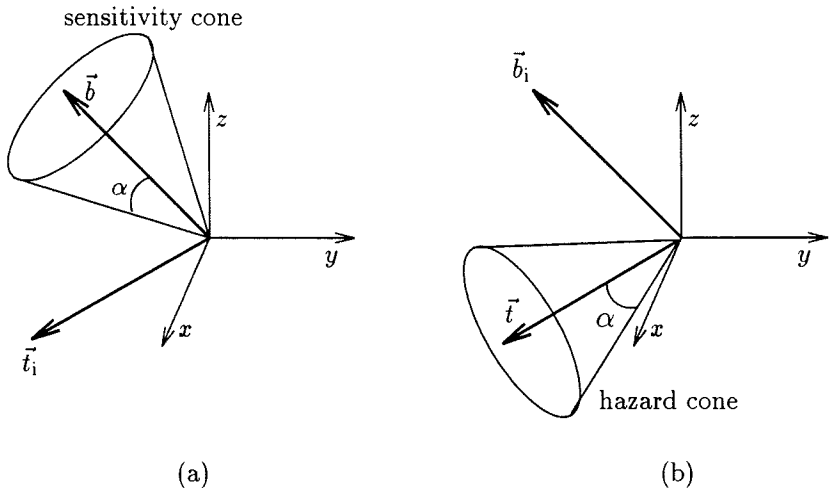

Figure 2.3: Pointing Constraint Model. (a) Sensitivity cone. (b) Equivalent hazard cone. The spacecraft frame $\mathcal{F}_S = (\vec{x}, \vec{y}, \vec{z})$ is shown for reference.

A simple avoidance constraint consists of a threat vector, an instrument boresight, and a cone of sensitivity taken with the instrument boresight as its axis. The avoidance constraint is violated whenever the spacecraft takes any attitude that causes the threat vector to lie within the sensitivity cone. A more convenient representation is to put the cone axis along the threat vector instead, now requiring that the instrument boresight $\vec{b}$ never fall within the newly formed hazard cone. Figure 2.3 illustrates these two paradigms.

To define the avoidance pointing constraint, we assume that each instrument is axis-symmetric about its boresight vector $\vec{b}$ and is vulnerable to a specific threat source, whose direction $\vec{t}$ relative to the spacecraft is known. The instrument's viewing field is taken to be a cone with the central axis along $\vec{b}$ and half-angle α. Threat sources are assumed to be so far away that they can be considered point sources.[1] The constraint function that keeps the threat source out of the instrument's viewing cone is

$$H_{\text{avoid}}(\vec{b}, \vec{t}, \alpha) := \vec{t} \cdot \vec{b} - \cos\alpha < 0. \tag{2.4}$$

Positive regions of the constraint function indicate violation of constraint. *All vectors are taken with respect to the spacecraft frame* $\mathcal{F}_S$. Note that $\vec{b}$ is constant with respect to the spacecraft frame, while $\vec{t}$ varies as the spacecraft slews through various attitudes. That is, $\vec{t} = \vec{t}(\mathcal{F}_S)$. The hazard cone half-angle α may be either an acute angle or an obtuse angle, but it must always satisfy $\alpha < \pi$.

Figure 2.4 shows a typical plot of the constraint function H_{avoid} as the spacecraft is rotated

[1] For nearby threat sources that are not points, one can define a "threat-extents" cone in the celestial sphere that contains the threat. Then define an effective sensitivity angle α_{eff} to be the sum of the instrument sensitivity angle α and the threat-extents cone half-angle α_t.

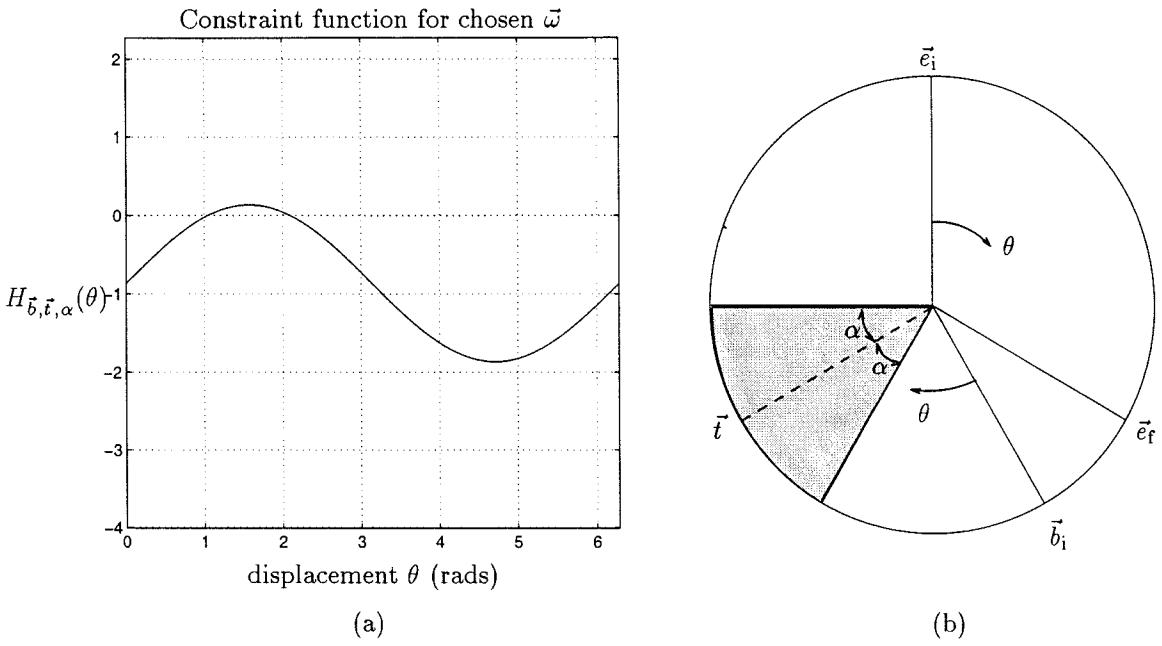

Figure 2.4: (a) Plot of a typical avoidance constraint curve. The horizontal axis measures the angular displacement θ of the spacecraft from its initial position $\theta = 0$ about a *chosen* axis $\vec{\omega}$. As $\vec{b}$ moves closer to $\vec{t}$, the constraint function takes on larger values. (b) The constraint seen looking down the $\vec{\omega}$ axis. As $\vec{e}$ goes through a full revolution, $\vec{b}$ simultaneously moves in a coordinated motion, passing through the constricted region (shaded).

about a *given* axis $\vec{\omega}$. Note that the value of the constraint function is not only dependent on the displacement, but also on the rotation axis selected for the maneuver. A different choice of $\vec{\omega}$ results in a different curve. From (2.4), it is apparent that H_{avoid} remains within the interval $[-2, 2]$. In the special cases where $\vec{\omega} = \pm\vec{b}$ or $\vec{\omega} = \pm\vec{t}$, the constraint curve is a constant.

Simple Aiming Constraints

Contrary to the avoidance constraint, an aiming constraint requires that the sighting vector to a target object always remain within the sensitivity cone of an instrument. For example, the boresight of the high-gain directional communications antenna on an interplanetary probe should remain sighted on the Earth.

Again assuming an axis-symmetric instrument with boresight $\vec{b}$ and sensitivity cone half-angle α, and a desired sighting vector $\vec{v}$, the constraint that maintains the instrument's view of the target

object is

$$H_{\text{aim}}(\vec{b}, \vec{v}, \alpha) := \vec{v} \cdot \vec{b} - \cos\alpha > 0. \tag{2.5}$$

We mentioned earlier that simple aiming constraints are dual to simple avoidance constraints. Specifically, if the instrument boresight $\vec{b}$ must remain within α radians of the sighting vector $\vec{v}$, then it is equivalent to state that the vector $\vec{b}$ must remain *outside* an imaginary hazard cone of half-angle $(\pi - \alpha)$ with central axis opposite to the sighting vector. Therefore, the conversion from an avoidance constraint to an aiming constraint is

$$H_{\text{aim}} := \vec{v} \cdot \vec{b} - \cos\alpha > 0 \Longleftrightarrow H_{\text{avoid}} := \vec{t} \cdot \vec{b} - \cos(\pi - \alpha) < 0, \tag{2.6}$$

with the imaginary avoidance threat source $\vec{t} = -\vec{v}$.

Henceforth we focus only on simple avoidance constraints, using the dual relationship (2.6) as needed to convert aiming constraints to avoidance constraints. To simplify the notation, hereafter the symbol H shall mean an avoidance constraint.

Multiple Pointing Constraints

In the case of multiple instruments, or a single instrument vulnerable to multiple threat sources, a complete set of avoidance constraint functions H_{jk} can be written for the spacecraft,

$$H_{jk} := \vec{t}_k \cdot \vec{b}_j - \cos\alpha_{jk} < 0,$$

where j refers to the instrument and k refers to the threat source, and α_{jk} is the instrument's effective sensitivity to the threat source.

Obstacles in $\mathcal{C}$: Hazardous Configurations

For each simple avoidance constraint there is a set of spacecraft configurations that are disallowed by the constraint. This set of hazardous configurations can be viewed as an obstacle in the configuration space $\mathcal{C}$. We therefore define an orientation obstacle

$$\mathcal{H} := \{\mathcal{F}_S \mid \vec{t} \cdot \vec{b} - \cos\alpha \geq 0\} \tag{2.7}$$

so that $\mathcal{H}$ is the set of hazardous configurations. Note that $\mathcal{H}$ results from the *violation* of the single simple avoidance constraint (2.4).

In the case of multiple avoidance constraints H_{jk}, we naturally define multiple obstacles $\mathcal{H}_{jk}$. The union of all the obstacles defines the *hazardspace,*

$$\mathcal{H}^* := \mathcal{H}_{11} \bigcup \mathcal{H}_{12} \bigcup \cdots \bigcup \mathcal{H}_{jk}. \tag{2.8}$$

Although other constraints can be defined and applied to create obstacles in the configuration space, we henceforth assume that all the obstacles contained in $\mathcal{H}^*$ result from simple avoidance constraints of the form (2.4). Note that while each constituent obstacle $\mathcal{H}$ is necessarily a simply-connected region in $\mathcal{C}$, the same is not always true for the collection $\mathcal{H}^*$.

Admissibility

To safely reorient the spacecraft around the orientation obstacles in $\mathcal{H}^*$, we must require at all times that the spacecraft configuration never violate any of the pointing constraints. This requirement leads to the definition of an *admissible configuration.*

> **Definition 2.4.** ***Admissible Configuration*:** A spacecraft configuration (orientation) $\mathcal{F}_S$ is admissible if all pointing constraints are satisfied when the spacecraft is in that orientation.

Using the concept of hazardous configurations, we define the space of admissible configurations, called the *freespace*, as

$$\mathcal{C}_{\text{free}} := \mathcal{C} - \mathcal{H}^*. \tag{2.9}$$

Thus any orientation in $\mathcal{C}_{\text{free}}$ is admissible. As with the hazardspace, the freespace $\mathcal{C}_{\text{free}}$ is not necessarily simply-connected.

We now extend admissibility to slew maneuvers and paths.

> **Definition 2.5.** ***Admissible Slew*:** A slew maneuver $M = M(\vec{\omega}, \theta)$ is admissible only if *all* intermediate orientations along the maneuver path in $\mathcal{C}$, including the orientations at both endpoints, are admissible. If *any* orientation along the path is inadmissible, then the slew maneuver M is inadmissible as a whole.

Thus, an admissible slew is one whose trajectory lies wholly in $\mathcal{C}_{\text{free}}$, including the endpoints. It follows that requiring a composite spacecraft path σ to never pass through a hazardous configuration is equivalent to imposing the same requirement individually on each of the component slews in the path.

> **Definition 2.6.** ***Admissible Path*:** A path $\sigma = (M_1, M_2, \ldots)$ is admissible if each of its constituent slew maneuvers $M_1, M_2, \ldots$ is admissible.

Simply Constrained Reorientation Problems

The simple avoidance constraints lead to the formulation of the constrained attitude transfer problem, defined as follows.

Problem 2.3. ***Attitude Transfer With Pointing Constraints.*** Let the initial orientation of a rigid spacecraft be given by a body frame $\mathcal{F}_{S_i}$ in $\mathcal{C}_{free}$, taken with respect to a reference frame $\mathcal{F}_{abs}$. Let $\mathcal{H}^*$ denote the union of all inadmissible orientations resulting from simple avoidance constraints of the form (2.4).

Given an admissible goal orientation $\mathcal{F}_{S_f}$, construct a path σ in $\mathcal{C}_{free}$, specifying a *discrete* sequence of slew maneuvers $(M_1, M_2, \ldots)$ that will direct the spacecraft from its initial orientation $\mathcal{F}_{S_i}$ to the desired final orientation $\mathcal{F}_{S_f}$.

Similarly we define the constrained aiming problem.

Problem 2.4. ***Aiming With Pointing Constraints.*** Let the initial orientation of a rigid spacecraft be given by a body frame $\mathcal{F}_{S_i}$ in $\mathcal{C}_{free}$, taken with respect to a reference frame $\mathcal{F}_{abs}$. Let $\mathcal{H}^*$ denote the union of all inadmissible orientations resulting from simple avoidance constraints of the form (2.4). Let the initial direction of a spacecraft aimsight be given by a direction vector $\vec{e}_i$.

Given a desired target direction $\vec{e}_f$ for the aimsight, construct a path σ in $\mathcal{C}_{free}$, specifying a *discrete* sequence of slew maneuvers $(M_1, M_2, \ldots)$ that will direct the spacecraft from its initial orientation $\mathcal{F}_{S_i}$ to any admissible final orientation $\mathcal{F}_{S_f} \in \mathcal{A}(\vec{e}_f)$.

It can be shown that Problems 2.3 and 2.4 with a single constraint H can always be solved using a single slew-maneuver. The details are given in Appendix B.

Extensions to the Simple Pointing Constraints

It is a simple matter to extend this pointing model to include instrumentation that is not mounted along an axis through the spacecraft center of mass. The other assumptions made during the development of the model can also be relaxed to expand the pointing constraint model (for example, to cope with threats that are very near or very small, so that the spacecraft can no longer be considered a point).

2.3.2 Maneuvering Limits

As mentioned earlier, McInnes describes a system for autonomous attitude motion planning using potential functions [14]; however, the resulting paths assume that the instantaneous axis of rotation can be continuously varied throughout the maneuver. While this might be practical for spacecraft equipped with momentum wheels, for spacecraft using thrusters the rotation axis cannot be so easily varied without consuming valuable propellant.

In this situation it is desirable to consider sequences of finite rotations, artificially modeling the maneuvering constraint as a limit on the number of finite rotations allowed. One complication that immediately arises from this approach is that the rotation axis changes abruptly from one slew maneuver to the next. Thus methods for planning continuously smooth paths, such as using calculus of variations, cannot be easily applied to generate attitude trajectories.

2.4 Constrained Reorientation with Maneuvering Limits

We can combine the constraint forms described in Section 2.3 to develop the *simply-constrained limited-maneuver reorientation problems,* as follows.

> **Problem 2.5.** ***Slew-Limited Attitude Transfer with Pointing Constraints.*** Let the initial orientation of a rigid spacecraft be given by a body frame $\mathcal{F}_{S_i}$ taken with respect to a reference frame $\mathcal{F}_{abs}$. Let $\mathcal{H}^*$ denote the union of all constrained orientations resulting from simple avoidance constraints of the form (2.4).
>
> Given a desired final orientation $\mathcal{F}_{S_f}$ and a maneuver limitation m, construct a path σ in $\mathcal{C}_{free}$, specifying a *discrete* sequence of n slew maneuvers $(M_1, M_2, \ldots, M_n)$, with $n \leq m$, that will direct the spacecraft from its initial orientation $\mathcal{F}_{S_i}$ to the final orientation $\mathcal{F}_{S_f}$.

> **Problem 2.6.** ***Slew-Limited Aiming with Pointing Constraints.*** Let the initial orientation of a rigid spacecraft be given by a body frame $\mathcal{F}_{S_i}$ taken with respect to a reference frame $\mathcal{F}_{abs}$. Let $\mathcal{H}^*$ denote the union of all inadmissible orientations resulting from simple avoidance constraints of the form (2.4). Let the initial direction of the spacecraft aimsight be given by a direction vector $\vec{e}_i$.
>
> Given a desired target direction $\vec{e}_f$ for the aimsight and maneuver limitation m, construct a path σ in $\mathcal{C}_{free}$, specifying a *discrete* sequence of n slew maneuvers $(M_1, M_2, \ldots, M_n)$, with $n \leq m$, that will direct the spacecraft from its initial orientation $\mathcal{F}_{S_i}$ to any final orientation $\mathcal{F}_{S_f} \in \mathcal{A}(\vec{e}_f)$.

For the purposes of this report, we limit the solutions to the constrained aiming problem to be made up of at most two slew maneuvers. That is, set $m = 2$. We refer to this problem as the *2-slew aiming problem with pointing constraints.*

2.5 A Criterion for Well-Posedness

The question arises whether the simply constrained reorientation problems defined above are solvable. Obviously, with a sufficient number of suitably placed configuration obstacles $\mathcal{H}$, it is possible

to create reorientation problems that have no solution regardless of the number of discrete slew maneuvers allowed. Applying additional restrictions on the number of slew maneuvers only further complicates the issue.

2.5.1 Well-Posedness and Reachability

The existence of slew solutions is used to define the concept of well-posedness.

> **Definition 2.7.** ***Well-Posedness*:** A simply constrained reorientation problem (either an attitude transfer problem or an aiming problem) is *well-posed* if there exists at least one admissible path σ composed of one or several ordered slew maneuvers that solves the problem.

Stated another way, if the corresponding orientation obstacles $\mathcal{H}_{jk}$ are arranged such that there is an admissible path σ in $\mathcal{C}_{\text{free}}$ that solves the problem, then the problem is well-posed; if not, it is ill-posed.

Therefore, for the attitude transfer problem to be well-posed, the final orientation must be *reachable* from the initial orientation.

> **Definition 2.8.** ***Reachable*:** An orientation $\mathcal{F}$ is *reachable* from a starting orientation $\mathcal{F}_0$ if there exists a sequence of *admissible* slew maneuvers connecting $\mathcal{F}_0$ to $\mathcal{F}$.

Reachability requires that both $\mathcal{F}_0$ and $\mathcal{F}$ be admissible. Reachability is also mutual: if frame $\mathcal{F}$ is reachable from $\mathcal{F}_0$, then $\mathcal{F}_0$ is also reachable from $\mathcal{F}$.

We see that the aiming problem is well-posed if at least one member orientation of the aimset $\mathcal{A}(\vec{e}_{\text{f}})$ is reachable from the initial orientation. Recalling the hazardspace $\mathcal{H}^*$, a reorientation problem is ill-posed if $\mathcal{H}^*$ divides the freespace $\mathcal{C}_{\text{free}}$ into disjoint regions such that the region containing the initial spacecraft orientation does not also contain any of the acceptable goal orientations. Unfortunately, except in the case of a single orientation obstacle, it is unclear how to test whether or not $\mathcal{H}^*$ does in fact divide $\mathcal{C}_{\text{free}}$ as just described. The sufficient conditions for single obstacle reachability are given in Appendix B.

2.5.2 Slew-Limited Well-Posedness and Reachability

We can further restrict the concept of well-posedness by imposing the maneuvering usage limit described in Section 2.3.2.

> **Definition 2.9.** ***Slew-Limited Well-Posedness*:** A simply constrained reorientation problem is *n-slew well-posed* if there exists at least one admissible path σ consisting of not more than n discrete slew maneuvers that solves the problem.

We extend the concept of reachability in the natural way, as follows.

Definition 2.10. ***n-Slew Reachable*:** An orientation $\mathcal{F}$ is said to be *n-slew reachable* from a starting orientation $\mathcal{F}_0$ if there exists a sequence of n admissible slew maneuvers connecting $\mathcal{F}_0$ to $\mathcal{F}$.

By construction, if $\mathcal{F}$ is n-slew reachable, it is also $(n+1)$-reachable. The converse is not always true. We can therefore define a *reachability number* for $\mathcal{F}$ indicating the minimum number of slews necessary to reach $\mathcal{F}$ from $\mathcal{F}_0$. An unreachable orientation has a reachability number of infinity.

2.5.3 General Well-Posedness

Reachability suggests a new way to view well-posedness of reorientation problems. Let $R(\cdot)$ be an operator that takes as its input a set $\mathcal{C}_0$ of starting orientations and returns the set $\mathcal{C}_1$ of all admissible orientations that are 1-slew reachable from *any* of the initial orientations in $\mathcal{C}_0$. We define the reachability operator using

$$\mathcal{C}_1 := R(\mathcal{C}_0). \tag{2.10}$$

By definition, $\mathcal{C}_1$ is a subset of the freespace $\mathcal{C}_{\text{free}}$. Note that we do not require all the input members of $\mathcal{C}_0$ to be admissible. By definition, though, inadmissible input orientations are unreachable. Thus,

$$R(\mathcal{H}^*) = \emptyset, \tag{2.11}$$

and so inadmissible members of $\mathcal{C}_0$ do not contribute to $\mathcal{C}_1$.

By recursively applying (2.10), we generate the set of orientations that are 2-slew reachable from an initial set $\mathcal{C}_0$ as

$$\mathcal{C}_2 := R(\mathcal{C}_1) = R(R(\mathcal{C}_0)). \tag{2.12}$$

Observe that while $\mathcal{C}_2$ is also a subset of $\mathcal{C}_{\text{free}}$, *it is not necessarily a subset of* $\mathcal{C}_1$. In other words, there may be orientations that are not reachable with one slew maneuver, but are reachable with two.

The set $\mathcal{C}_n$ is generated by extending (2.12) in the natural way,

$$\mathcal{C}_n := R^n(\mathcal{C}_0), \tag{2.13}$$

with the superscript indicating the multiplicity of the operation.

Applying the reachability operator to the 2-slew aiming problem, we define

$$\left.\begin{aligned} \mathcal{C}_1 &= R(q_i), \\ \mathcal{C}_2 &= R^2(q_i). \end{aligned}\right\} \tag{2.14}$$

Recall that the aimset $\mathcal{A}(\vec{e}_f)$ becomes a closed curve $Q(\vec{e}_f)$ in $\mathcal{C}$. Well-posedness of the 2-slew aiming problem requires that at least one point on $Q(\vec{e}_f)$ be contained in either $\mathcal{C}_1$ or $\mathcal{C}_2$, that is,

$$(Q(\vec{e}_f) \cap \mathcal{C}_1) \bigcup (Q(\vec{e}_f) \cap \mathcal{C}_2) \neq \emptyset. \tag{2.15}$$

Simplifying, we find that well-posedness requires

$$Q(\vec{e}_f) \bigcap (\mathcal{C}_1 \cup \mathcal{C}_2) \neq \emptyset. \tag{2.16}$$

We can extend this argument in the natural way to create the general well-posedness criterion for the n-slew limited aiming problem,

$$Q(\vec{e}_f) \bigcap (\mathcal{C}_1 \cup \mathcal{C}_2 \cup \cdots \cup \mathcal{C}_n) \neq \emptyset. \tag{2.17}$$

In closing, we note that the above well-posedness relationships also apply to attitude transfer problems if we reduce the curve $Q(\vec{e}_f)$ to a single point q_f.

2.5.4 A Preliminary Test for Well-Posedness

The well-posedness condition of (2.17) is somewhat difficult to evaluate in practice. However, a preliminary test is easy to implement:

$$Q(\vec{e}_f) \bigcap \mathcal{C}_{\text{free}} \neq \emptyset. \tag{2.18}$$

If (2.18) fails, then none of the desired final orientations are admissible and the problem is ill-posed. This test effectively defines an *admissible aimset.* We note that an admissible aimset is a necessary condition for well-posedness, but it is *not* sufficient: it is possible for all the final orientations to be admissible and yet also be unreachable. Appendix A outlines an algorithm for establishing the admissibility of an aimset according to (2.18).

Chapter 3

Motion Planning Algorithm for the 1-Slew Aiming Problem

The single slew attitude motion planning algorithm presented here is capable of determining the set of individual slew maneuvers that will safely solve the 1-slew aiming problem. The solutions returned reorient the aimsight $\vec{e}$ from its initial position $\vec{e}_{\mathrm{i}}$ to the desired final position $\vec{e}_{\mathrm{f}}$ without violating any of the given pointing constraints.

3.1 Objective and Algorithm Overview

The purpose of the 1-slew aiming planner is to solve the constrained aiming problem (Problem 2.4) using only one admissible slew maneuver, if possible. The solution is the set of all admissible slew maneuvers that do so. The algorithm applies a brute-force search to look for "non-conventional" slew axes that will solve the problem.

Because it is only necessary to specify the final attitude to within a rotation about the target-vector $\vec{e}_{\mathrm{f}}$, it is easiest to view solutions to the problem on the surface of the unit sphere $\mathcal{S}$, often called the celestial sphere. Under rotation, an instrument boresight traces a circular arc on $\mathcal{S}$. Pointing constraints are easily plotted as well, by intersecting the hazard cone with the sphere, generating a hazard circle. As long as the boresight path never enters the hazard circle, the pointing constraint is satisfied under the rotation.

3.2 Procedure

The algorithm first establishes the admissibility of the aimset $\mathcal{A}(\vec{e}_f)$ according to criterion (2.18). Assuming $\mathcal{A}(\vec{e}_f)$ is admissible, it then proceeds as follows:

1. Compute the set $\mathcal{W}$ of all candidate rotation axes $\vec{\omega}$ that will directly slew the aimsight from $\vec{e}_i$ into alignment with the target-vector $\vec{e}_f$.

2. For each candidate axis $\vec{\omega}$ in $\mathcal{W}$, determine the angular displacement θ necessary to satisfy the pointing requirement. The rotation axis and its corresponding angular displacement together define the candidate slew maneuver $M = M(\vec{\omega}, \theta)$. Let $\mathcal{M}$ denote the set of all such candidate slew maneuvers constructed from each $\vec{\omega}$ in $\mathcal{W}$. (The members of $\mathcal{M}$ solve the *unconstrained* aiming problem.)

3. Test each member M in $\mathcal{M}$ for admissibility against the constraints H_{jk}. Define the set $\mathcal{M}_{\text{unsafe}}$ to hold all inadmissible slew maneuvers in $\mathcal{M}$. Let

$$\mathcal{M}_{\text{safe}} := \mathcal{M} - \mathcal{M}_{\text{unsafe}} \tag{3.1}$$

   denote the set of all admissible slew maneuvers that solve the 1-slew aiming problem with simple pointing constraints.

4. Apply an optimization algorithm to select one of the remaining safe maneuvers in $\mathcal{M}_{\text{safe}}$.

The process is presented in detail in the sections that follow.

3.2.1 Compute the Candidate Rotation Axes Set $\mathcal{W}$

Observe that the sphere $\mathcal{S}$ contains all possible axes of rotation for the spacecraft. It is apparent that not all axes in $\mathcal{S}$ can rotate the initial aimsight $\vec{e}_i$ into $\vec{e}_f$. Let $\mathcal{W}$ be the subset of $\mathcal{S}$ whose members *can* perform the desired rotation. The first task of the 1-slew aiming planner is to determine the subset $\mathcal{W}$.

In general, the initial aimsight and the target-vector are not coaxial. That is, $||\vec{e}_i \times \vec{e}_f|| \neq 0$. The case where the two vectors are coaxial is handled separately.

Non-coaxial Case. We first examine the non-coaxial case. Two solutions to the *unconstrained* aiming problem are readily apparent. The first, the eigenslew $M(\vec{\omega}_{\text{eig}}, \theta_{\text{eig}})$ as formed in Definition (2.3), is guaranteed to provide the minimum displacement path for swinging the aimsight $\vec{e}$ from $\vec{e}_i$ to $\vec{e}_f$ [20]. For notational convenience, we identify the first apparent solution axis $\vec{\omega}_1$ with the eigenaxis,

$$\vec{\omega}_1 = \vec{\omega}_{\text{eig}} = \frac{\vec{e}_i \times \vec{e}_f}{||\vec{e}_i \times \vec{e}_f||}. \tag{3.2}$$

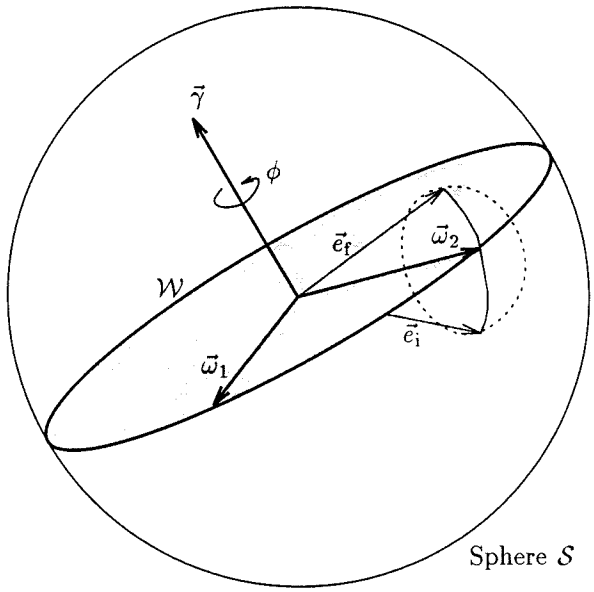

Figure 3.1: Plane of candidate rotation axes. The plane, with normal vector $\vec{\gamma}$, intersects the unit sphere $\mathcal{S}$ as shown. The apparent rotation vectors $\vec{\omega}_1$ and $\vec{\omega}_2$ are also indicated, with sample arc-paths for the aimsight $\vec{e}$.

The second apparent axis, $\vec{\omega}_2$, lies in the plane formed by $\vec{e}_i$ and $\vec{e}_f$, and midway between the two vectors. The second axis is

$$\vec{\omega}_2 = \frac{(\vec{e}_i + \vec{e}_f)}{\|\vec{e}_i + \vec{e}_f\|}. \tag{3.3}$$

It follows that the corresponding angular displacement for this axis is 180°. From these two candidate axes, we can now generate the complete set $\mathcal{W}$ of candidate rotation axes.

In order to swing $\vec{e}_i$ directly into $\vec{e}_f$, all axes $\vec{\omega}$ in $\mathcal{W}$ must satisfy

$$\angle(\vec{e}_i, \vec{\omega}) = \angle(\vec{e}_f, \vec{\omega}). \tag{3.4}$$

Symmetry arguments show that the all candidate $\vec{\omega}$ lie in the plane that passes through the origin and symmetrically bisects the angle between $\vec{e}_i$ and $\vec{e}_f$, as shown in Figure 3.1. Define the normal

$$\vec{\gamma} = \vec{\omega}_1 \times \vec{\omega}_2. \tag{3.5}$$

Considering only the unit vectors that lie in this plane, we obtain the great circle $\mathcal{W}$ as shown. The set $\mathcal{W}$ of candidate rotation axes is one-dimensional, as expected from the single degree of freedom present in the unconstrained aiming problem.

With regard to the initial spacecraft reference frame, the members of $\mathcal{W}$ can be expressed in matrix notation as

$$\mathcal{W} = \{\boldsymbol{\omega}(\phi) | \boldsymbol{\omega}(\phi) = \exp(\phi\hat{\gamma}) \cdot \boldsymbol{\omega}_1\}, \tag{3.6}$$

where

$$\gamma = \begin{bmatrix} \gamma_x \\ \gamma_y \\ \gamma_z \end{bmatrix} \tag{3.7}$$

and $\hat{\gamma}$ is the skew-symmetric matrix representation of the vector γ, i.e.,

$$\hat{\gamma} = \begin{bmatrix} 0 & -\gamma_z & \gamma_y \\ \gamma_z & 0 & -\gamma_z \\ -\gamma_y & \gamma_z & 0 \end{bmatrix}. \tag{3.8}$$

Coaxial Case. In the case that $\vec{e}_\mathrm{i}$ and $\vec{e}_\mathrm{f}$ *are* coaxial, then equation (3.2) fails (since $\|\vec{e}_\mathrm{i} \times \vec{e}_\mathrm{f}\| = 0$). There are two subcases: $\vec{e}_\mathrm{i} = \vec{e}_\mathrm{f}$ and $\vec{e}_\mathrm{i} = -\vec{e}_\mathrm{f}$. The first subcase is trivial: no maneuvering is necessary.

For the degenerate subcase $\vec{e}_\mathrm{i} = -\vec{e}_\mathrm{f}$, the candidate set $\mathcal{W}$ is also a great circle whose members satisfy equation (3.4) as before. However, in this case, there is no unique eigenaxis—the angular displacement from $\vec{e}_\mathrm{i}$ to $\vec{e}_\mathrm{f}$ is the same regardless of the candidate $\vec{\omega}$ chosen. To get around this difficulty, set $\vec{\gamma} = \vec{e}_\mathrm{i}$ and choose $\vec{\omega}_1$ to be *any* arbitrary unit vector perpendicular to $\vec{\gamma}$. The set $\mathcal{W}$ is then computed using the parameterization (3.6) as before.

3.2.2 Determine the Candidate Slew Set $\mathcal{M}$

Once the set of candidate axes $\mathcal{W}$ is defined, the motion planner determines the displacements for each member of $\mathcal{W}$.

Note that for each $\vec{\omega}$ in $\mathcal{W}$, there are *two* candidate slew maneuvers: clockwise and counter-clockwise. However, by symmetry the reciprocal axis $-\vec{\omega}$ is also a member of the candidate set, so that we need only consider counter-clockwise displacements. The solution to the first Paden-Kahan subproblem, described in [16], provides the counter-clockwise angular displacement θ necessary to rotate $\vec{e}_\mathrm{i}$ into $\vec{e}_\mathrm{f}$ for a given $\vec{\omega}$. Appendix C provides the Paden-Kahan solution for reference.

The candidate axis $\vec{\omega}$ and its corresponding displacement θ together define a candidate slew maneuver with respect to the spacecraft frame $\mathcal{F}_\mathrm{S}$:

$$M = M(\vec{\omega},\, \theta)\,. \tag{3.9}$$

Recalling from equation (3.6) that $\vec{\omega}$ is itself a function of ϕ (and therefore so is θ), we can define a set $\mathcal{M}$ of candidate slew maneuvers

$$\mathcal{M} := \{M(\phi) | M(\phi) = M(\vec{\omega}(\phi),\, \theta(\phi))\}\,. \tag{3.10}$$

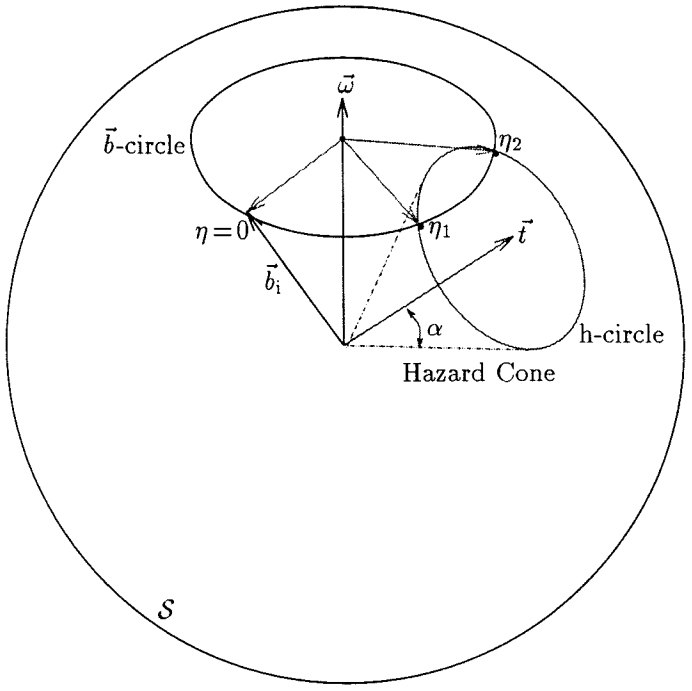

Figure 3.2: Illustration of h-circle (created by intersection of hazard cone with unit sphere) and $\vec{b}$-circle (path taken by an instrument boresight under full rotation about rotation axis $\vec{\omega}$).

If there are no constraints to be applied against these slew maneuvers, then the algorithm may skip the next step: the set $\mathcal{M}$ provides all possible single slew solutions to the *unconstrained* 1-slew aiming problem.

3.2.3 Remove Unsafe Slews From $\mathcal{M}$

For the *constrained* 1-slew aiming problem, the motion planner verifies each candidate maneuver in $\mathcal{M}$ against all the disallowed configurations in $\mathcal{H}^*$. To simplify the discussion that follows, we again visualize the constraints on the surface of $\mathcal{S}$.

The intersection of the sphere $\mathcal{S}$ with the constraint hazard cone (axis $\vec{t}$ and half-angle α) is a circle. This circle, called the hazard circle or *h-circle*, has its center along $\vec{t}$ as shown in Figure 3.2. For a given slew maneuver $M(\vec{\omega}, \theta)$, the constraint's corresponding instrument boresight $\vec{b}$ traces a portion of a circle, called the *$\vec{b}$-circle*. The question of verifying each constraint becomes one of determining at what point(s), if any, the $\vec{b}$-circle intersects the h-circle.

Solving for the intersections is equivalent to solving the second Paden-Kahan subproblem, also described in [16] and presented in Appendix C. Unless the two circles overlap, there are at most two such intersections corresponding to counter-clockwise angular displacements η_1 and η_2 about the slew-axis $\vec{\omega}$. Table 3.1 interprets the results, where n is the number of intersections and $\eta_1 \leq \eta_2$.

n	Condition	Action	Comments
0	n/a	None.	The $\vec{b}$-circle and the h-circle do not intersect; this constraint is always satisfied under rotation about $\vec{\omega}$.
1	$\theta < \eta_1 = \eta_2$	None.	$M(\vec{\omega}, \theta)$ passes the constraint under test.
	$\eta_1 = \eta_2 \leq \theta$	Disqualify $M(\vec{\omega}, \theta)$.	$M(\vec{\omega}, \theta)$ slews $\vec{b}$ through the hazard cone.
2	$\theta < \eta_1 < \eta_2$	None.	$M(\vec{\omega}, \theta)$ passes the constraint under test.
	$\eta_1 \leq \theta \leq \eta_2$	Disqualify $M(\vec{\omega}, \theta)$.	The final position of $\vec{b}$ is unsafe under $M(\vec{\omega}, \theta)$.
	$\eta_1 < \eta_2 \leq \theta$	Disqualify $M(\vec{\omega}, \theta)$	$M(\vec{\omega}, \theta)$ slews $\vec{b}$ through the hazard cone.
∞	n/a (overlapping)	Disqualify $M(\vec{\omega}, \theta)$.	The $\vec{b}$-circle and the h-circle overlap. No solution is possible. Note that this problem is ill-posed; the *initial* condition is unsafe.

Table 3.1: Interpretation of Paden-Kahan results. Note that $\eta_1 \leq \eta_2$, and n is the number of intersections.

Both η_1 and η_2 are measured using the initial spacecraft orientation as a reference. As a practical matter, the last entry in the table never occurs in practice since it requires that the problem be initially ill-posed: the definition of the constrained aiming problem requires that the initial attitude of the spacecraft be admissible.

The algorithm independently checks each constraint H_{jk} for violation under the slew $M(\vec{\omega}, \theta)$. If *any* constraint is violated, then $M(\vec{\omega}, \theta)$ is disqualified because it is inadmissible. The process is repeated for each slew in $\mathcal{M}$.

We define the set $\mathcal{M}_{\text{safe}}$ to be all slews $M(\vec{\omega}, \theta)$ that are not disqualified according to Table 3.1. All members of $\mathcal{M}_{\text{safe}}$ are therefore admissible; each is a solution to the 1-slew aiming problem. It is also possible that $\mathcal{M}_{\text{safe}}$ will be the null set, indicating that there are no single slew solutions.

3.2.4 Select an Optimal Slew From $\mathcal{M}_{\text{safe}}$

At this point, we apply an optimization process over all the admissible slews in $\mathcal{M}_{\text{safe}}$ to determine the best slew maneuver to execute. Examples of optimization might include minimizing fuel-consumption, minimizing the angular displacement traversed by the aimsight $\vec{e}$, or maximizing solar power received during the slew.

We define a number r that denotes the "reachability" of a final orientation from a given starting

orientation $\mathcal{F}_{S_i}$ using a given slew M,

$$r := r(\mathcal{F}_{S_i}, M).$$

The optimizer ranks each slew M in $\mathcal{M}$ according to the optimality metric r, selecting the member with the largest r. Thus, the optimal slew is

$$M_{\text{opt}} := M|_{r_{\max}}, \quad r_{\max} = \max_{\mathcal{M}}\{r\}. \tag{3.11}$$

An obvious metric for r is the constraint function 2.4. Two other metrics are described in the following sections.

MARG optimization

The MARG optimization routine selects the best slew maneuver on the basis of "overshoot margin." It selects the maneuver that allows the most excess admissible angular displacement θ_{over} beyond the slew trajectory endpoint. The instrument boresight obtaining the least overshoot margin defines the metric for the slew trajectory M:

$$r = \min_{M}\{\theta_{1,\text{over}}, \ \ldots, \ \theta_{n,\text{over}}\}. \tag{3.12}$$

In the event that r has no distinct maximum over the slews in $\mathcal{M}$, the MARG optimizer then chooses the least total displacement from those slew maneuvers with $r = r_{\max}$.

This metric does not consider proximity to hazard cones, although unsafe slews are rejected outright. The MARG routine may select a path that takes a particular instrument along an arc that is very close to its hazard. Therefore, MARG assumes good spacecraft control of the commanded rotation axis, while being tolerant of displacement errors.

ANGSEP optimization

The ANGSEP optimization routine, on the other hand, does consider proximity to obstacles, selecting from $\mathcal{M}$ the maneuver that maximizes the least angular separation β between an instrument and its hazard cone. With the angular separation defined over the slew trajectory M as

$$\beta = \min_{M}(\angle(\vec{b}, \vec{t}) - \alpha),$$

the optimization metric, taken over the n instruments, becomes

$$r = \min_{M}\{\beta_1, \ldots, \beta_n\}. \tag{3.13}$$

Note that the ANGSEP routine only compares the *nearest* points of approach; it does not take an average of the angular separation. Thus it is possible that ANGSEP will select a path that maintains

a low but constant angular separation while rejecting a path whose average separation is better but "bottoms out" closer than the former path. It can be shown by geometry that there are at most three critical points at which β needs to be evaluated: at the initial point, the final point, and the closest point of *possible* approach, found by intersecting the great circle from $\vec{t}_j$ to $\vec{\omega}$ with the $\vec{b}$-circle drawn about $\vec{\omega}$. Further, because all slews in $\mathcal{M}$ start from the same initial frame, the initial values of β are the same. ANGSEP discards the initial separations when ranking the slews in $\mathcal{M}$.

The ANGSEP routine disregards the size of the hazard cone; it *only* considers the angular separation between the edge of the cone and the corresponding instrument. ANGSEP is thus more tolerant of errors in $\vec{\omega}$ than MARG. However, paths with good overshoot margin may be rejected by ANGSEP, which assumes tight overshoot control when evaluating β at the slew's intended endpoint.

Other optimization routines

Naturally, other optimization routines could be considered, as well as combinations of the two routines mentioned above. Appendix D presents MATLAB source code for both the ANGSEP and MARG routines.

3.3 Two Case Studies

As a simple demonstration of the 1-slew aiming planner, in this section we will first consider motion planner in the presence of a single avoidance constraint. Next we will extend the example to also include a narrow aiming constraint.

Example 3.1. Single Avoidance Constraint

Consider a rigid spacecraft whose main engine is directed along $\vec{e}_{\rm i} = [0, 0, 1]^T$ in the spacecraft frame $\mathcal{F}_{\rm S}$. It is desired to reorient the spacecraft so that the engine is directed along the vector $\vec{e}_{\rm f} = [\frac{1}{\sqrt{3}}, \frac{1}{\sqrt{3}}, \frac{-1}{\sqrt{3}}]^T$, in the absolute frame. (The absolute frame $\mathcal{F}_{\rm abs}$ is taken to be coincident with the initial spacecraft frame $\mathcal{F}_{\rm S_i}$.) The spacecraft carries an onboard sensor, mounted along sensitivity axis $\vec{b} = [0, \frac{1}{\sqrt{2}}, \frac{1}{\sqrt{2}}]^T$. The sensor is never allowed to be within $\alpha = \pi/6$ radians of the vector to a local bright body at $\vec{t} = [0, -1, 0]^T$ in the absolute frame. Figure 3.3a depicts the initial situation, with the threat cone, instrument vector, initial aimsight, and target-vector shown as indicated.

The 1-slew aiming algorithm determines the set $\mathcal{W}$ of candidate axes, also shown. Figure 3.3b illustrates the set of candidate slew maneuvers in graphical form, using ϕ to parameterize the members of $\mathcal{W}$ according to equation (3.6). For each $\vec{\omega}(\phi)$, the graph gives the necessary counter-clockwise displacement $\theta^+(\phi)$ to achieve the reorientation objective. The clockwise displacement

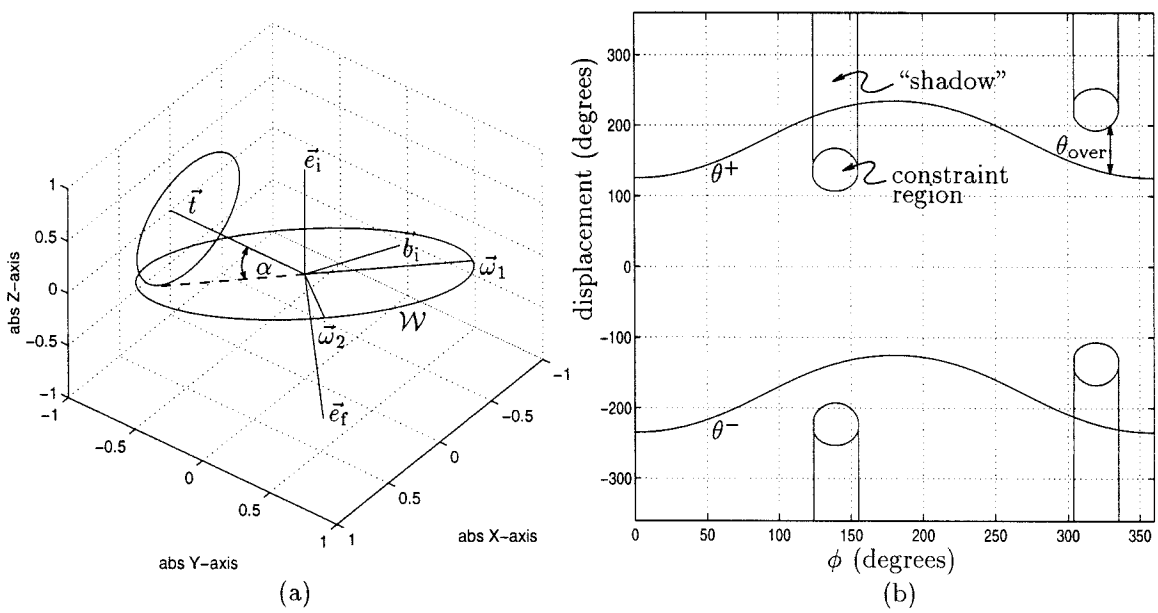

Figure 3.3: (a) Initial situation for the single avoidance constraint of Example 3.1. Also shown is the set $\mathcal{W}$ as determined from the 1-slew planning algorithm. (b) Final displacements and admissible slews as a function of ϕ.

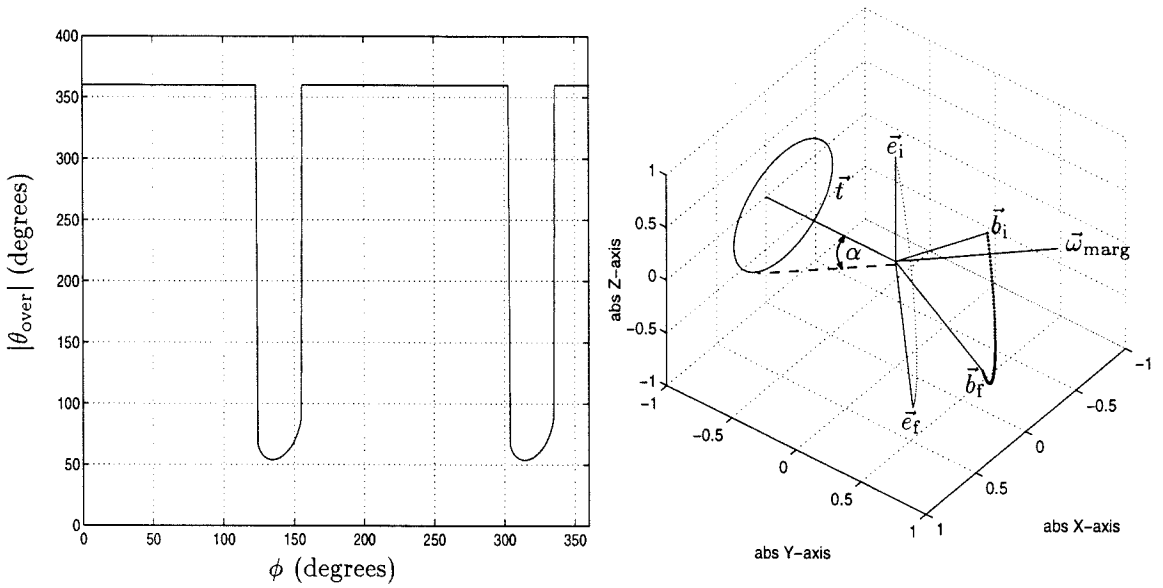

Figure 3.4: (a) Best overshoot margins as a function of ϕ. (b) Optimal MARG maneuver, with traces for both the engine and sensor.

$\theta^{-}(\phi)$ is also shown, as well as the location and extents of the constraint obstacle. Slew trajectories in this diagram proceed upwards and downwards from the horizontal axis, so that the unreachable displacements are "shadows" cast outwards from the constraint obstacles. Observe that a single hazard cone leads to several constraint shadows in this diagram. Also note the symmetries that occur: the displacement curves show even symmetry about $\phi = \pi/2$, while the obstacle shadows invert in each $\pi/2$ interval.

The obstacle plot of Figure 3.3 allows us to define a measure of the *single-slew departibility* of $\mathcal{F}_{S_i}$ to the aimset $\mathcal{A}(\vec{e}_f)$. We define the departibility fraction d for the frame $\mathcal{F}_{S_i}$ as that portion of $\mathcal{W}$ which allows admissible slews to $\mathcal{A}(\vec{e}_f)$. From the figure we observe that there is an admissible slew maneuver (*either* clockwise or counter-clockwise) for all members of $\mathcal{W}$. We thus say that under the given constraints, $\mathcal{F}_{S_i}$ is fully departible to $\mathcal{A}(\vec{e}_f)$ with a departibility fraction $d = 1$.

Next, Figure 3.4a shows the overshoot margin as described for the MARG routine. The plot shows the best overshoot margin for each axis in $\mathcal{W}$ by assuming that the spacecraft will choose the direction with the most overshoot margin. Notice that most candidate axes provide a full 360 degrees of overshoot, indicating that these slew paths will not ever intersect the hazard cone. The dips in the plot indicate that rotation about $\vec{\omega}(\phi)$ beyond the destination curve $\theta(\phi)$ will eventually cause a constraint violation (at about 55 degrees of overshoot in the worst case). Although not shown in this example, negative or zero overshoot would indicate that the axis in question was completely

unsafe.

Figure 3.4b plots the engine and sensor paths for the selected best slew maneuver, as if etched on the surface of the celestial sphere $\mathcal{S}$. (The sphere itself is removed from the drawing for clarity.) With several maneuvers providing a complete 360 degrees of overshoot, the MARG routine selects the eigenaxis $\vec{\omega}_1$ for its minimal angular displacement. The optimal slew maneuver is

$$M_{\text{marg}} = M\left(\vec{\omega} = \begin{bmatrix} \frac{-1}{\sqrt{2}} \\ \frac{1}{\sqrt{2}} \\ 0 \end{bmatrix}, \theta = 125.26^\circ\right).$$

Figure 3.5 indicates the ANGSEP routine results. In part (a), the *least* angular separation β for slews in each direction (CCW and CW) is given, as the rotation axis is varied through $\mathcal{W}$. Because the initial angular separation β_i is constant, regardless of the choice of axes $\vec{\omega}$, it is "filtered out" from the separation curve. (The horizontal dashed line in the figures indicates β_i for reference.) For a given $\vec{\omega}(\phi)$, the larger value of the two angular separation curves indicates the best rotation direction. The "optimal" angular separation plot, shown in part (b) of the figure, indicates the largest possible angular separation at each axis $\vec{\omega}(\phi)$, with the preferred direction indicated at the bottom as a pulse waveform. The "pulse length" is 180 degrees, as we expect from the symmetry of the problem. Note that the ANGSEP plots do not indicate the angular separation for rotations of more or less than the exact necessary displacement $\theta(\phi)$. The ANGSEP curves are valid *only* for the slew maneuver that satisfies

$$M(\phi) = M(\vec{\omega}(\phi),\, \theta(\phi))\,,$$

as ϕ ranges over the members of $\mathcal{M}$.

Figure 3.5c illustrates the optimal maneuver selected by the ANGSEP routine. The optimal maneuver selected by ANGSEP is

$$M_{\text{ang}} = M\left(\vec{\omega} = \begin{bmatrix} -0.1217 \\ 0.9456 \\ 0.3016 \end{bmatrix}, \theta = 137.32^\circ\right).$$

Observe how ANGSEP selects a slew maneuver with axis more closely antiparallel to the threat vector to maximize the angular separation, while MARG chose the eigenaxis maneuver to minimize angular displacement. The table below compares the overshoot margin and angular separation for the selected maneuvers.

	MARG	ANGSEP
θ	125.26°	137.32°
θ_{over}	360.00°	360.00°
β	93.90°	140.26°

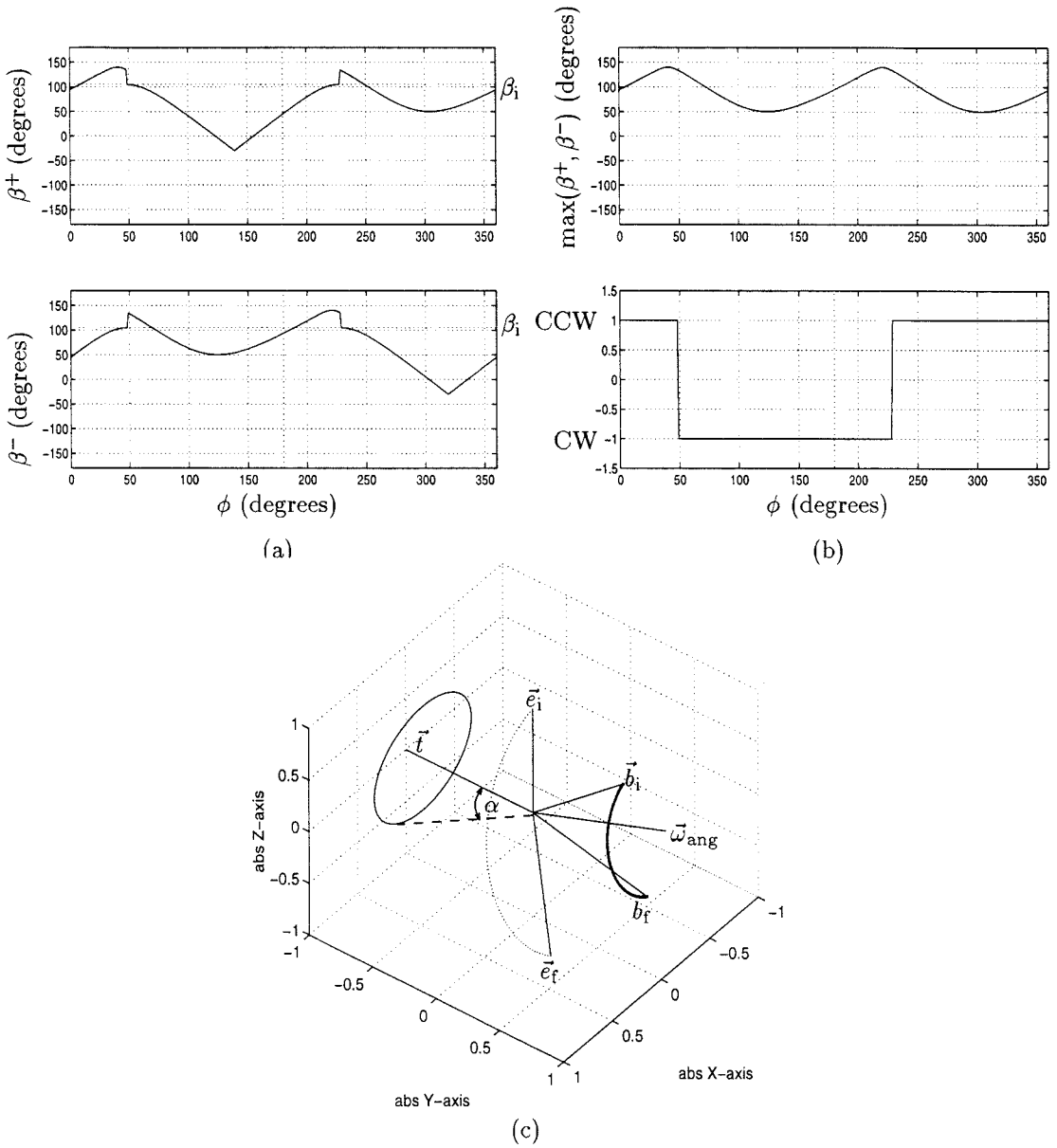

Figure 3.5: (a) Angular separation results for both CCW maneuvers (top) and CW maneuvers (bottom). (b) Final angular separation criteria from ANGSEP routine as a function of ϕ. Shown beneath are the preferred directions of travel (positive counter-clockwise). (c) Optimal ANGSEP maneuver, with traces for both the engine and the sensor.

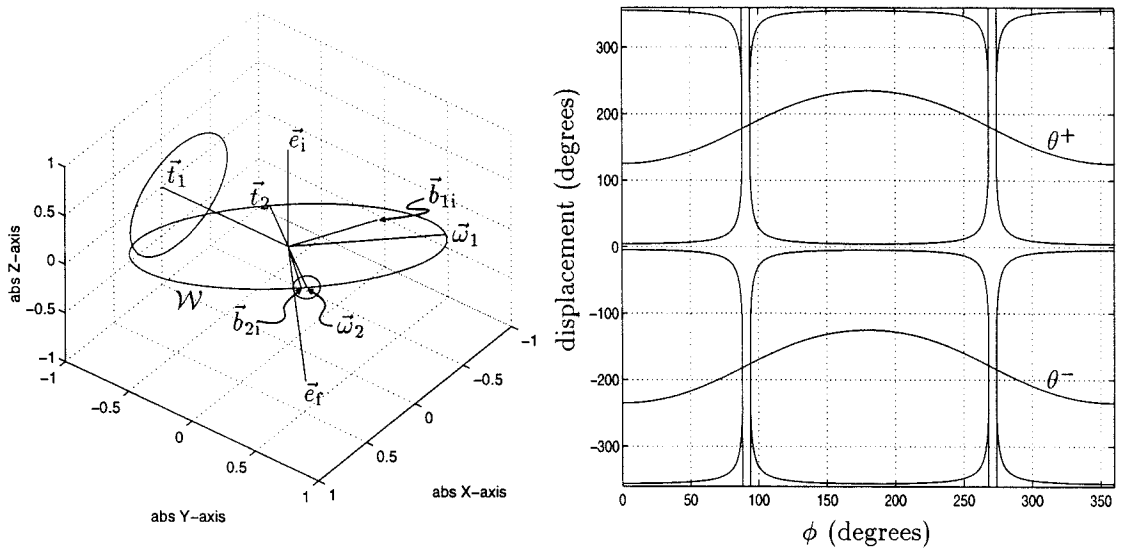

(a) (b)

Figure 3.6: (a) Example initial situation with the previous avoidance constraint and an additional aiming constraint. Note $\mathcal{W}$ remains unchanged. (b) Final displacements and obstructed slews as a function of ϕ. The narrow aiming constraint dominates the avoidance constraint, greatly reducing the allowable slews.

Example 3.2. Avoidance Constraint with Narrow Aiming Constraint

We now add a narrow aiming constraint to the previous example case. In addition to satisfying the previous reorientation requirement and the avoidance constraint, the spacecraft must also keep a navigational star at $\vec{v}_2 = [0.6280, 0.6280, 0.4597]^T$ within a narrow telescope viewing field of 5 degrees half-angle along the telescope axis. We assume that the spacecraft begins with the telescope axis pointed slightly off target by approximately 2 degrees, so that $\vec{b}_2 = [0.6523, 0.6029, 0.4594]^T$.

The aiming constraint is converted to an avoidance constraint by setting $\vec{t}_2 = -\vec{v}_2$ and $\alpha = 175$ degrees. Figure 3.6a depicts the initial spacecraft set-up. Note that $\mathcal{W}$ remains as before.

The narrow aiming constraint severely reduces the number of safe slew axes to be found in $\mathcal{W}$, as indicated in Figure 3.6b. In fact, the aiming constraint in this example dominates the situation, completely overshadowing the earlier avoidance constraint. There are now only two narrow avenues for admissible slew maneuvers. The departibility of $\mathcal{F}_{S_i}$ to $\mathcal{A}(\vec{e}_f)$ is much reduced by the narrow aiming constraint, with a departibility number $d = 0.0278$.

Figure 3.7a illustrates the overshoot margin for the telescope only (instrument $\vec{b}_2$). The overshoot margin for the star sensor (instrument $\vec{b}_1$) remains as in the previous example, shown in Figure 3.4.

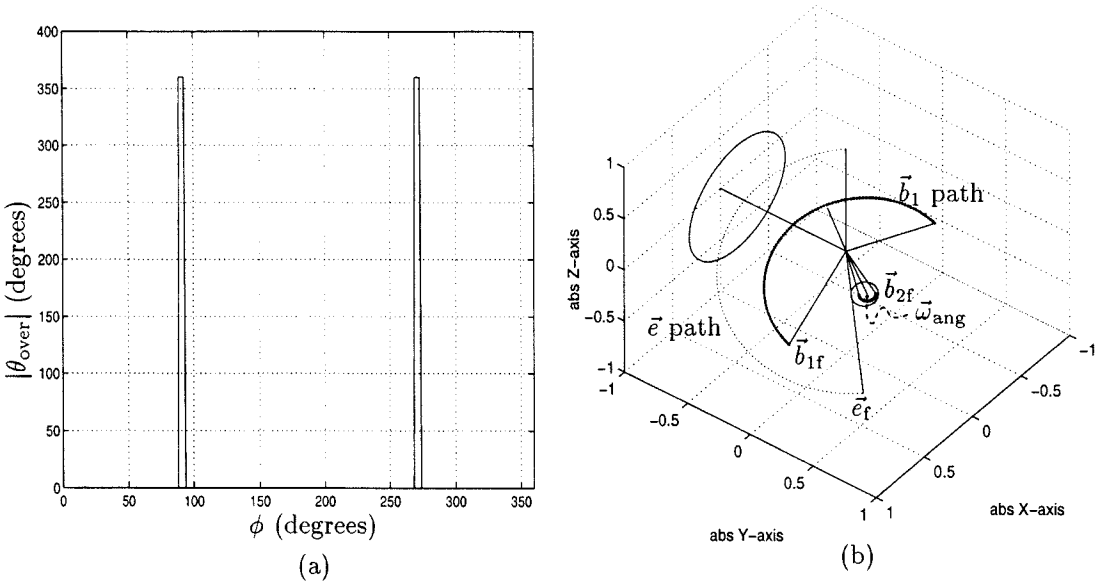

Figure 3.7: (a) Slew overshoot margin (for telescope only) as a function of ϕ. (b) Optimal MARG maneuver, with traces for both the engine $\vec{e}$ and sensors $\vec{b}_1$ and $\vec{b}_2$.

The optimal MARG slew maneuver, shown in part (b) of the figure, is

$$M_{\text{marg}} = M\left(\vec{\omega} = \begin{bmatrix} -0.6641 \\ -0.5901 \\ -0.4591 \end{bmatrix}, \theta = 176.90^\circ\right).$$

Figure 3.8 provides the angular separations for each instrument *individually*. Figure 3.9a combines the individual angular separation plots into a pair of combined plots (one for each direction), by taking the *minimum* of the angular separations for each direction (so that the worst angular separation for each instrument is captured in the plot). Then in part(b) the overall ANGSEP curves are combined into an "optimal" plot by taking the *maximum* angular separation over the two directions, as described for the previous example.

Figure 3.10 illustrates the optimal ANGSEP maneuver. The maneuver selected is

$$M_{\text{ang}} = M\left(\vec{\omega} = \begin{bmatrix} 0.6402 \\ 0.6155 \\ 0.4596 \end{bmatrix}, \theta = 181.04^\circ\right).$$

Observe that the angular displacement is greater than 180 degrees. While rotating clockwise about the same axis would yield a smaller displacement, that path would take the sensor $\vec{b}_1$ closer to the bright body threat at $\vec{t}_1$.

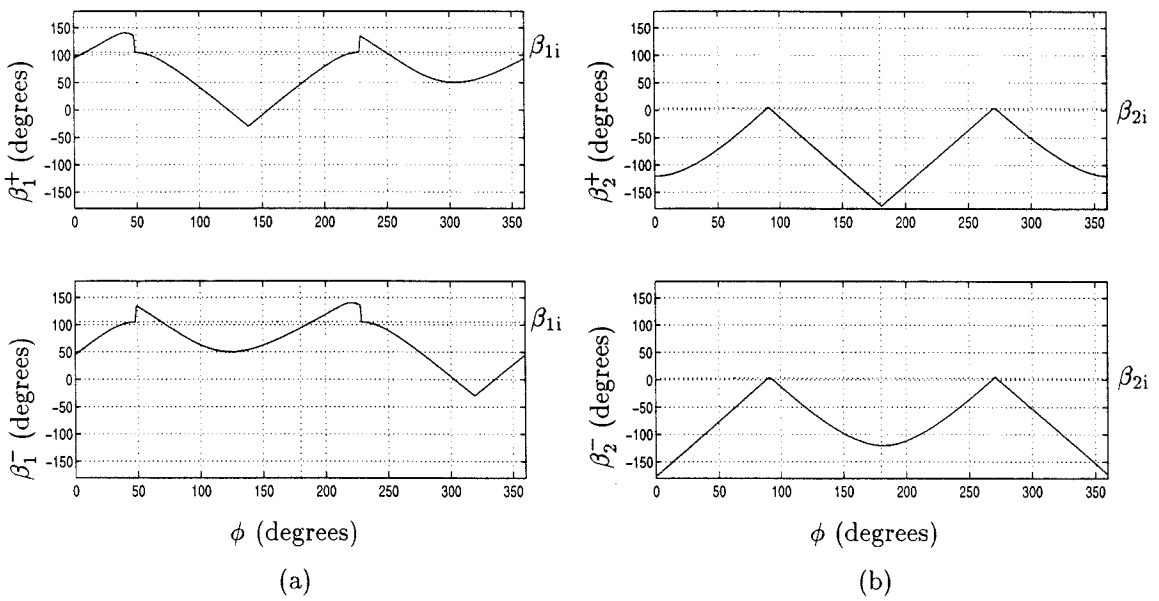

Figure 3.8: (a) Angular separation criteria for the avoidance constraint H_1. Counter-clockwise results are presented above the clockwise results. (b) Angular separation results for the narrow aiming constraint H_2.

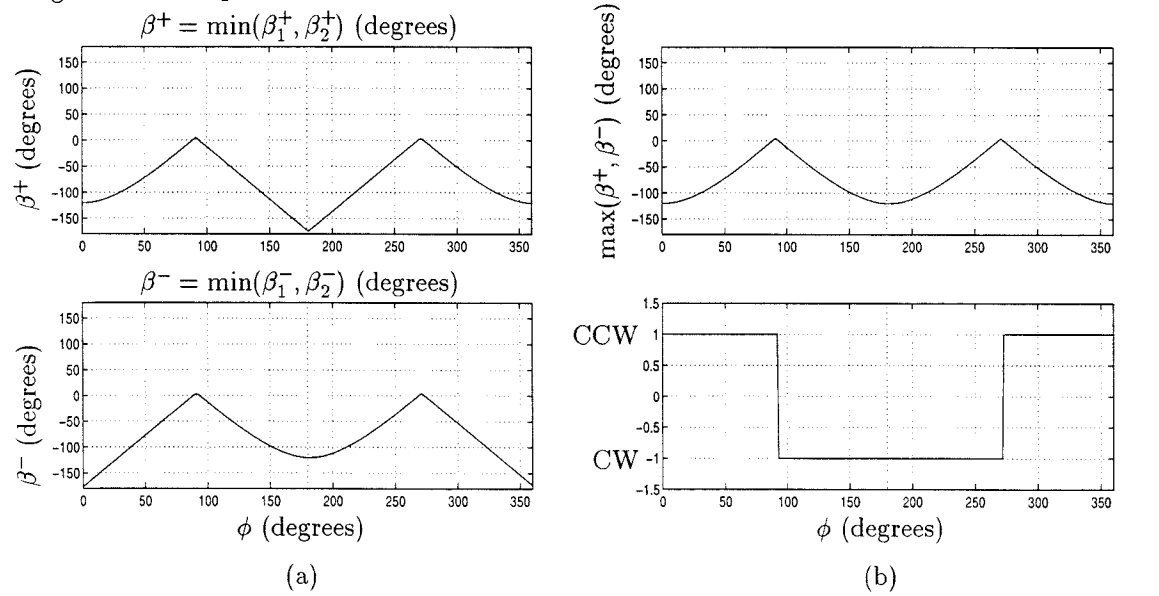

Figure 3.9: (a) Combined ANGSEP results for both instruments, CCW maneuver (top) and CW maneuver (bottom). (b) Final ANGSEP results (for either direction and all instruments) as a function of ϕ. Shown beneath are the preferred directions of travel (positive counter-clockwise).

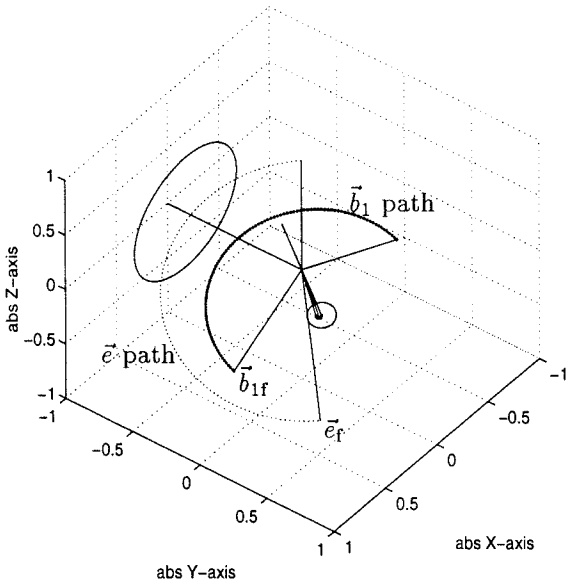

Figure 3.10: Optimal ANGSEP maneuver, with traces for both the engine $\vec{e}$ and sensors $\vec{b}_1$ and $\vec{b}_2$. Note how $\vec{b}_2$ keeps a tighter lock on $\vec{v}_2$.

In comparison with the optimal MARG maneuver, observe that the MARG routine causes the telescope path to swing near to losing lock on the target star, while the ANGSEP routine keeps the telescope path more tightly contained. The tighter containment from the ANGSEP routine results from the distinct local maximum in the overall ANGSEP plot. The MARG margin results have no distinct maximum, so MARG then resorts to selecting the minimum displacement slew. The following table compares the chosen maneuvers (recall that the β_i is removed from consideration). The angular separation listed is for the telescope.

	MARG	ANGSEP
θ	176.90°	181.04°
θ_{over}	360.00°	360.00°
β_2	1.00°	4.98°

Chapter 4

Motion Planning Algorithm for the 2-Slew Constrained Aiming Problem

The two slew attitude motion planning algorithm presented here extends the 1-slew aiming planner to determine an *ordered pair* of slew maneuvers that will solve the 2-slew aiming problem with pointing constraints. The returned ordered pair of slews reorients the aimsight $\vec{e}$ from its initial position $\vec{e}_{\mathrm{i}}$ to the desired final position $\vec{e}_{\mathrm{f}}$ without violating any of the pointing constraints.

4.1 Solution Design for the 2-Slew Aiming Problem

Figure 4.1 represents the 2-slew aiming problem as a 1-slew attitude transfer problem followed by a 1-slew aiming problem. Solutions consist of an attitude transfer from the initial orientation $\mathcal{F}_{\mathrm{S_i}}$ to some intermediate orientation $\mathcal{F}_{\mathrm{S_{ii}}}$, followed by a secondary slew from the intermediate orientation to some valid final orientation in the aimset $\mathcal{A}(\vec{e}_{\mathrm{f}})$. The two slew maneuvers are sequenced together to generate a composite slew path σ, specified as

$$\sigma := (M_1, M_2). \tag{4.1}$$

The intermediate orientation is free to range over the whole set of orientations in the freespace $\mathcal{C}_{\mathrm{free}}$, generally allowing three degrees of freedom. Together with the single degree of freedom allowed by the final aimset $\mathcal{A}(\vec{e}_{\mathrm{f}})$, there are a total of four degrees of freedom in the problem. The space to be searched for a solution is thus quite large compared to the search space of the 1-slew problem.

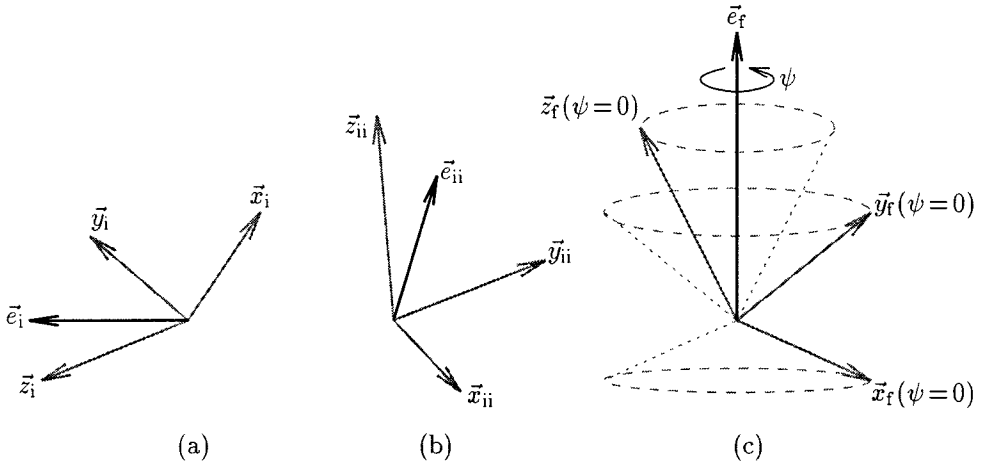

Figure 4.1: (a) The spacecraft starts in an initial frame $\mathcal{F}_{S_i}$ with the initial aimsight vector $\vec{e}_i$ as shown. (b) A single slew maneuver brings the spacecraft to an intermediate orientation $\mathcal{F}_{S_{ii}}$. (c) A second slew maneuver brings the spacecraft to any admissible orientation in $\mathcal{A}(\vec{e}_f)$.

The search for an optimal path depends on finding a good intermediate orientation $\mathcal{F}_{S_{ii}}$ that is easily reachable from $\mathcal{F}_{S_i}$ and also easily departible to $\mathcal{A}(\vec{e}_f)$. Typically, there are significant optimality tradeoffs between the reachability of $\mathcal{F}_{S_{ii}}$ and its departibility to $\mathcal{A}(\vec{e}_f)$.

The schematic of Figure 4.1 is extensible to allow more slew maneuvers. In general, each additional allowed slew maneuver creates another three degrees of freedom. The rest of this chapter shall consider the 2-slew limit in detail.

4.2 Algorithm Overview

The purpose of the 2-slew aiming planner is to solve the slew-limited constrained aiming problem (Problem 2.6) using only two slew maneuvers. Acceptable solutions include all allowable *ordered pairs* of admissible slew maneuvers. At no time must the spacecraft ever assume any of the hazardous configurations in $\mathcal{H}^*$.

The procedure presented below does *not* first check for single slew maneuver solutions; it only searches for solutions that require two slew maneuvers. It is assumed that this algorithm is executed only after the 1-slew aiming planner has failed to find a solution. The 2-slew motion planner conducts a brute force search to first locate all admissible and reachable intermediate spacecraft attitudes $\mathcal{F}_{S_{ii}}$. From each of these attitudes, it then applies the 1-slew motion planner described in the previous chapter.

4.3 Procedure

To simplify the discussion, recall that any spacecraft frame $\mathcal{F}_S$ can be represented as a point q in the configuration space $\mathcal{C}$. In the sequel, the spacecraft orientation is assumed to start at an initial orientation $\mathcal{F}_{S_i}$ with corresponding initial configuration q_i. The frame $\mathcal{F}_{S_{ii}}$ denotes the intermediate spacecraft frame with corresponding q_{ii}, while the aimset $\mathcal{A}(\vec{e}_f)$ maps to a closed curve $Q(\vec{e}_f)$ in configuration space.

For convenience, the 2-slew aiming problem is formally presented here, using configuration space notation.

> **Problem 4.1.** ***Constrained 2-slew Aiming Problem.*** Let the initial configuration of a rigid spacecraft be given by a point q_i in $\mathcal{C}_{free}$, taken with respect to a reference configuration q_{abs}. Let $\mathcal{H}^*$ denote the union of all inadmissible configurations resulting from simple avoidance constraints of the form (2.4).
>
> Given a desired target curve $Q(\vec{e}_f)$, construct a 2-slew path σ in $\mathcal{C}_{free}$, specifying an ordered pair of discrete slew maneuvers (M_1, M_2) that will direct the spacecraft from its initial configuration q_i to any final configuration $q_f \in Q(\vec{e}_f)$.

The algorithm proceeds as follows:

1. Let q_{ii} range over all points in $\mathcal{C}$ in an ordered fashion, checking each q_{ii} for admissibility and 1-slew reachability. Discard all inadmissible and unreachable q_{ii}. The remaining q_{ii} define $\mathcal{C}_1$. (Recall that $\mathcal{C}_1$ is the set of admissible orientations that are 1-slew reachable from q_i.)

2. For each q_{ii} in $\mathcal{C}_1$, construct a composite path as follows:

   (a) compute the primary slew M_1 by solving the 1-slew attitude transfer problem from q_i to q_{ii}.

   (b) compute the *set* of possible second slews, $\mathcal{M}_2$, by solving the 1-slew aiming problem from q_{ii} to $Q(\vec{e}_f)$.

   (c) select the secondary slew M_2 by applying an optimization algorithm to those slews in $\mathcal{M}_2$.

   Note that the 1-slew aiming problem is not guaranteed to have a solution for all q_{ii} in $\mathcal{C}_1$. Define the set $\mathcal{P}$ to contain all admissible composite paths $\sigma = (M_1, M_2)$.

3. Apply optimization to select the best admissible composite path from those paths in $\mathcal{P}$.

The algorithm is presented in detail in the following sections. Note that several of these steps may be done in parallel to increase software efficiency. However, the outline still provides a good basis for understanding the actual procedure.

4.3.1 Construct the Intermediate Reachable Set $\mathcal{C}_1$

The algorithm builds $\mathcal{C}_1$ from scratch, by first checking each candidate intermediate configuration q_{ii} for admissibility. If the candidate q_{ii} is not admissible, the algorithm immediately rejects it and proceeds to evaluate a new q_{ii}. If the candidate q_{ii} is admissible, the algorithm then tests it for 1-slew reachability. However, the test for 1-slew reachability is tantamount to solving the 1-slew constrained attitude transfer problem, so this test can be deferred until the next step.

4.3.2 Construct the Set of Composite Paths $\mathcal{P}$

Having established so far that q_{ii} is in $\mathcal{C}_{\text{free}}$, the algorithm next determines if it is also in $\mathcal{C}_1$. If so, it then attempts to construct a complete admissible 2-slew path. Such paths are used to build up a set $\mathcal{P}$ of admissible 2-slew paths. The details of the substeps are provided below.

(a) Compute the primary slew M_1

The algorithm now establishes the reachability of the candidate q_{ii}, in the process solving the 1-slew attitude transfer problem.

> **Problem 4.2.** ***Constrained One-Slew Attitude Transfer.*** Let the initial configuration of a rigid spacecraft be given by a body frame q_{i} in $\mathcal{C}_{\text{free}}$, taken with respect to a reference configuration q_{abs}. Let $\mathcal{H}^*$ denote the union of all inadmissible configurations resulting from simple avoidance constraints of the form (2.4).
>
> Given an admissible goal configuration q_{ii}, find an admissible slew M_1 that will direct the spacecraft from its initial configuration q_{i} to the desired goal configuration q_{ii}.

Due to the 1-slew limit, the actual procedure of solving Problem 4.2 is not much more involved than solving the unconstrained attitude transfer problem. The algorithm simply computes the two solutions, $M_{1\text{CCW}}$ and $M_{1\text{CW}}$, for the unconstrained attitude transfer problem according to Chasles' theorem (see Appendix C). It then tests each slew for admissibility against the constraints H_{jk}. The admissibility test is the same test performed in Section 3.2.3 using the results of the second Paden-Kahan subproblem.

If neither slew is admissible, then Problem 4.2 has no solution, meaning that q_{ii} is unreachable (and therefore not in $\mathcal{C}_1$). The unreachable q_{ii} is immediately discarded, and the algorithm proceeds to the next candidate q_{ii}.

If either slew is admissible, then q_{ii} is in $\mathcal{C}_1$. The admissible slew is recorded in M_1. If both slews are admissible, an optimization routine selects the best slew to record in M_1.

(b) Compute the set of secondary slews $\mathcal{M}_2$

Having determined q_{ii} to be in $\mathcal{C}_1$, the algorithm now solves the 1-slew aiming problem from q_{ii} to $Q(\vec{e}_f)$ using the 1-slew aiming planner described in Chapter 3. The 1-slew planner returns a set of single slews in $\mathcal{M}_2$. If $\mathcal{M}_2$ is the null-set, then it is not possible to reach any member of the aimset $Q(\vec{e}_f)$ from q_{ii}. In this case, q_{ii} is discarded for being *non-departible* to $Q(\vec{e}_f)$.

(c) Construct the path $\sigma = (M_1, M_2)$

The secondary slew M_2 is selected from set $\mathcal{M}_2$ using an optimization routine, in same style as the methods of Chapter 3. The candidate slew path is constructed from the primary and secondary slew maneuvers as

$$\sigma := (M_1, M_2).$$

This candidate slew path is stored into the set $\mathcal{P}$ for later comparison with all other members of $\mathcal{P}$.

4.3.3 Choose an Optimal Path in $\mathcal{P}$

At this point the algorithm uses an optimization routine to select an optimal ordered pair of slew maneuvers from the candidate set $\mathcal{P}$. The fact that there are now two discrete slews, coupled with the higher degree of freedom in the problem, lead to interesting tradeoffs during the optimization process. For example, the primary and secondary slews may be accorded different weights, representing the relative importance of departing along a superior trajectory or arriving along a superior trajectory. Furthermore, the procedure may allow compensation effects: a superior primary slew may offset deficiencies in its associated secondary slew. Without compensation, the algorithm may rank each path according to the worst constituent slew maneuver, selecting the path with the least overall "danger."

We now briefly describe the two optimization strategies employed in the case studies at the end of this chapter. Both strategies proceed by assessing the suitability of candidate q_{ii} according to two criteria: reachability from q_i and departiblity to $Q(\vec{e}_f)$.

CD/M Optimization

The CD/M optimization routine represents an attempt to quickly rank the reachability and departibility of the intermediate frame q_{ii} without actually investing the time to compute and optimize the departing slew maneuver M_2 to $Q(\vec{e}_f)$.

The reachability of q_{ii} is first established using the constraint function 2.4. Each q_{ii} is ranked by the worst (most positive) value of the constraint function encountered along the slew trajectory from q_i to q_{ii}, taken over all the applied constraints. Unreachable q_{ii} are immediately discarded.

The procedure next solves the 1-aim slew aiming problem, computing the set $\mathcal{M}_2$ of slew maneuvers from q_{ii} to $Q(\vec{e}_{\text{f}})$. However, rather than immediately pausing to select the best secondary slew trajectory M_2 from the available $\mathcal{M}_2$, the routine instead computes the departibility fraction d, representing the fraction of $\mathcal{M}_2$ that is admissible (as mentioned in Example 3.1). Computing the departibility fraction for the set $\mathcal{M}_2$ as a whole is simpler than measuring some other metric, such as overshoot margin, for each member of the set. The q_{ii} are ranked according to the departiblity fraction; all non-departible q_{ii} (with $d=0$) are discarded.

Once all the q_{ii} have been ranked, the optimization routine first selects the most reachable, then choosing from those q_{ii} the most departible. Observe that the intermediate frame q_{ii} is actually selected before the complete slew path is determined. Once the intermediate frame is chosen, the algorithm then proceeds to optimize among a much smaller set of candidate secondary slews using the same MARG routine used in Chapter 3.

CA Optimization

The CA algorithm also uses the constraint function to rate the reachability of q_{ii}; however, unlike CD/M, it does stop at each q_{ii} to determine the best departure slew in $\mathcal{M}_2$. It then uses that slew's trajectory when ranking the departure characteristics of q_{ii} to $Q(\vec{e}_{\text{f}})$. The CA algorithm uses the ANGSEP method of Chapter 3 to evaluate the departibility of q_{ii}.

4.4 Case Studies

Visualization of 2-slew results is somewhat difficult on the surface of the sphere $\mathcal{S}$, mainly because it becomes difficult to keep track of which instruments and hazard cones are paired together in an avoidance constraint. In the examples that follow, we consider a special case in which the instrument under constraint is also the device we wish to aim. This case is called the *constrained aimsight* case.

As we shall see, the resolution at which we let q_{ii} range over $\mathcal{C}$ plays a strong role in the results. For these examples, the intermediate attitudes were represented by a sequence of Eulerian angles $(\psi_{\text{r}}, \psi_{\text{p}}, \psi_{\text{y}})$ representing relative rotations about the spacecraft roll, pitch, and yaw axes. Although this representation is known to be redundant, it effectively imposes a grid onto $\mathcal{C}$ with adjacent elements in the grid being separated by a single rotation $\Delta\psi$ about one of the spacecraft axes.

Once the intermediate orientation q_{ii} is reached, solution of the 1-slew aiming problem requires searching over the subsequent set $\mathcal{W}_2$ of candidates axes. The search resolution imposed on $\mathcal{W}_2$ is $\Delta\phi$.

The 1-slew planner is known to fail for the given combinations of hazards in all following examples.

Example 4.1. Triply Constrained Aimsight

Consider a rigid spacecraft with a single light sensitive instrument initially directed along $\vec{b}_i = [0.3558, -0.5966, 0.7193]^T$. The sensor must be redirected along $\vec{b}_f = [-0.3558, 0.5966, 0.7193]^T$ with respect to the initial spacecraft frame (taken as the absolute reference). Thus, in the notation of the general reorientation problems, we have $\vec{e}_i = \vec{b}_i$ and $\vec{e}_f = \vec{b}_f$. However, the sensor is especially sensitive to radiation from a source at $\vec{t}_1 = [0, 0, -1]^T$, with sensitivity $\alpha_1 = 135°$. Furthermore, there are two other radiative sources at $\vec{t}_2 = [0, -0.4462, 0.8949]^T$ and $\vec{t}_3 = [0, 0.4462, 0.8949]^T$ to which the instrument has a lesser sensitivity $\alpha_2 = \alpha_3 = 23.5°$. The instrument boresight $\vec{b}$ must never fall within any of these three hazard cones during the maneuvers.

We first apply the 2-slew aiming planner using the CD/M optimization procedure. The results are shown in Figure 4.2 at various resolutions. Part (a) of the figure illustrates the hazard circles and the returned instrument path as etched on the surface of $\mathcal{S}$. Observe that the hazards are constructed so that the instrument must traverse a narrow channel. At its narrowest point, the channel width is 6 degrees of arc. The initial and goal points for the instrument are separated from the hazard cones by 1 degree of arc.

Part (b) illustrates the results as seen looking down from the "north pole" of sphere $\mathcal{S}$. For this example, the Eulerian grid imposed on $\mathcal{C}$ is a 10×10×10 grid, so that $\Delta\psi = 36°$ between grid elements. The grid resolution imposed on $\mathcal{W}_2$ is $\Delta\phi = 3.6°$. As seen in the figure, at these grid resolutions the primary slew path tracks the edge of the first hazard cone, maintaining 1 degree of angular separation. The intermediate point $\vec{b}_{ii}$ is chosen so that secondary slew path just averts tangency with the hazard cone about $\vec{t}_3$.

Parts (c) and (d) of the figure illustrate the effects of increasing the Eulerian resolution to $\Delta\psi = 12°$ and then to $\Delta\psi = 3.6°$. The major difference is that as the resolution is increased, the chosen path traverses the channel on the primary slew and the angular clearances between hazards increases. By good fortune, the medium resolution result has a $\mathcal{C}$ grid point so that the primary slew to q_{ii} neatly bisects the channel. Although the higher resolution grid has a finer mesh, the spacing of the grid points is such that the primary slew to q_{ii} is always biased to one side or the other of the channel, so that no "perfect" path is found. With improved resolution, the center path through the channel can be recovered, but at ever higher costs in computational effort.

Table 4.1 presents the results of the 2-slew planner for all three resolutions.

Figure 4.3 provides a comparison between the CD/M and CA optimization methods at the same resolution ($\Delta\psi = 12°$, $\Delta\phi = 3.6°$). The CD/M algorithm takes the primary slew well beyond the channel in order to reach an intermediate position with a larger departibility fraction, where there are a larger number of potential secondary slews. In the case of the CA algorithm, the small angular

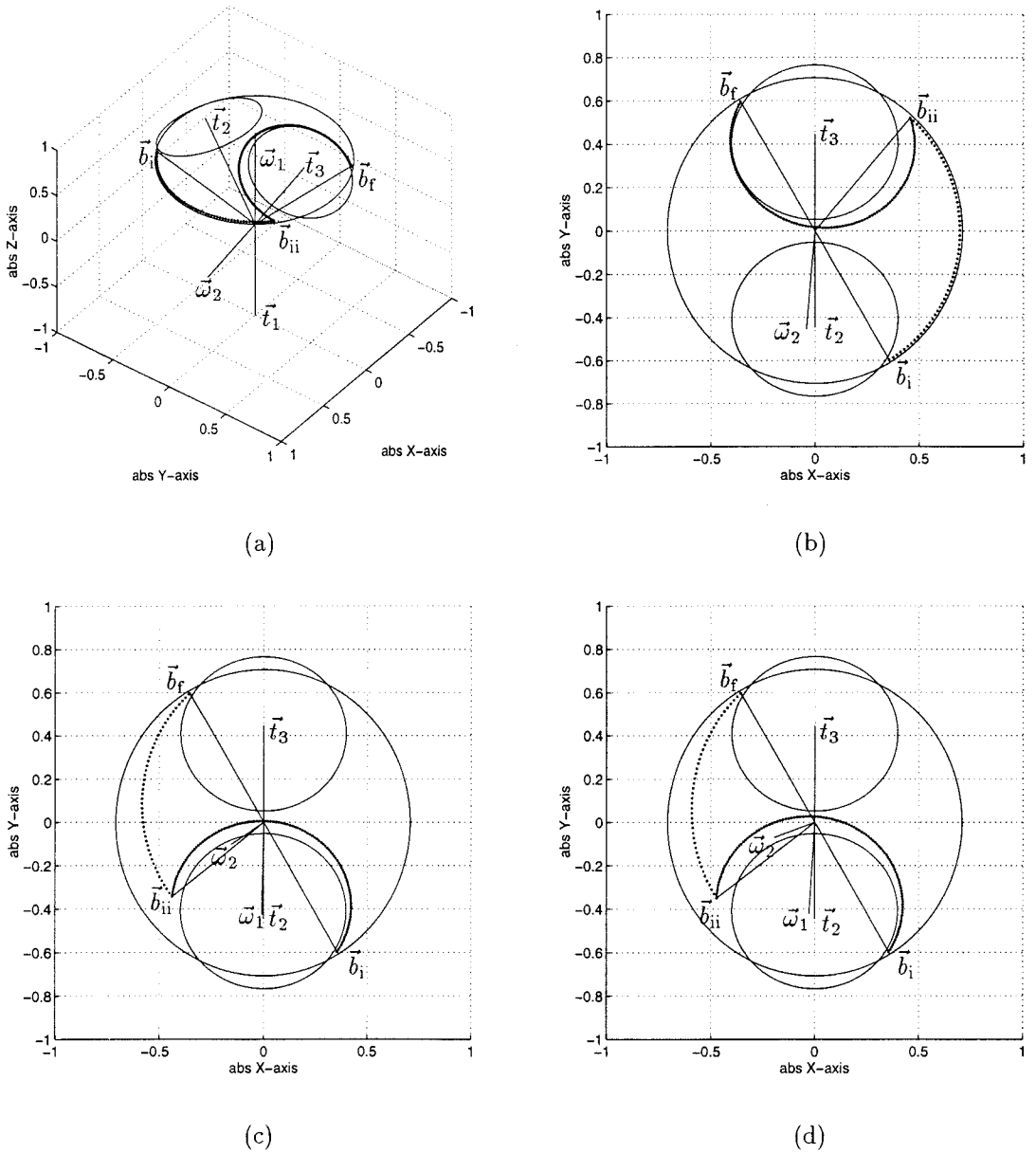

Figure 4.2: CD/M results for triply-constrained aimsight. (a) 3d view with $\Delta\psi = 36°$ and $\Delta\phi = 3.6°$. (b) "Top down" view of maneuver results of (a), $\Delta\psi = 36°$ and $\Delta\phi = 3.6°$. The primary axis $\vec{\omega}_1$ is straight out of the page. (c) Top down view at resolution $\Delta\psi = 12°$, $\Delta\phi = 3.6°$. (d) Results at resolution $\Delta\psi = 3.6°$, $\Delta\phi = 3.6°$.

	(a) $\Delta\psi=36°,\ \Delta\phi=3.6°$	(b) $\Delta\psi=12°,\ \Delta\phi=3.6°$	(c) $\Delta\psi=3.6°,\ \Delta\phi=3.6°$
$\vec{\omega}_1$	$[0, 0, 1]^T$	$[-0.0096, -0.4270, 0.9042]^T$	$[-0.0271, -0.4227, 0.9058]^T$
θ_1	108.00°	206.65°	208.63°
$\vec{\omega}_2$	$[-0.4202, 0.1800, -0.8894]^T$	$[0.3851, 0.7054, -0.5951]^T$	$[0.4422, 0.6403, -0.6281]^T$
θ_2	225.46°	85.14°	81.11°
$\vec{b}_{ii}$	$[0.4574, 0.5228, 0.7193]^T$	$[-0.4385, -0.3434, 0.8305]^T$	$[-0.4711, -0.3499, 0.8097]^T$

Table 4.1: CD/M results for triply constrained aimsight. Note that $\vec{\omega}_1$ is given in $\mathcal{F}_{S_i}$, $\vec{\omega}_2$ is in $\mathcal{F}_{S_{ii}}$, and $\vec{b}_{ii}$ is in $\mathcal{F}_{abs}$.

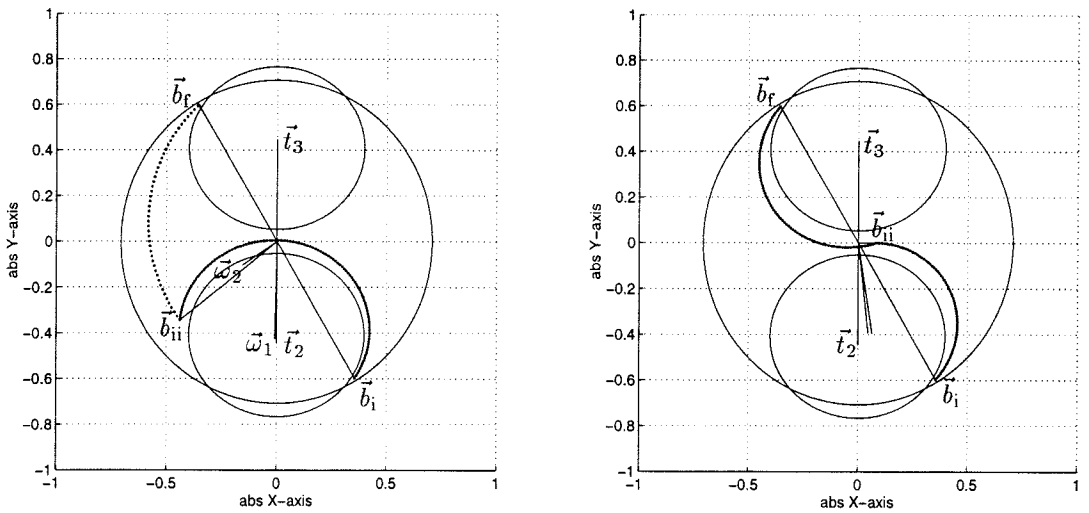

(a) (b)

Figure 4.3: CD/M and CA comparison for $\Delta\psi=12°$, $\Delta\phi=3.6°$ (a) CD/M, as shown earlier. (b) CA.

	CD/M	CA
$\vec{\omega}_1$	$[-0.0096, -0.4270, 0.9042]^T$	$[0.0642, -0.3964, 0.9158]^T$
θ_1	206.65°	128.17°
$\vec{\omega}_2$	$[0.3851, 0.7054, -0.5951]^T$	$[-0.6685, 0.6013, -0.4377]^T$
θ_2	85.14°	147.49°
$\vec{b}_{\text{ii}}$	$[-0.4385, -0.3434, 0.8305]^T$	$[0.0808, -0.0003, 0.9967]^T$

Table 4.2: CD/M and CA results for triply constrained aimsight at the same resolution: $\Delta\psi = 12°$, $\Delta\phi = 3.6°$. The rotation vector $\vec{\omega}_1$ is given in $\mathcal{F}_{\text{S}_\text{i}}$, $\vec{\omega}_2$ is $\mathcal{F}_{\text{S}_\text{ii}}$, and $\vec{b}_{\text{ii}}$ is in $\mathcal{F}_{\text{abs}}$.

separations imposed by the starting and desired stop positions of the instrument allow the CA routine to select a path that closely tracks the hazards cones, while not getting any closer than necessary. Depending on our particular requirements, we might select either result as qualitatively being the better choice. Table 4.2 presents a numerical comparison of the two routines.

Example 4.2. Quadruply Constrained Aimsight

For the second example we impose an additional constraint on the aimsight, creating two separate channels, as follows.

Consider a rigid spacecraft with a single light sensitive instrument initially directed along $\vec{b}_\text{i} = [0.2425, -0.6509, 0.7193]^T$. The sensor must be redirected along $\vec{b}_\text{f} = [-0.2425, 0.6509, 0.7193]^T$ with respect to the initial spacecraft frame (taken as the absolute reference). The sensor must avoid the hazard cones formed by the following threat vectors and sensitivity angles:

$$\begin{aligned}
\vec{t}_1 &= [0, 0, -1]^T, & \alpha_1 &= 135°;\\
\vec{t}_2 &= [0, -0.5807, 0.8141]^T, & \alpha_2 &= 14.5°;\\
\vec{t}_3 &= [0, 0.5807, -0.8141]^T, & \alpha_3 &= 14.5°;\\
\vec{t}_4 &= [0, 0, 1]^T, & \alpha_4 &= 15°.
\end{aligned}$$

These hazard cones form two channels, each 6 degrees of arc. As before the instrument initial position is 1 degree of arc from the first hazard cone.

Applying the 2-slew aiming planner with resolution $\Delta\psi = 12°$ and $\Delta\phi = 3.6°$ gives the results shown in Figure 4.4. We again observe that CD/M shows a strong preference for an easily departible intermediate frame. Additionally, the CD/M result is superior in terms of total arclength. Table 4.3 provides the numerical data for the maneuvers.

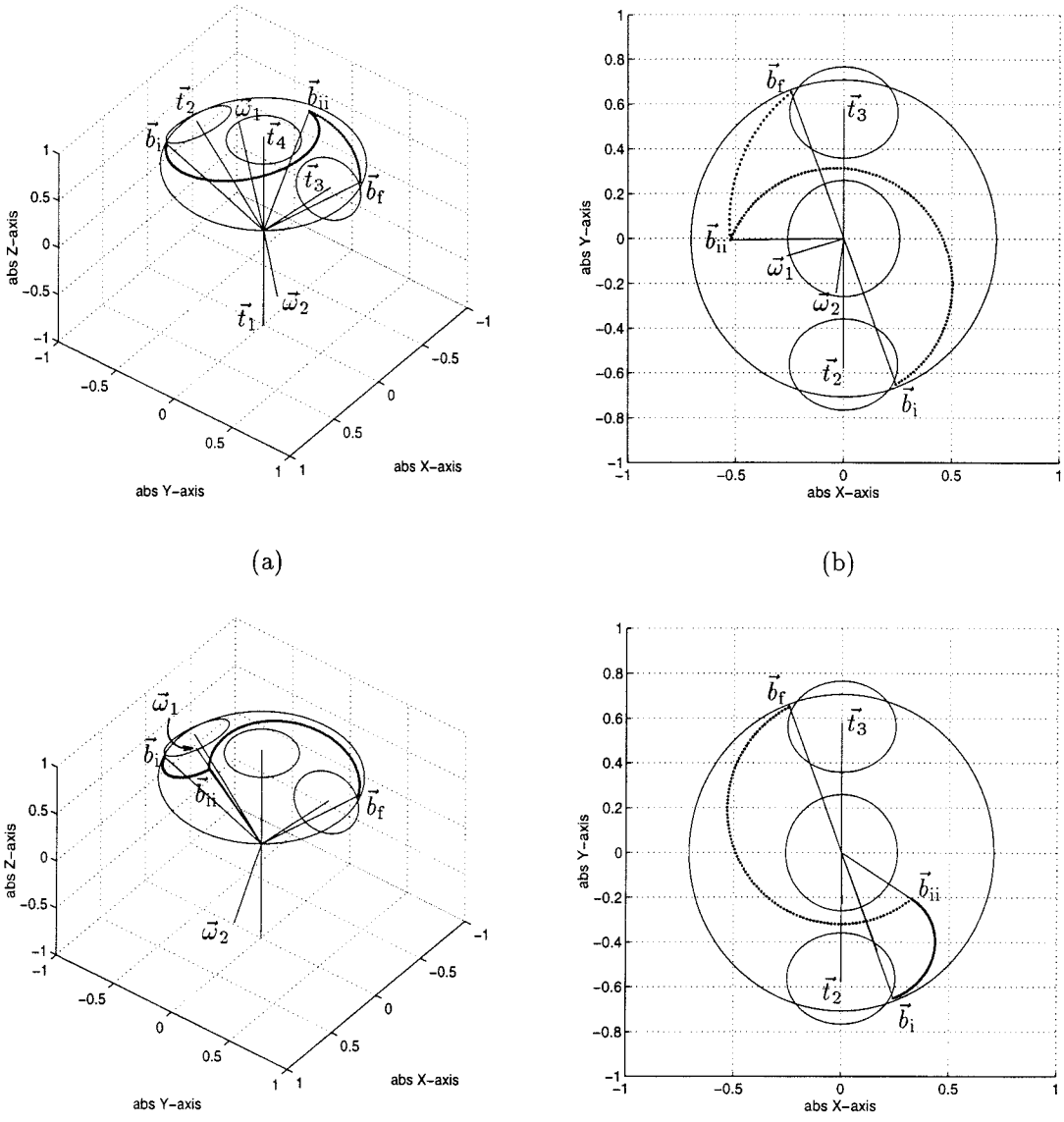

(a) (b)

(c) (d)

Figure 4.4: CD/M and CA results for the quadruply constrained aimsight, with $\Delta\psi = 12°$ and $\Delta\phi = 3.6°$. (a) CD/M. (b) CA.

	CD/M	CA
$\vec{\omega}_1$	$[-0.0352, -0.2410, 0.9699]^T$	$[0.1673, -0.4358, 0.8844]^T$
θ_1	217.48°	125.85°
$\vec{\omega}_2$	$[0.4548, 0.2770, -0.8465]^T$	$[-0.7119, 0.5244, -0.4671]^T$
θ_2	59.49°	191.66°
$\vec{b}_{\text{ii}}$	$[-0.5246, -0.0077, 0.8513]^T$	$[0.3252, -0.2061, 0.9229]^T$

Table 4.3: CD/M and CA results for quadruply constrained aimsight at the same resolution: $\Delta\psi =$ 12°, $\Delta\phi = 3.6°$. The vector $\vec{\omega}_1$ is given in the frame $\mathcal{F}_{\text{S}_\text{i}}$, $\vec{\omega}_2$ is in $\mathcal{F}_{\text{S}_\text{ii}}$, and $\vec{b}_{\text{ii}}$ is in $\mathcal{F}_{\text{abs}}$.

Chapter 5

An Alternative View: Stereographic Projection

As we have seen, it becomes difficult to visualize the orientation and pointing constraints of the spacecraft on the celestial sphere $\mathcal{S}$ as more and more slew maneuvers are allowed. In this chapter we present an alternative method for visualizing the spacecraft orientation, hazards, and aimset of a reorientation problem: stereographic projection. The stereographic projection is a mapping that takes the curved surface of the sphere $\mathcal{S}$ into a plane. We use the projection plane to aid visualization of attitude motion.

In this chapter, we drop the general vector notation (such as $\vec{t}$) in favor of the column vector notation (such as $\mathbf{t}$) to simplify the derivations.

5.1 Fundamentals of the Stereographic Projection

Consider the unit sphere $\mathcal{S}$ to be resting on a plane P as shown in Figure 5.1. Assign a coordinate reference frame $\mathcal{F}_{\text{st}}$ in $\mathbb{R}^3$ at the center of the sphere, with its x and y axes forming a plane parallel to P. Also assign a reference frame $\mathcal{F}'_{\text{st}}$ to points within the plane, with coordinate axes x' and y' parallel to the x and y axes of $\mathcal{F}_{\text{st}}$. From now on we shall use primed notation to indicate points in the plane, and unprimed notation to indicate points on the sphere.

We define the "north pole" $\mathbf{z_n}$ as the point where the z axis intersects $\mathcal{S}$. Thus we have

$$\mathbf{z_n} = [0 \;\; 0 \;\; 1]^T.$$

Let $\mathbf{p}$ be any point on the surface of the sphere. We construct the stereographic projection by drawing the straight line segment from the north pole $\mathbf{z_n}$ through the specified point $\mathbf{p}$, intersecting

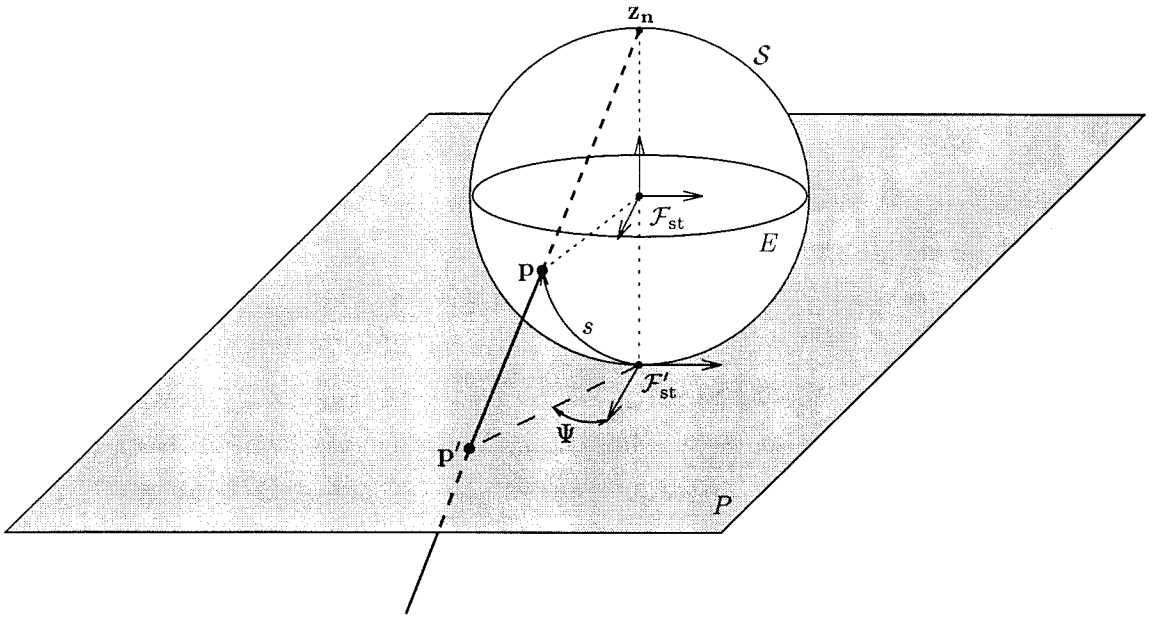

Figure 5.1: Stereographic projection of $\mathbf{p}$ onto $\mathbf{p}'$. [8].

the plane at a point $\mathbf{p}'$. With the exception of the north pole, for each point on the sphere there is a corresponding point in the plane. We shall consider the north pole to map to infinity, that is,

$$\|\mathbf{z}'_{\mathbf{n}}\| = \infty.$$

Given the coordinates of $\mathbf{p} = [x, y, z]^T$, with $\|\mathbf{p}\| = 1$, we define the forward stereographic projection $\mathbf{p}' = [x', y']^T$ as

$$\left.\begin{aligned} x' &= x/(1-z), \\ y' &= y/(1-z). \end{aligned}\right\} \tag{5.1}$$

The inverse projection from $\mathbf{p}'$ to $\mathbf{p}$ is

$$\left.\begin{aligned} x &= \frac{2x'}{(x')^2 + (y')^2 + 1}, \\ y &= \frac{2y'}{(x')^2 + (y')^2 + 1}, \\ z &= \frac{(x')^2 + (y')^2 - 1}{(x')^2 + (y')^2 + 1}. \end{aligned}\right\} \tag{5.2}$$

Observe that the forward projection performs as required for $\mathbf{p} = [0, 0, 1]^T = \mathbf{z}$, returning an unbounded $\mathbf{p}'$. Furthermore, in the limit the inverse projection returns the north pole point $\mathbf{z_n}$ for any $\mathbf{p}'$ as $\|\mathbf{p}'\|^2 = (x')^2 + (y')^2$ tends to infinity.

Observations on the stereographic projection

As we have already observed, the north pole $\mathbf{z_n}$ maps to infinity in the plane, which we construe in a manner similar to that of attaching a "point at infinity" in the complex plane [8]. Additionally, the "south pole" $\mathbf{z_s}$ maps to the origin in the plane,

$$\mathbf{z_s} = [0 \;\; 0 \;\; -1]^T \Longleftrightarrow \mathbf{z}'_\mathbf{s} = [0 \;\; 0]^T.$$

Furthermore, we observe that the "equator" E on the sphere maps to the unit circle E' in the plane. Points in the "southern hemisphere" map to the interior of E', while points in the "northern hemisphere" map to the exterior of E'. As can be seen from (5.1), we have

$$\|\mathbf{p}'\| \to \infty \;\; \text{as} \;\; \|\mathbf{p} - \mathbf{z_n}\| \to 0$$

so that points near the north pole are mapped very far from the origin in the plane [8].

The stereographic projection is also a conformal mapping [8], meaning that the angle between oriented curves on $\mathcal{S}$ is preserved under the mapping of those curves to P. We later show in Section 5.2 that circles drawn on the sphere $\mathcal{S}$ map to either circles or straight lines in the plane P.

Finally, we make some observations about the projection of distance and azimuth. Consider again the point $\mathbf{p}$ on the sphere, connected to the south pole with an arc of minimum length drawn on $\mathcal{S}$. The arclength s, measured from $\mathbf{z_s}$, is $s = \rho r = \rho$, where ρ is the angle between $\mathbf{p}$ and $\mathbf{z_s}$ (recall $r = 1$ on the unit sphere). It is not much work to show

$$\cos\rho = \mathbf{p}^T\mathbf{z_s} = -z.$$

Let d' be the radial distance of the projected point $\mathbf{p}'$ from the origin of P. Thus, using (5.1),

$$(d')^2 = (x')^2 + (y')^2 = \left(\frac{x}{1-z}\right)^2 + \left(\frac{x}{1-z}\right)^2.$$

Substituting for the $(-z)$ term, we obtain

$$(d')^2 = \frac{x^2+y^2}{1+\cos\rho} = \frac{x^2+y^2}{1+\cos s}. \tag{5.3}$$

Equation (5.3) relates arclength from the south pole to projected radial distance in the plane.

Defining azimuth Ψ as the angle in the xy-plane measured from the x-axis, it is apparent that the azimuth of the projected ray $\mathbf{p}'$ in $\mathcal{F}'_{\text{st}}$ is the same as the original azimuth of $\mathbf{p}$ in $\mathcal{F}_{\text{st}}$ (since $\text{atan2}(x, y) = \text{atan2}(x', y')$). This is expected from the conformality of the stereographic projection. Of course, the azimuths of the north and south poles are undefined.

Infinity in the Plane P

Let $\mathbf{p}$ start at the south pole and proceed at constant speed along an arbitrary azimuth towards the north pole (tracing a line of "longitude"). As $\mathbf{p}$ proceeds along its path, the projection $\mathbf{p}'$ starts at

the origin and proceeds outward along a ray with the same azimuth. Note that although the rate of advance of $\mathbf{p}$ is constant, the rate of advance of $\mathbf{p}'$ increases without limit. As $\mathbf{p}$ approaches the north pole, the magnitude of $\mathbf{p}'$ becomes arbitrarily large, although its azimuth remains fixed.

Because arbitrarily large $\mathbf{p}'$ can be generated along any azimuth, we take the "point at infinity" to be an abstract region that surrounds the finite regions of the plane P. Necessarily, the azimuth of this "point at infinity" is undefined [8].

5.2 Circular Projections

We have seen that instruments trace circular paths under rotation about an axis $\boldsymbol{\omega}$, and that hazard cones intersect the sphere in a circle. Clearly a study of the projection of circles is indicated. First, however, we must define some terminology relating to circles etched on the sphere.

Circles on the Sphere

We can construct a circle C on the sphere $\mathcal{S}$ by intersecting the sphere with a plane A in $\mathbb{R}^3$, as shown in Figure 5.2a. The circle so constructed lies completely within in the plane, with its center also in the plane. Of course, the distance from the center to any point on C is constant. We define $\bar{\mathbf{o}}_C$ to be the center of C, using an overbar to indicate that the center lies in the plane of C. Except for tangent planes, $\bar{\mathbf{o}}_C$ does *not* lie on the surface of the sphere (since $\|\bar{\mathbf{o}}_C\| \leq 1$).

Nonetheless, we can define a "center" point on the *surface* of $\mathcal{S}$ by requiring that the minimal arclength measured from this center to all points on C be constant. This definition is equivalent to requiring the angle between this *surface center* and all points on C to be constant, visualized as the intersection of a radially directed cone with the sphere. As shown in Figure 5.2b, the intersection of the cone with the sphere defines the circle C, the cone axis passes through the surface center, and the cone half-angle defines the angular radius of the circle. Note that by extension the cone axis penetrates the sphere through two antipodal points, each of which is a surface center by definition. Therefore, circles on the sphere have *two* surface centers, denoted as $\mathbf{o}_{C,1}$ and $\mathbf{o}_{C,2}$ (without an overbar). We note that $\mathbf{o}_{C,2} = -\mathbf{o}_{C,1}$. Necessarily, one of the surface centers lies in the northern hemisphere and the other lies in the southern hemisphere, unless C is a meridian.

Just as planar concentric circles share a common center, it is possible for circles on $\mathcal{S}$ to share the same surface centers. These circles are called *coaxial circles,* since the radial cones used to generate these circles share a common axis between the two surface centers. Varying the half-angle of the intersecting cone produces the various coaxial circles. Coaxial circles are also called *parallel circles* because the circles reside in parallel planes, such as the latitude circles traced on the Earth. We later show that while parallel circles share the same surface centers, their stereographic projections

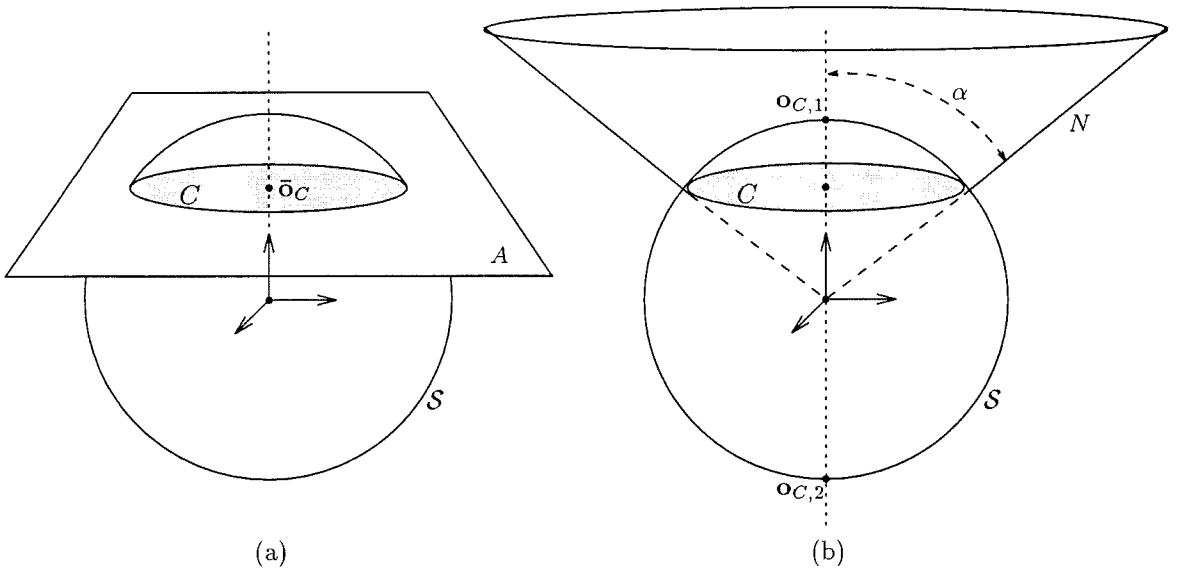

Figure 5.2: (a) Circle C constructed by intersecting plane A with sphere $\mathcal{S}$. The center of the circle is $\bar{o}_C$. (b) Circle C constructed by intersecting a radial cone N with sphere $\mathcal{S}$. The intersection of the cone axis with the sphere defines the surface centers $o_{C,1}$ and $o_{C,2}$.

are not themselves concentric.

5.2.1 Stereographic Projection of a Spherical Circle

This section develops the projection of a spherical circle C onto the plane, drawing observations on the various forms the projected curve C' may take. Recall from geometry the equations of the unit sphere and the general equation of a plane A, given here respectively as

$$x^2 + y^2 + z^2 = 1, \tag{5.4}$$

$$ax + by + cz = d. \tag{5.5}$$

The coefficients (a, b, c) in Eq. (5.5) define the normal vector to the plane A. We restrict the discussion to planes that intersect the sphere by requiring that $|d| \leq 1$. Note that for $d = 0$ the plane passes through the center of the sphere. The locus of points that satisfy both equations (5.4) and (5.5) defines the circle C.

Great Circles ($d = 0$)

We first generate the great circles on the sphere by setting $d = 0$, so that the plane bisects the sphere into two even hemispheres. Applying the inverse mapping relations (5.2) to the planar equation

with $d=0$, we obtain,

$$2ax' + 2by' + c\left[(x')^2 + (y')^2\right] = c. \tag{5.6}$$

We now consider two cases, $c=0$ and $c\neq 0$.

1. For $c=0$, the plane is a vertical plane, producing a great circle on $\mathcal{S}$ resembling a meridian on the Earth. The meridian passes through both the north pole and the south pole. Equation (5.6) reduces to the equation of a line through the origin in the stereographic plane:

$$ax' + by' = 0. \tag{5.7}$$

Thus, for $c= d= 0$, the spherical circle C maps to a *line* C' through the origin.

2. For $c\neq 0$, first divide by c and then complete the square, obtaining

$$\left[x' + \frac{a}{c}\right]^2 + \left[y' + \frac{b}{c}\right]^2 = 1 + \frac{a^2+b^2}{c^2}. \tag{5.8}$$

Equation (5.8) is the equation of a circle in the stereographic plane P, with center at

$$\mathbf{o}_{C'} = \left(\frac{-a}{c}, \frac{-b}{c}\right)$$

and radius

$$r' = \sqrt{\left(1 + \frac{a^2}{c^2} + \frac{b^2}{c^2}\right)}.$$

So, with $d=0$ and $c\neq 0$, the spherical circle C maps to a circle C' in the stereographic plane. The circle C' surrounds the origin since $r' > ||\mathbf{o}_{C'}||$.

Minor Circles ($d \neq 0$)

We now generate minor circles by requiring $d\neq 0$ and $|d|\leq 1$ in the original planar equation (5.5). We proceed as before, applying the inverse mapping relations to the planar equation. With not too much effort, we obtain

$$2ax' + 2by' + (c-d)\left[(x')^2 + (y')^2\right] = (c+d). \tag{5.9}$$

As before, there are two main cases: $(c-d)=0$ and $(c-d)\neq 0$.

1. For $(c-d)=0$, the plane passes through the north pole. Simplifying equation (5.9), we obtain the equation of a line in the stereographic plane:

$$2ax' + 2by' = (c+d). \tag{5.10}$$

Thus, for $c-d=0$, the spherical circle C through the north pole maps to a *line* C' that does *not* pass through the origin. The line has slope $m = -\frac{a}{b}$.

2. For $(c-d) \neq 0$, we first divide equation (5.9) by the factor $(c-d)$ and then complete the square. After some simplification, we obtain

$$\left[x' + \frac{a}{c-d}\right]^2 + \left[y' + \frac{b}{c-d}\right]^2 = \frac{a^2+b^2+c^2-d^2}{(c-d)^2}. \tag{5.11}$$

This result is a circle C' in the plane, with center and radius

$$\begin{aligned} \mathbf{o}_{C'} &= \left(\frac{a}{d-c}, \frac{b}{d-c}\right), \\ r' &= \sqrt{\frac{a^2+b^2+c^2-d^2}{(c-d)^2}}. \end{aligned}$$

The circle C' may or may not surround the origin, depending on the size and position of the spherical circle C.

General Observations

In general, a circle C etched on $\mathcal{S}$ maps to a circle C' in the plane P. If C passes through the north pole, however, then C' is a line. We consider the line to be a circle of infinite radius, with the "center" of the circle located at infinity (along an "azimuth" perpendicular to the line C'). The stereographic projection maps circles on the sphere into generalized circles in the plane.

In addition, the projections of the surface centers of C generally do not map to the center of C'. The latitude circles (circles on the sphere formed with horizontal planes) are the only exceptions, with projections in the plane that are circles centered at the origin.

However, the center $\mathbf{o}_{C'}$ of the projected circle C' does lie on the projection of the meridian that passes through both surface centers ($\mathbf{o}_{C,1}$ and $\mathbf{o}_{C,2}$) of C. In other words, the projections $(\mathbf{o}_{C,1})'$ and $(\mathbf{o}_{C,2})'$ of the surface centers form a line in the stereographic plane which contains the center of C'. This line is further detailed in the next section. Figure 5.3 illustrates the mapping of the centers for a minor circle as shown.

5.2.2 Parallel Circles on the Sphere

A set of parallel circles is generated by intersecting a radial cone with the sphere, varying the cone half-angle while keeping the axis fixed. For this reason, parallel circles on the spherically curved surface $\mathcal{S}$ are considered analogous to concentric circles drawn on a flat surface.

In general, however, the projections of these parallel circles are not themselves concentric. Consider the projections of three vertical parallel circles C_1, C_2, and C_3, as shown in Figure 5.4. The central parallel circle C_2 is a meridian and so projects to a line C_2' through the origin, taken to be a circle of infinite radius and "centered" at infinity. The other two parallel circles are diametrically opposite, and project into circles as shown.

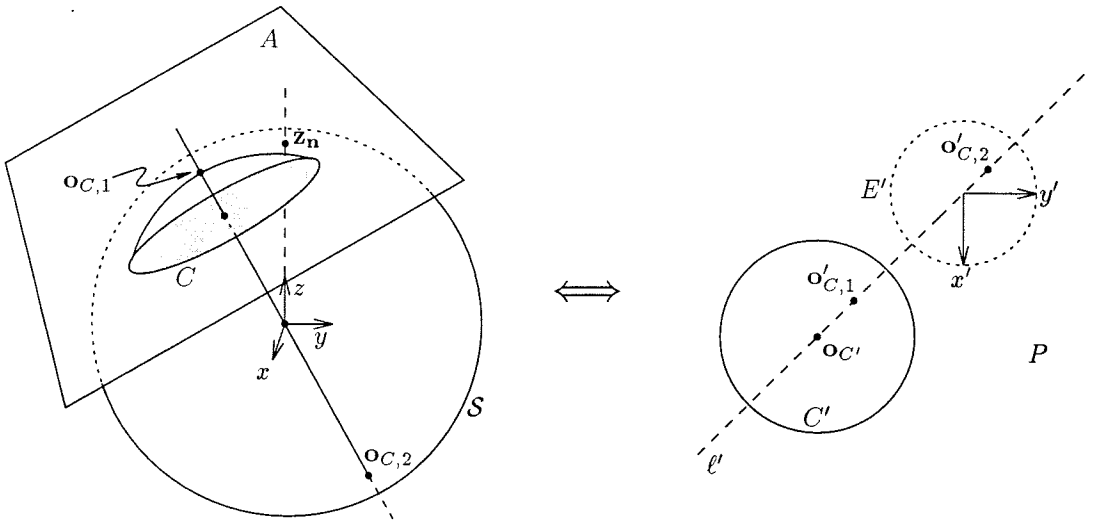

Figure 5.3: On the left, circle C is generated with a cutting plane A through sphere $\mathcal{S}$. The projection C' is shown on the right (plane P), with projections $\mathbf{o}'_{C,1}$ and $\mathbf{o}'_{C,2}$ of the surface centers as indicated. For reference, the equatorial projection E' is also shown.

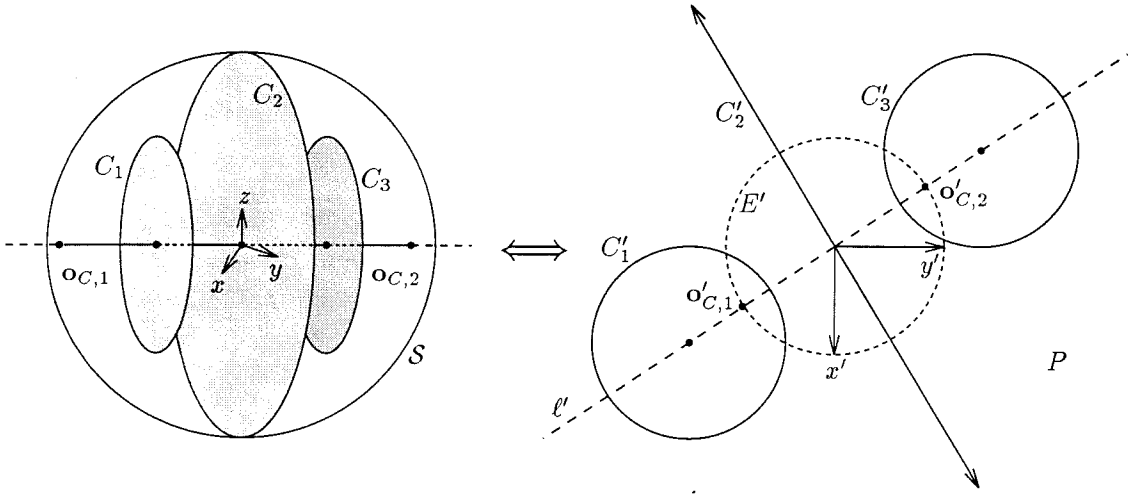

Figure 5.4: Projection of three parallel circles. The common axis for the spherical circles is as shown at the left. Note that although the three circles share common surface centers, the projections at right are *not* concentric. The line of centers ℓ' is indicated, drawn through the projections of the surface centers.

While the projections C'_j are not concentric, their centers do lie on a line ℓ' through the origin, called the *line of centers.* The line of centers is drawn through the projections of the surface centers. Note that ℓ' is perpendicular to the meridian projection C'_2. Recall also that since ℓ' is itself a line through the origin, it inversely maps to a meridian ℓ on the sphere. The meridian ℓ passes through the common surface centers of the C_j circles, bisecting each circle equally.

If the parallel circles on the sphere are "latitudes," then the projections are in fact concentric. The common center is at the origin of the plane P. The line of centers ℓ' degenerates to two discrete points: the origin and the "point at infinity" (corresponding to the north and south poles, which are the surface centers).

Finally, observe that the projections C'_j do not intersect one another, consistent with the non-intersection of the parallel circles C_j on the sphere.

5.2.3 Arcs on the Sphere

In closing this section, we note that portions of circles (arcs) on the sphere $\mathcal{S}$ are mapped to either arcs or line segments in the stereographic plane P. This allows us to easily map lines and spherical polygons into the plane, since they are constructed from arcs of great circles [22].

5.3 Application to Motion Planning

In this section we apply stereographic techniques to the problem of spacecraft attitude motion planning. We assume the spacecraft model as described in Chapter 2. Of course, we must take special care to handle vector traces and hazard circles that pass through the north pole, since these projections become unbounded in the plane. Nonetheless, the stereographic projection provides a useful tool for visualizing the traces of the aimsight and instrument boresight vectors.

5.3.1 Boresight Paths in the Plane

We know that the aimsight $\mathbf{e}$ and all the instrument boresights trace circular arcs on the sphere $\mathcal{S}$ under a given rotation axis $\boldsymbol{\omega}$. In fact, if the arcs were extended to complete circles (as if under a complete 2π revolution), the circles would be parallel.

Under the stereographic projection, the boresight paths project into generalized circular arcs in the plane. Since the spherical traces are arcs of parallel circles, the projected curves have centers that lie along a common line of centers, as detailed in Section 5.2.2. The ray from the origin through the projection $\boldsymbol{\omega}'$ defines the line of centers, since the rotation vector $\boldsymbol{\omega}$ and its antipode $(-\boldsymbol{\omega})$ are the surface centers of the circular arcs.

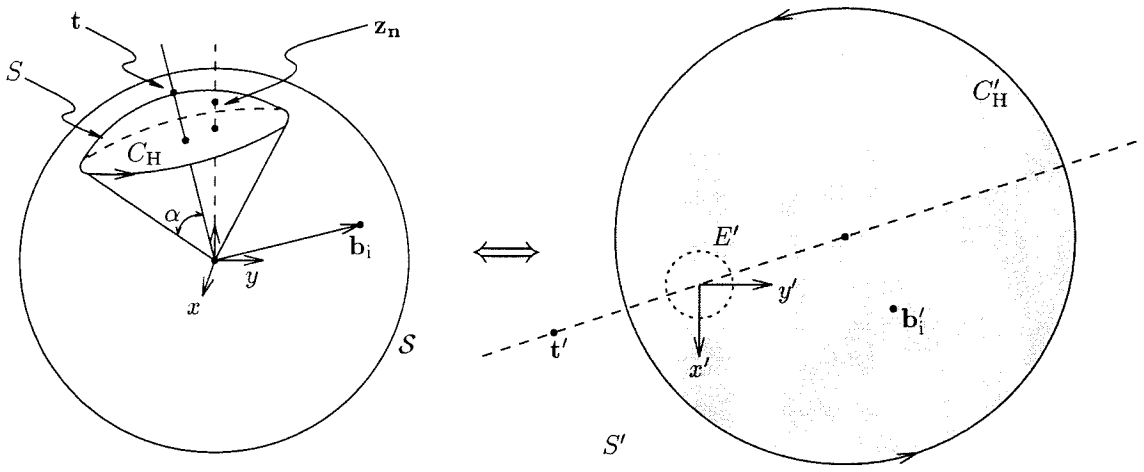

Figure 5.5: At left, hazard cone with threat axis $\mathbf{t}$ and half-angle α intersects $\mathcal{S}$, creating a surface patch S bounded by the directed curve C_H. Observe that the north pole $\mathbf{z_n}$ is contained in S. At right, the threat projection $\mathbf{t}'$ lies *outside* the projected hazard circle C'_H. All points outside C'_H are in S', so that the instrument $\mathbf{b}'$ must remain within the shaded region.

5.3.2 Hazards in the Plane

As described in Chapter 2, we represent a simple pointing constraint with a hazard cone and its corresponding instrument boresight vector $\mathbf{b}$. As long as $\mathbf{b}$ remains outside the cone, the constraint is satisfied. The stereographic projection is particularly useful for graphically illustrating these constraints, but we must carefully consider how points "inside" and "outside" the constraint cone map to the plane.

Let a threat vector $\mathbf{t}$ and and half-angle α define a single hazard cone, describing a hazard circle C_H through intersection with the sphere $\mathcal{S}$. Let C_H be a directed closed curve oriented so that $\mathbf{t}$ always lies to the left of the curve in the usual sense.[1] We say that C_H *encloses* or contains $\mathbf{t}$. Let S be the surface patch enclosed by C_H according to the left-side enclosure rule just defined, as illustrated in Figure 5.5. Note that $\mathbf{t}$ is part of S by definition. The constraint is satisfied provided the instrument boresight $\mathbf{b}$ never enters S.

Upon stereographic projection into the plane P, the directed spherical circle C_H maps into a directed generalized circle C'_H, and the surface patch S accordingly maps into a region S'. However, S' is *not* enclosed within C'_H in the usual sense. Rather, S' lies on the *right* of the directed curve C'_H. Recall the threat vector $\mathbf{t}$ must map to a point $\mathbf{t}'$ inside the region S', graphically confirming this counter-intuitive result.[2]

[1] Observe that the direction of travel around C_H is counter-clockwise when viewed from $\mathbf{t}$ according to the familiar right-hand rule.

[2] In other words, using the conventional notions of enclosure, the interior of C_H on the sphere maps to the exterior

In the plane, the avoidance constraint is satisfied as long as the projected instrument boresight $\mathbf{b}'$ remains never enters the region S' (that is, $\mathbf{b}'$ remains to the *left* of C'_{H}). Note that well-posedness of the reorientation problems requires that all instrument boresights start in safe positions, so that

$$\mathbf{b}'_{\mathrm{i}} \notin S'.$$

Naturally, for each instrument boresight there is a different associated hazard region S'.

5.3.3 Coping with Infinity

There is no way to map the surface of $\mathcal{S}$ into a Euclidean plane without introducing at least one singularity [21]. We have seen that under the stereographic projection there is one singularity at the north pole. Consequently, any boresight path or hazard circle that passes through the north pole causes difficulty with numerical motion planning algorithms. Choosing a different stereographic frame $\mathcal{F}_{\mathrm{st}}$ may alleviate the problem but cannot guarantee that it will never occur.

Hazard circles can be easily handled: the projection C'_{H} clearly divides the plane P into two regions. The projected threat vector $\mathbf{t}'$ identifies the hazardous region S' in the plane. If S' is bounded, then the instrument boresight $\mathbf{b}'$ is free to pass through the north pole. If S' is an unbounded region ($\mathbf{z_n}$ is on or to the right of C'_{H}) then the instrument boresight is never allowed to pass through the north pole.

Tracking the aimsight through the north pole is another matter, however. Since the objective of the aiming problem is to redirect the aimsight, accurate knowledge of the path of the aimsight is essential. If the aimsight passes through or near the north pole, numerical resolution degrades.

There are several possibilities for coping with this problem. One method simply never allows the aimsight $\mathbf{e}$ to pass through or near the north pole, neatly avoiding the problems of boundedness altogether. Effectively, this method creates a simple avoidance constraint on the aimsight itself. If there are such constraints on the aimsight in the initial problem statement (as in the examples of Chapter 4), then an elegant solution is evident: choose $\mathcal{F}_{\mathrm{st}}$ so that the north pole is coincident with the threat vector, thus restricting the motion of the aimsight to the finite plane without introducing any new constraints on the problem.

In general, however, there are no such constraints on the aimsight. (Recall that avoidance constraints operate against instrument boresights which are not required to be coincident with the aimsight.) In this case the technique is to control when the aimsight may be at the north pole; one approach is to choose the frame $\mathcal{F}_{\mathrm{st}}$ so that the north pole is aligned with the *initial* position of the

of C'_{H} in the plane.

aimsight. Thus, in the frame $\mathcal{F}_{st}$, we have

$$\begin{aligned} \mathbf{e}_i &= \mathbf{z_n}, \\ \|\mathbf{e}_i'\| &= \infty. \end{aligned}$$

Since the objective of reorientation maneuvering is to re-target the aimsight $\mathbf{e}$, it is safe to say that $\mathbf{e}$ must depart from its initial position $\mathbf{e}_i$ in order to reach the target-vector $\mathbf{e}_f$. Furthermore, the aimsight must depart $\mathbf{e}_i$ along a *line* in P.

Thus, for 1-slew aiming problems, the projected path of the aimsight will always be a straight line passing through the projected final position $\mathbf{e}_f'$. For the 2-slew aiming problem, there are two possibilities for the primary slew maneuver. The first maneuver will either be a "rotation in place" with $\boldsymbol{\omega} = \mathbf{e}$ (essentially creating a 1-slew problem with different initial conditions), or it will take $\mathbf{e}'$ along a straight line to an intermediate position $\mathbf{e}_{ii}'$. Furthermore, it is apparent that $\mathbf{e}$ cannot ever return to its initial position without trivializing the problem.

5.3.4 Orientations in the Plane

While the stereographic projection readily lends itself to the mapping of boresights and hazards, representation of spacecraft orientation is not as straightforward. The reason is simple: there are only two dimensions to the plane, but orientation has three degrees of freedom. To describe spacecraft orientation requires following the motion of not one but *two* points in P representing the projections of two spacecraft body vectors. Nonetheless, the projection is still useful for aiming problems, where the set of acceptable final orientations is described by a single target-vector $\mathbf{e}_f$.

5.4 Illustrative Examples

In this section we illustrate how slew maneuvers appear in the stereographic plane using Example 3.2 and both examples from Chapter 4. In all the examples that follow, the stereographic frame $\mathcal{F}_{st}$ is taken coincident with the absolute frame throughout the maneuvers.

5.4.1 Illustration of 1-slew Motion

Figure 5.6 illustrates the stereographic projection of the MARG results from Example 3.2. The initial position of the aimsight is $\mathbf{e}_i = [0, 0, 1]^T$, so that $\mathbf{e}_i'$ projects to infinity. The constraint cones map to circles as shown, with the narrow aiming constraint creating a tight circle towards the upper right. The MARG generated maneuver creates the aimsight and instrument boresight paths as indicated in the figure. Part (b) provides closeup view of the narrow aiming constraint. Recall that

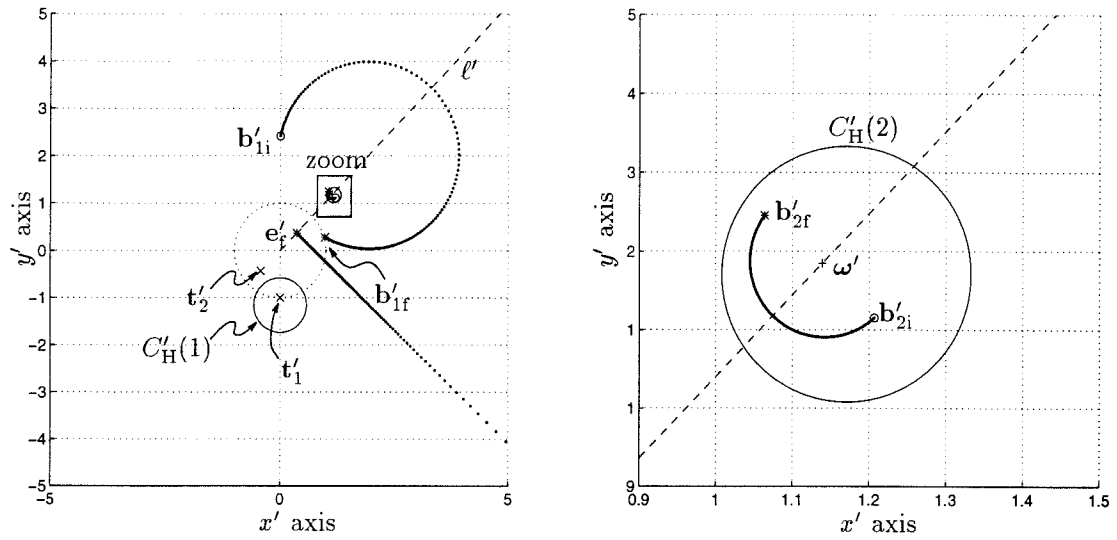

Figure 5.6: Stereographic Projection of MARG results for Example 3.2. The equatorial projection E' (dotted circle) is indicated for reference. The diagonal dashed line ℓ' is the line of centers for the maneuver. (a) Wide view. (b) Close-up view of the narrow aiming constraint.

the paths will be portions of parallel circles on the sphere, with rotational center $\boldsymbol{\omega}'$ on the line of centers as marked.

For comparison, the ANGSEP results are presented in Figure 5.7. Observe how the $\mathbf{b}'_2$ boresight is held much more tightly within the constraint circle for a small change in $\boldsymbol{\omega}'$.

5.4.2 Illustration of 2-slew Motion

Figure 5.8 illustrates a two slew sequence in the stereographic plane using the CD/M results of Example 4.1 (the triply constrained aimsight). The initial situation is shown at the top, with a close-up view towards the upper right. The lower plots illustrate the maneuver sequence. The first slew maneuver causes the instrument boresight $\mathbf{b}'$ to trace a very large circle in the plane, proceeding off the right edge of the graph and re-entering at the left. The second slew then takes the instrument from its intermediate position to the desired final position.

Figure 5.9 illustrates a two slew sequence using the CA results from Example 4.2 (quadruply constrained aimsight). The initial maneuver is shown at left, with the finishing maneuver indicated at the right.

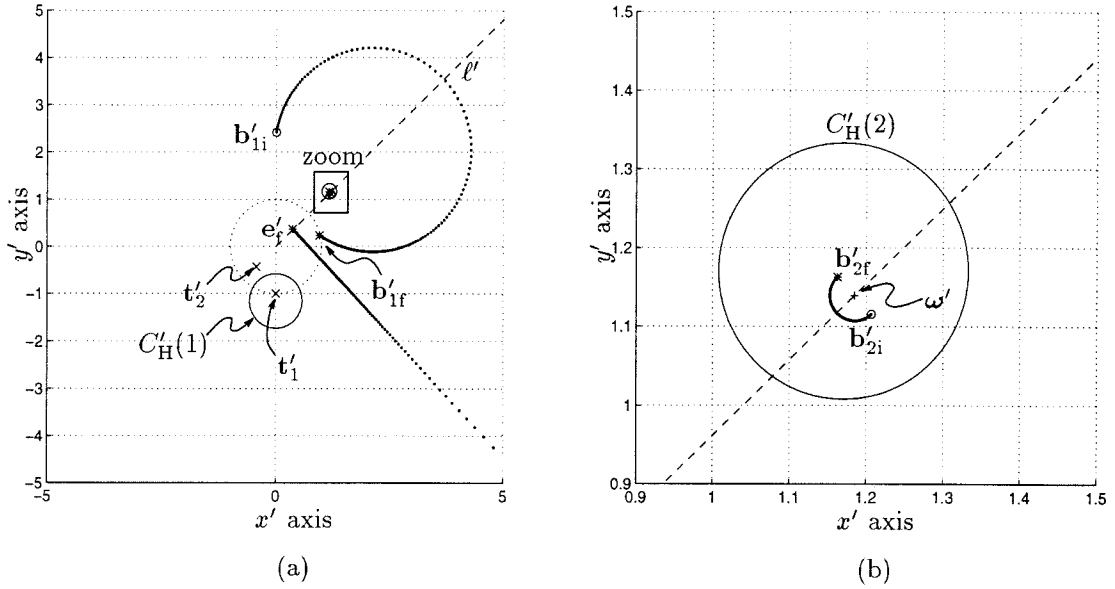

Figure 5.7: Stereographic Projection of ANGSEP Results for Example 3.2. (a) Wide view. (b) Zoomed view onto the narrow aiming constraint.

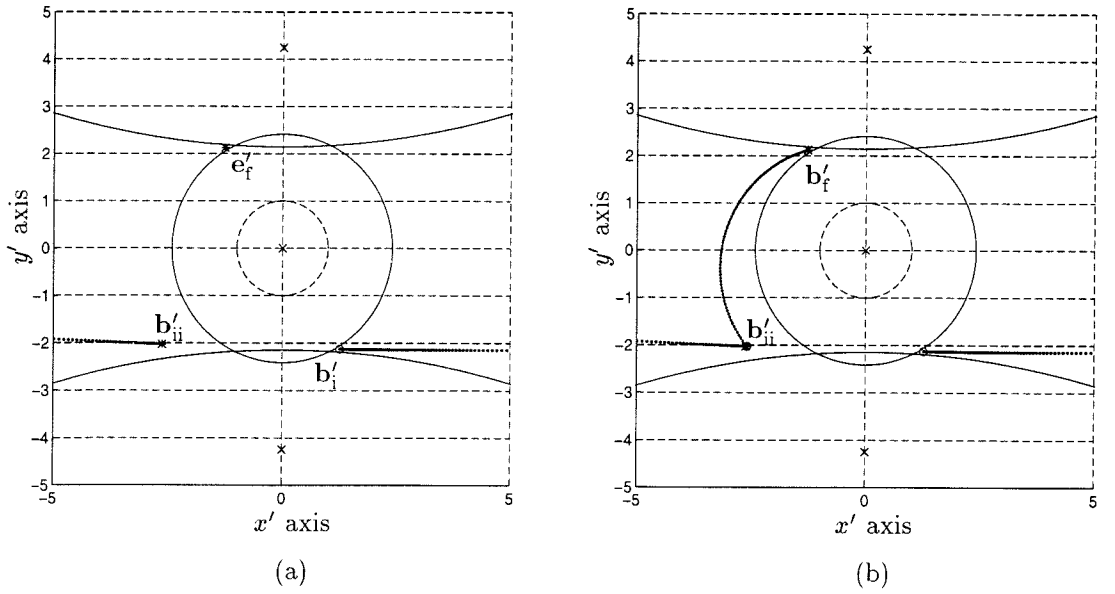

Figure 5.8: Stereographic Projection of Example 4.1: CD/M Results (a) Wide view. (b) Zoomed view. (c) Primary slew path of aimsight (travels counter-clockwise about a *very* large circular arc, "wrapping" around in this view) (d) Continuation through secondary slew path.

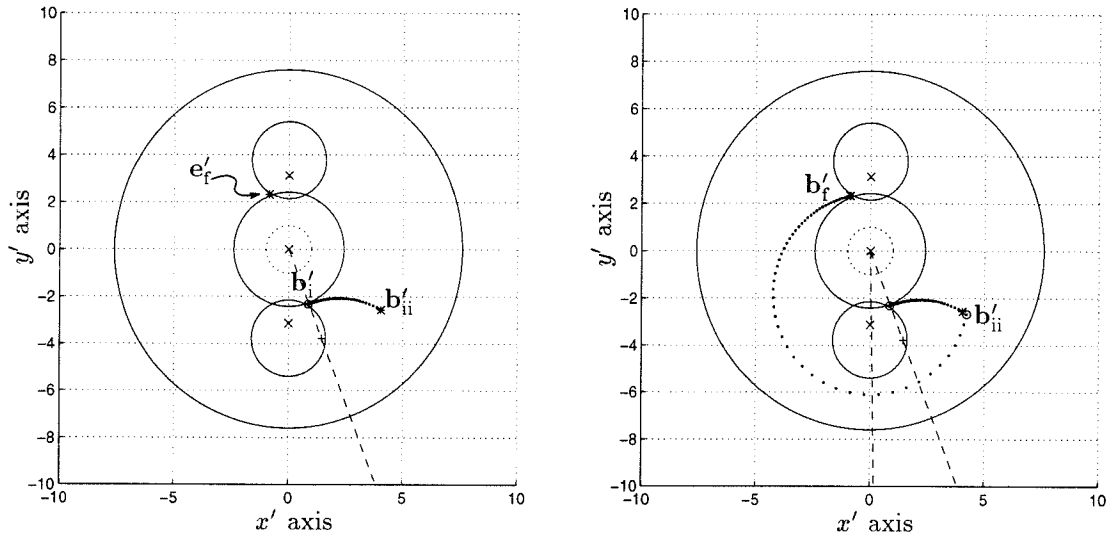

Figure 5.9: Stereographic Projection of Example 4.2: CA Twin-channel Results (a) Primary slew path of aimsight. (b) Continuation through secondary slew path.

Chapter 6

Conclusions

This report has established a framework for the discussion of attitude motion planning problems under simple pointing constraints. We presented several techniques for representing the attitude motion planning problem, in particular concentrating on aiming problems. We also imposed an artificial maneuvering usage limit to avoid arbitrary complexity in the search for solutions.

6.1 Results

In Chapters 3 and 4 we present algorithms that will solve simply constrained 1-slew and 2-slew aiming problems. Appendix C also presents a quick routine for solving the unconstrained 1-slew attitude transfer problem. The algorithms satisfy three of the four desired motion planning features described in Chapter 1: autonomy, admissibility, and optimality. The fourth feature, completeness, is only partially provided using the preliminary test of Section 2.5.4.

The algorithms presented allow for autonomous spacecraft reorientation under simple pointing constraints. Each algorithm proceeds from what is basically a brute force approach, with some refinements to reduce the search space. The brute force search will find a solution, provided that one exists and that the resolution of the search is sufficiently fine.

Admissibility is established by rejecting all slew maneuvers that do not always satisfy the pointing constraints. Although not implemented, the algorithms are written so that the admissibility requirement can be relaxed to allow for a temporary violation of the constraints—effectively creating "soft" pointing constraints as opposed to the "hard" constraints of the form (2.4). Thermal requirements might be an example of a soft constraint: an instrument may be allowed to point towards a heat source for brief periods of time, accumulating heat up to some critical threshold value before it must be pointed away to "cool off."

Two measures for determining optimality were briefly illustrated: MARG and ANGSEP. The MARG routine seeks the admissible slew with the largest displacement overshoot margin, while the ANGSEP routine favors admissible slews with the most angular separation from nearby hazard cones. As presented, both routines accord equal importance to all constraints, although a weighting scheme can be employed to favor particularly sensitive instruments or avoid particularly dangerous threats. The algorithms are general enough that optimization of another desired parameter (for example, fuel consumption or slew time) can be incorporated into the routine. However, these additional parameters may require knowledge of the spacecraft dynamics and severely increase computational load.

The last desired feature, completeness, is only partially provided. Even though a brute force search may fail to find to a solution at a particular search resolution, that is no guarantee that no solutions exist. It may simply be that a finer search grid is required. At the moment there is no facility that determines *a priori* whether or not solutions exist to a particular reorientation problem, nor what search grid resolution is required to find them. Thus, establishing completeness for the planning algorithms is closely tied to determining the conditions for well-posedness of the reorientation problems. While the necessary conditions for well-posedness were established in Section 2.5, using these conditions is tantamount to solving the problem itself. We have not determined a set of sufficient conditions or some other metric that will determine well-posedness without first solving the problem in the process. However, Section 2.5.4 does provide a "quick-and-dirty" test for certain classes of *ill*-posedness.

6.2 Improvements and Future Work

The brute force approach is computationally intensive. While there are surely improvements that can be made to the code in terms of computational efficiency, ultimately the limiting factor in applying the algorithms herein is the manner in which solutions are sought. Furthermore, although the algorithms may fail to find a solution at a particular search resolution, that is no guarantee that solutions do not exist. Clearly, a metric is needed that will impose a limit on the search resolution required to find a solution. Such a metric will most likely combine the relative sizes of the hazard cones and their positions.

"Intelligent" approaches to attitude motion planning under pointing constraints could greatly reduce the search space. We present two possibilities below without extensive analysis. Both approaches involve steering using instrument boresights first, followed by an attempt to target the aimsight onto its desired final position.

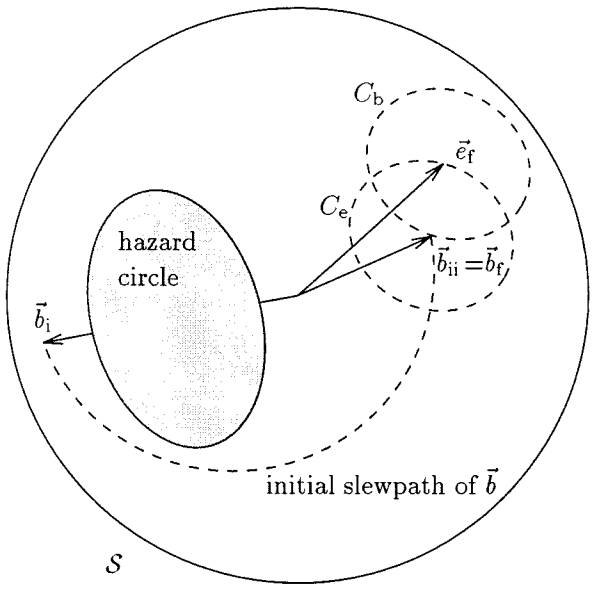

Figure 6.1: Using boresight circles to reduce the search for secondary slew axes.

6.2.1 Intermediate Boresight Reduction of Secondary Slew Axes

In this approach, we first consider the aimset $\mathcal{A}(\vec{e}_f)$ that represents the set of acceptable final attitudes. We note that if the spacecraft is pointed so that the aimsight $\vec{e}$ is directed along the target-vector $\vec{e}_f$, then each boresight $\vec{b}_k$ must lie on a circle about $\vec{e}_f$, called the final boresight circle. Further, all instrument final boresights must lie on parallel circles about $\vec{e}_f$. Then by considering only secondary slews that use any instrument boresight as the rotation axis $\vec{\omega}_2$, we drastically reduce the search space for secondary slew maneuvers to only those maneuvers with axes on the final boresight circles. Under the secondary slew, the chosen instrument boresight rotates in place while the aimsight $\vec{e}$ slews into its desired final position.

We then look for all primary slew maneuvers that will place an instrument boresight on its final circle, intending that that boresight then becomes the secondary rotation axis. We illustrate the procedure in Figure 6.1 for the simple case of only one constraint.

The constant body angle λ between the instrument boresight and the aimsight determines the final boresight circle about the target vector $\vec{e}_f$ (indicated as the circle C_b with angular radius λ). Next we assume an intermediate position $\vec{b}_{ii}$ of the boresight on C_b, so that the intermediate aimsight $\vec{e}_{ii}$ must also lie on a similar circle C_e of angular radius λ centered about $\vec{b}_{ii}$. We now solve the 1-slew aiming problem that takes the *boresight* from its initial position $\vec{b}_i$ to our chosen $\vec{b}_{ii}$. Recall that the 1-slew aiming problem returns a *set* of solutions, each yielding an intermediate attitude $\mathcal{F}_{S_{ii}}$. From each $\mathcal{F}_{S_{ii}}$ we validate the secondary maneuver against all pointing constraints using $\vec{\omega}_2 = \vec{b}_{ii}$. The

angular displacement is returned according to the attitude transfer problem, with $\vec{\omega}_2$ known.

We then march $\vec{b}_{\text{ii}}$ about all positions on C_{b}, repeating the process at each step. The procedure is simply extended to multiple instrument boresights by constructing the appropriate C_{b} for each $\vec{b}$ as needed and repeating the procedure for all instruments.

6.2.2 Motion Planning in the Stereographic Plane

Although it is difficult to use the plane to represent full orientation, we can use the plane to help drastically reduce the search space for solutions with a clever choice of the projection frame $\mathcal{F}_{\text{st}}$. The procedure is outlined as follows, for a spacecraft subject to several avoidance constraints $H_1, \ldots, H_n$. The constraints are sorted according to sensitivity angle, so that

$$\alpha_1 \geq \alpha_2 \geq \ldots \geq \alpha_n.$$

Thus the most restrictive constraint is H_1 and the least restrictive constraint is H_n.

1. Set the stereographic projection frame $\mathcal{F}_{\text{st}}$ so that the z-axis lies along the direction of the most restrictive threat source, $\mathbf{t}_1$.

2. Project the hazard circles onto the stereographic plane for all constraints. The projected hazard circle for $\mathbf{t}_1$ will necessarily be centered at the origin of the plane. Denote this circle $C'_{\text{H}}(1)$.

3. Project the initial instrument boresights. Observe that $\mathbf{b}'_1$ is enclosed within (to the left of) the directed hazard circle projection $C'_{\text{H}}(1)$, and must remain within that circle during all slew maneuvers.

4. Every point interior to $C'_{\text{H}}(1)$ defines a *set* of frames $\mathcal{B}$ with a common instrument boresight vector. In fact, the set $\mathcal{B}$ is really an aimset with $\mathbf{b}_1$ as the generating parameter. To avoid confusion, we refer to this set as the *boreset* $\mathcal{B}(\mathbf{b}_1)$.

5. Select a particular boreset $\mathcal{B}$ by choosing an intermediate boresight point $\mathbf{b}'_{1\text{i}}$ inside $C'_{\text{H}}(1)$. Compute all possible primary slews from the initial boresight $\mathbf{b}_{1\text{i}}$ to the chosen boreset by solving the 1-slew aiming problem. For each primary slew solution returned, construct the secondary slew by solving the attitude transfer problem that takes $\mathbf{e}$ from its intermediate position to its final position $\mathbf{e}_{\text{f}}$.

6. Repeat for all boresets within $C'_{\text{H}}(1)$, selecting the best of all computed 2-slew solutions as the optimal 2-slew solution.

Figure 6.2 illustrates the procedure.

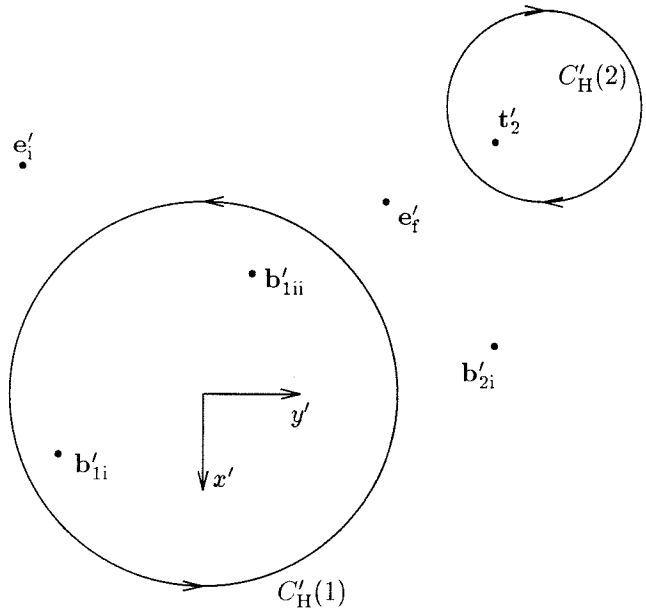

Figure 6.2: Motion Planning in the stereographic plane using boresets.

Appendix A

Test for Aimset Admissibility

This appendix describes a procedure for determining whether or not the spacecraft pointing requirement $\mathcal{A}(\vec{e}_f)$ is feasible for the aiming problem with simple pointing constraints. Simply put, it answers the question: Is the pointing requirement $\mathcal{A}(\vec{e}_f)$ admissible according to condition (2.18)?

The answer given is complete in the sense that if there are such final orientations, they are returned as part of the answer. Note that the test does not determine whether or not those final orientations are *reachable*, that is, it does not indicate that a path exists to take the spacecraft from its initial orientation $\mathcal{F}_{S_i}$ to the specified admissible final orientations in $\mathcal{A}(\vec{e}_f)$. The test therefore does not determine the well-posedness of a reorientation problem.

A.1 Overview

The underlying concept for the aimset admissibility test is simple. All spacecraft orientations $\mathcal{F}_S$ in the aimset $\mathcal{A}(\vec{e}_f)$ are examined for violations of any of the pointing constraints H_{jk}. If *each* member frame in $\mathcal{A}(\vec{e}_f)$ fails to pass any of the constraints, then *all* of $\mathcal{A}(\vec{e}_f)$ is inadmissible, and any reorientation problem with pointing requirement $\mathcal{A}(\vec{e}_f)$ is ill-posed. A brute force search is avoided by taking advantage of the simple rotational parameterization of the aimset and relying on the rigid spacecraft assumption.

For a rigid spacecraft, the body angle λ between the aimsight and a boresight vector $\vec{b}$ must remain constant. Therefore, if the spacecraft meets the pointing requirement (when the aimsight $\vec{e}$ is directed along the target-vector $\vec{e}_f$), the boresight vector must lie somewhere on a cone about the target-vector $\vec{e}_f$ with the same body angle λ. This cone intersects the celestial sphere in a circle, denoted the $\vec{b}_f$-circle. Together with the target-vector, the $\vec{b}_f$-circle represents the complete aimset $\mathcal{A}(\vec{e}_f)$ of desired final orientations for the spacecraft (since two direction vectors determine an

orientation). Some of these orientations likely will violate the pointing constraints for this instrument (or for some other instrument), creating "unsafe" regions along the $\vec{b}_{\mathrm{f}}$-circle. If the entire $\vec{b}_{\mathrm{f}}$-circle is obstructed by these unsafe regions, then there are no possible final orientations in the aimset $\mathcal{A}(\vec{e}_{\mathrm{f}})$ that are safe. The aimset is therefore inadmissible.

The procedure outlined above can be extended to n instruments, as detailed below.

A.2 Procedure

Given:

1. A rigid spacecraft.
2. An initial direction for a spacecraft aimsight, $\vec{e}_{\mathrm{i}}$.
3. n spacecraft body vectors for instrumentation boresights, $\vec{b}_{1\mathrm{i}}, \ldots, \vec{b}_{n\mathrm{i}}$.
4. Corresponding simple *avoidance* constraints for each instrument of the form

$$(\vec{t}_k \cdot \vec{b}_k) - \cos\alpha_k < 0, \quad 1 \leq k \leq n, \tag{A.1}$$

   where $\vec{t}_k$ is the threat source and α_k is the nearest angle that $\vec{b}_k$ is allowed to approach $\vec{t}_k$.
5. An aimset $\mathcal{A}(\vec{e}_{\mathrm{f}})$ defined by a desired target-vector $\vec{e}_{\mathrm{f}}$ along which the aimsight $\vec{e}_{\mathrm{i}}$ is to be directed.

Procedure:

1. Compute the spacecraft body-angles λ_k between the initial aimsight $\vec{e}_{\mathrm{i}}$ and each initial instrument vector $\vec{b}_{k\mathrm{i}}$, using

$$\lambda_k = \angle\left(\vec{e}_{\mathrm{i}}, \vec{b}_{k\mathrm{i}}\right), \quad 1 \leq k \leq n. \tag{A.2}$$

   The body-angles are depicted in Figure A.1 for the case $n = 3$.
2. On the surface of the celestial sphere $\mathcal{S}$ construct n parallel circles representing the possible final directions $\vec{b}_{k\mathrm{f}}$ of the instruments as follows: For each instrument k, intersect a cone with central axis $\vec{e}_{\mathrm{f}}$ and half-angle λ_k with the sphere $\mathcal{S}$.

   The circle so created is termed the $\vec{b}_{k\mathrm{f}}$-circle for the kth instrument. This circle represents set of possible final directions for the kth instrument under the condition that the aimsight is aligned along the target-vector. These circles are indicated in Figure A.2.

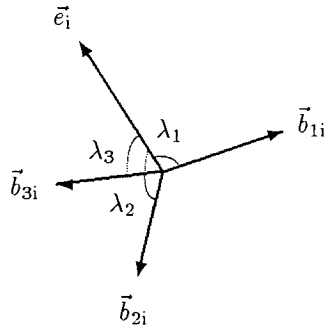

Figure A.1: Spacecraft body angles for $n = 3$.

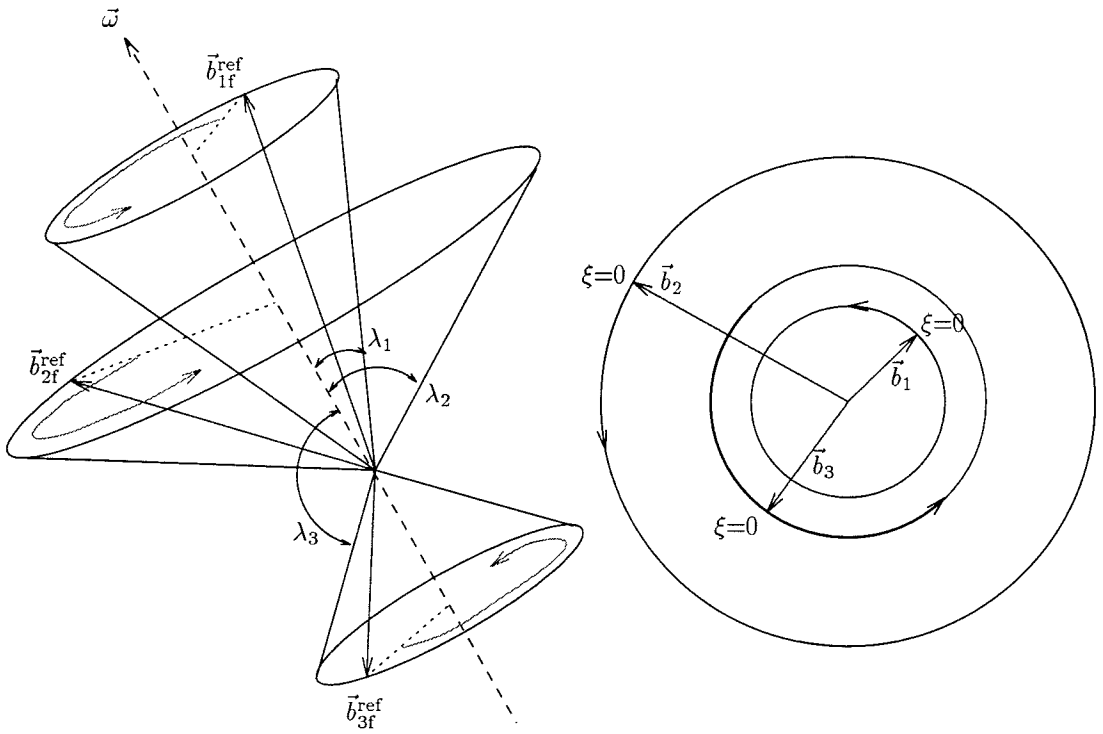

(a) (b)

Figure A.2: (a) Cones used to create $\vec{b}_{k\rm f}$-circles. One of the points on a chosen circle, in this case the $k = 1$ circle, is chosen as a reference for ξ. The target-vector $\vec{e}_{\rm f}$ and the chosen reference $\vec{b}^{\rm ref}_{1\rm f}$ determine a reference orientation $\mathcal{F}^{\rm ref}_{S_{\rm f}}$, from which the corresponding $\xi = 0$ ("ref") directions for the other instruments computed. (b) The view as seen looking down along the $\vec{e}_{\rm f}$ vector.

3. Parameterize the *set* of final orientations, $\mathcal{A}(\vec{e}_f) := \{\mathcal{F}_{S_f}\}$, using the target-vector $\vec{e}_f$ and any *one* of the $\vec{b}_{kf}$-circles. For example, using the first circle ($k = 1$), it is readily seen that the members of $\mathcal{A}(\vec{e}_f)$ are generated by sweeping a chosen $\vec{b}_{1f}$ completely around the circle. Denote the position of the $\vec{b}_{1f}$ vector along the first circle with a parameter ξ, measured as a counter-clockwise angle about an axis $\vec{e}_f$ from some arbitrarily chosen vector $\vec{b}_{1f}^{ref}$ on the circle, also indicated in Figure A.2. Thus ξ is a parameterization of $\mathcal{A}(\vec{e}_f)$ that represents rotation of some reference frame about $\vec{e}_f$, that is,

$$\mathcal{F}_{S_f}(\xi) = \exp(\widehat{e_f} \cdot \xi) \cdot \mathcal{F}_{S_f}^{ref}, \quad 0 \leq \xi \leq 2\pi, \tag{A.3}$$

with $\mathcal{F}_{S_f}^{ref}$ taken to be the frame determined by the vectors $\vec{e}_f$ and $\vec{b}_{1f}^{ref}$. Note that choosing a value for ξ automatically specifies *all* spacecraft instrument vectors $\vec{b}_{1f}, \ldots, \vec{b}_{nf}$ since ξ fully identifies a unique spacecraft body frame. Therefore, ξ is also simultaneously a parameterization of *all* the $\vec{b}_{kf}$-circles, with the references $\vec{b}_{kf}^{ref}$ for each circle determined by the positions of the each corresponding instrument in the ξ-reference frame $\mathcal{F}_{S_f}^{ref}$.

4. Test each member frame $\mathcal{F}_{S_f}$ in $\mathcal{A}(\vec{e}_f)$ for admissibility. Discard those members for which any instrument final position is in violation of the corresponding instrument pointing constraint. If the entire set $\mathcal{A}(\vec{e}_f)$ is discarded, then the aiming problem is *ill-posed.* Otherwise, the aimset $\mathcal{A}(\vec{e}_f)$ is admissible.

In practice, carrying out the test for the last step is quite simple. Intersecting the $\vec{b}_{kf}$-circle for each instrument with that instrument's corresponding threat-cone will divide the $\vec{b}_{kf}$-circle into two regions: safe and unsafe, as shown in Figure A.3.

The ξ coordinates at the boundaries of the safe and unsafe regions, ξ_1 and ξ_2, will determine what portion of the range $[0, 2\pi]$ must be considered unsafe for that instrument. Note that ξ coordinates must be measured from the corresponding instrument's reference position at $\xi = 0$, that is, from $\vec{b}_{kf}^{ref}$. The admissible final orientations can then be generated from those values of ξ that lie in the safe regions for *all* instruments. If no values of ξ are safe, then the problem is not well-posed.

Figure A.4 illustrates two simple three-instrument examples of the final step of this procedure. In the first example, the test indicates the problem is not well-posed. In the second, the test indicates the aimset is admissible, i.e., there are orientations that satisfy the pointing requirement while not violating any instrument constraints.

It is important to realize that even though the test indicates such safe orientations exist, it may turn out that there are no safe paths to these orientations from the initial orientation. Admissibility of the aimset is not sufficient to claim well-posedness, but it is necessary. Figure A.5 illustrates one such case where the aiming problem has no solution and the admissibility test passes. In this figure,

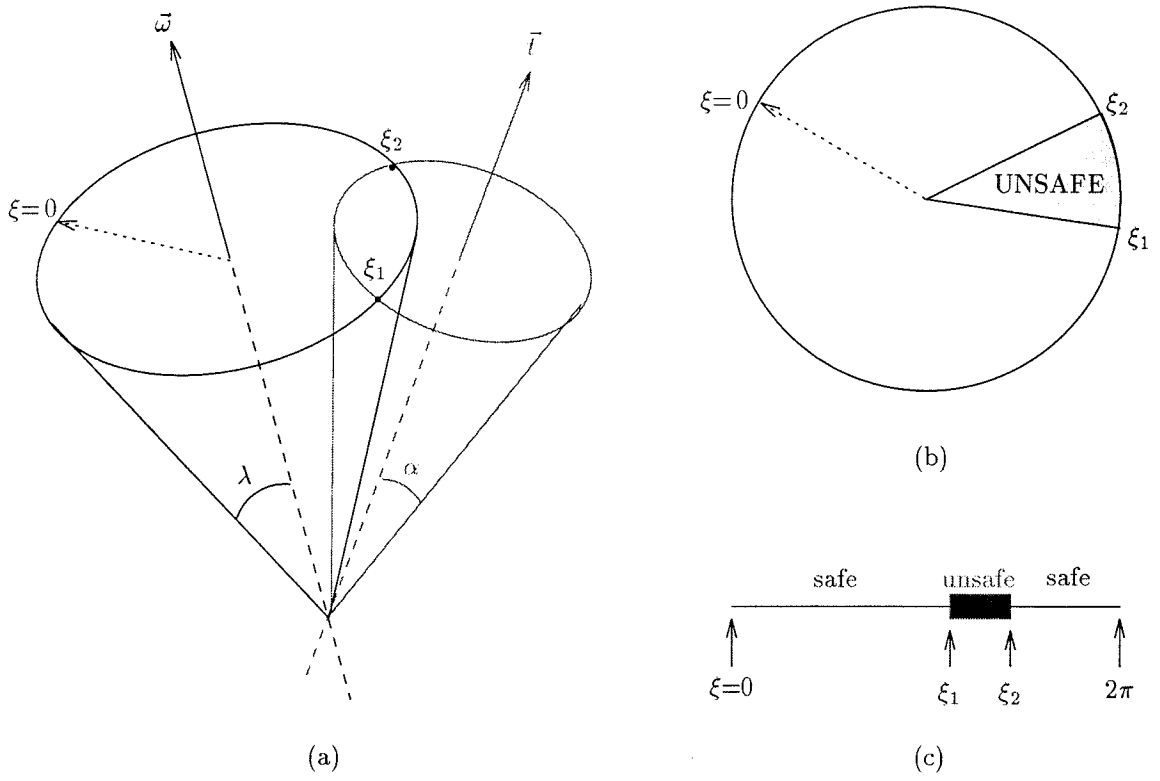

Figure A.3: Intersection of threat cone with $\vec{b}_{kf}$-circle. (a) The circle penetrates and exits the cone at the points labeled ξ_1 and ξ_2. (The cone containing the $\vec{b}_{kf}$-circle is shown for visual clarification.) (b) As seen looking down axis $\vec{\omega}$. (c) "Unwrapping" the circle into a linear map of safe and unsafe regions.

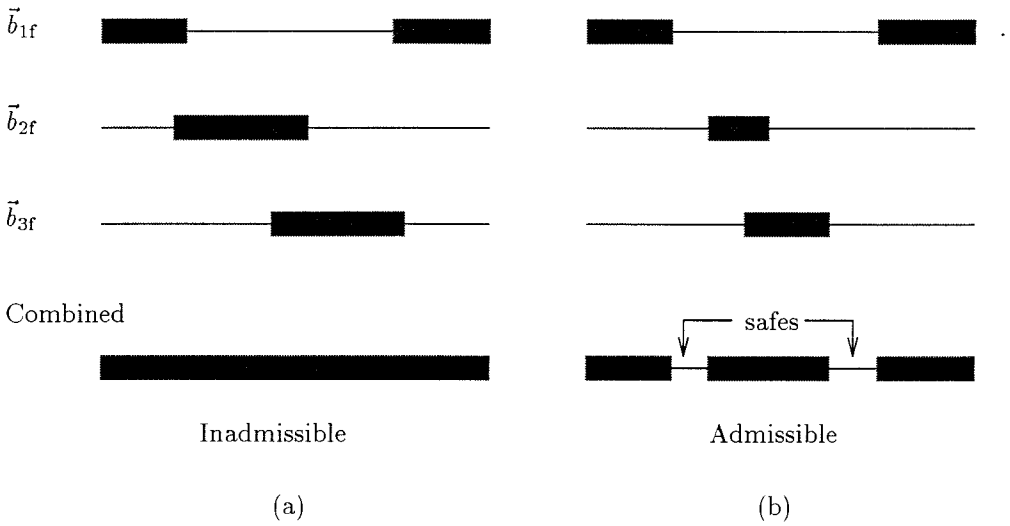

Figure A.4: Combination of safe and hazardous ξ-intervals. (a) Inadmissible aimset (b) Admissible—with two disjoint admissible regions.

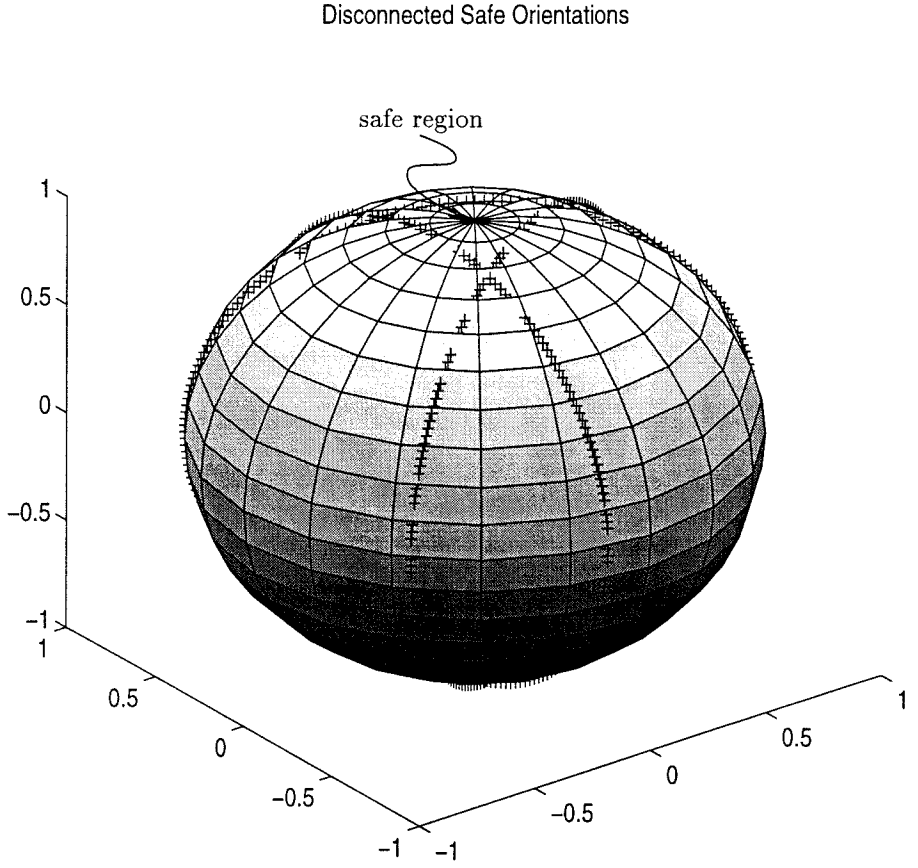

Figure A.5: Celestial sphere indicating the safe pointing region in the "northern hemisphere." There is another identical region at the "south pole." Since the two regions are disconnected there is no safe traverse between them.

the aimsight and the instrument-vector are coincident, that is,

$$\vec{e} = \vec{b}$$

in the spacecraft body frame $\mathcal{F}_S$. (This is an example of the constrained aimsight problem discussed in Section 4.4.) The target-vector $\vec{e}_f$ is diametrically opposite the initial aimsight $\vec{e}_i$, but it is topologically separated from it by the three indicated hazard cones (depicted by their h-circles on the surface $\mathcal{S}$).

Appendix B

Existence of Solutions for the Single-Constraint Aiming Problem

It was claimed in Section 2.3.1 that it is always possible to find a solution to the well-posed aiming problem with a single avoidance constraint (Problem 2.4). The proof is given here.

We first note that the well-posed single-constraint *attitude* transfer problem also always has a one-slew solution. The proof is by geometry, as follows: Chasles' Theorem specifies a single rotation axis $\vec{\omega}$ for the solution, about which the spacecraft may rotate clockwise or counter-clockwise, resulting in two possible slew maneuvers. For the given admissible initial and final orientation, there are corresponding initial and final directions for the instrument, denoted $\vec{b}_\mathrm{i}$ and $\vec{b}_\mathrm{f}$ respectively. Consider these points to lie on the surface of the celestial sphere $\mathcal{S}$. By definition, both points must also lie on the $\vec{b}$-circle about $\vec{\omega}$. The configuration obstacle $\mathcal{H}$ is drawn as a hazard circle on the surface of $\mathcal{S}$. Assume initially that the hazard circle does not intersect the $\vec{b}$-circle, and enlarge the hazard circle until it just intersects the $\vec{b}$-circle. For the problem to remain well-posed, the hazard circle may not enclose either the initial or the final instrument boresights. Therefore, the region of intersection with the $\vec{b}$-circle must be between these two points, obstructing *either* the CCW slew path or the CW slew path. We cannot continue to enlarge the hazard circle so as to also obstruct the other path without first enclosing either the initial or the final instrument locations, thereby violating well-posedness.

Using a similar approach, we now show that the single-constraint aiming problem always has a one-slew solution. The parameters for the single-constraint aiming problem are as follows:

1. a single avoidance constraint H with threat vector $\vec{t}$ and sensitivity angle α,

2. the initial instrument boresight $\vec{b}_\mathrm{i}$,

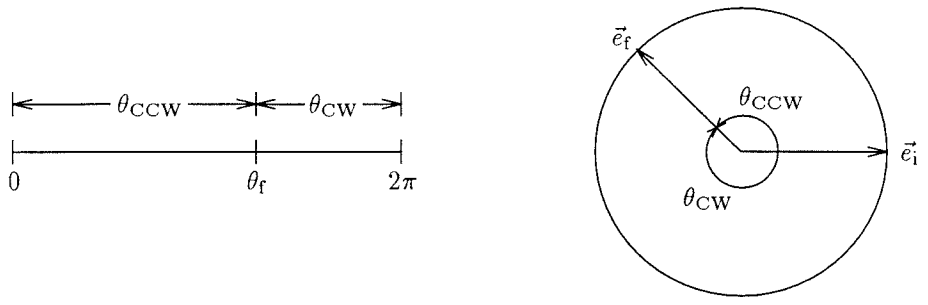

Figure B.1: Topology of single-slew axis maneuver. (a) Unwrapped linear plot of fundamental interval. (b) Circular plot of fundamental interval with $\vec{e}_i$ and $\vec{e}_f$ indicated (as viewed along rotation axis $\vec{\omega}$).

3. admissible initial spacecraft orientation $\mathcal{F}_{S_i}$,

4. initial spacecraft aimsight $\vec{e}_i$,

5. desired *admissible* aimset $\mathcal{A}(\vec{e}_f)$ based on target vector $\vec{e}_f$.

Theorem B.1. Given the single-constraint aiming problem as specified above, there is at least one safe slew maneuver M that will directly take the spacecraft from its initial orientation $\mathcal{F}_{S_i}$ to a final orientation $\mathcal{F}_{S_f}$ satisfying $\vec{e} = \vec{e}_f$.

Proof. From the admissibility of $\mathcal{A}(\vec{e}_f)$, there must be at least one safe final attitude $\mathcal{F}_{S_f}$ for which the final instrument vector $\vec{b}_f$ does not lie within α radians of $\vec{t}$.

According to the Chasles' Theorem [16], there exists a single axis $\vec{\omega}$ about which the spacecraft may rotate *either* counter-clockwise or clockwise from $\mathcal{F}_{S_i}$ to $\mathcal{F}_{S_f}$. Let θ_f be the *counter-clockwise* angular displacement. Define these two candidate slew maneuvers as $M_{CCW} = M(\vec{\omega},\ \theta_f)$ and $M_{CW} = M(\vec{\omega},\ \theta_f - 2\pi)$.

We can divide the fundamental displacement interval into two regions, as shown in Figure B.1. Recall that both $\mathcal{F}_{S_i}$ and $\mathcal{F}_{S_f}$ are admissible orientations. Therefore the obstacle must lie wholly within either the CCW interval, the CW interval, or neither interval. Regardless, there is at least one unobstructed interval. That interval may be safely traversed from the initial frame $\mathcal{F}_{S_i}$ at θ_i to the final frame $\mathcal{F}_{S_f}$ at θ_f using a single slew maneuver. □

Thus, the aimset admissibility condition of (2.18),

$$\mathcal{A}(\vec{e}_f) \bigcap \mathcal{C}_{free} \neq \emptyset,$$

is sufficient to show well-posedness of the single-constraint aiming problem.

Appendix C

Referenced Algorithms

C.1 Unconstrained Attitude Transfer

In the absence of constraints on orientation, Chasles' theorem states that only a single slew is needed to achieve a reorientation. The algorithm for computing the slew maneuver parameters is simple [16]:

Given: A relative rotation matrix $\mathbf{F}$ representing the desired final attitude as measured with respect to the initial attitude.

Solution: Let f_{ij} represent the elements of the matrix $\mathbf{F}$. Then the rotation axis $\boldsymbol{\omega}$ and the displacement θ can be computed as follows, with the components of $\boldsymbol{\omega}$ given in the initial attitude frame.

1. First, set

$$\theta = \arccos\left(\frac{\text{trace}(\mathbf{F}) - 1}{2}\right). \tag{C.1}$$

2. If $\theta = 0$ then $\boldsymbol{\omega}$ may be arbitrarily chosen. This case is trivial.

3. If $\theta = \pi$ then we set the components of $\boldsymbol{\omega}$ as

$$\left.\begin{aligned} \omega_1 &= \sqrt{(f_{11}+1)/2} \\ \omega_2 &= \sqrt{(f_{22}+1)/2} \\ \omega_3 &= \sqrt{(f_{33}+1)/2}. \end{aligned}\right\} \tag{C.2}$$

4. Else, for $\theta \in (0, \pi)$ set $\boldsymbol{\omega}$ according to

$$\boldsymbol{\omega} = \begin{bmatrix} \omega_1 \\ \omega_2 \\ \omega_3 \end{bmatrix} = \frac{1}{2\sin\theta}\begin{bmatrix} f_{32} - f_{23} \\ f_{13} - f_{31} \\ f_{21} - f_{12} \end{bmatrix}. \tag{C.3}$$

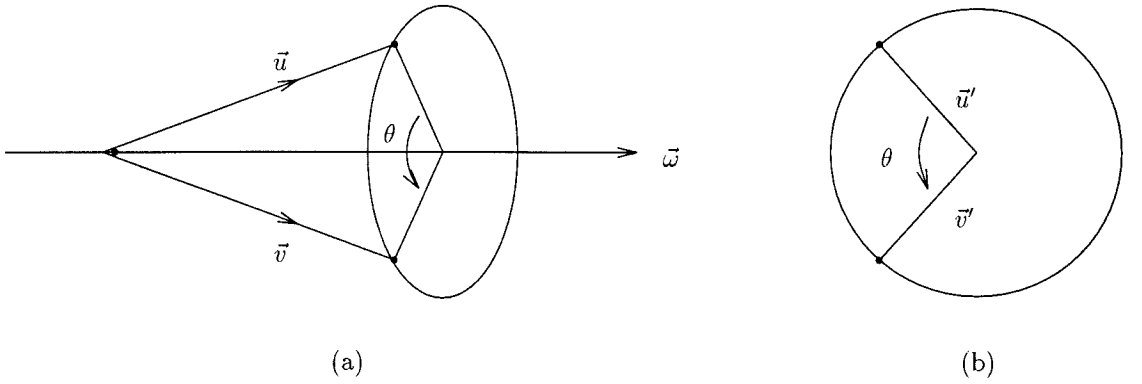

Figure C.1: First Paden-Kahan subproblem. (a) Rotating $\vec{u}$ into $\vec{v}$ about $\vec{\omega}$. (b) As seen looking down $\vec{\omega}$.

Unless the angular displacement is zero, there are only two solutions to the unconstrained attitude problem: $M_1 = M(\vec{\omega}, \theta)$ and $M_2 = M(\vec{\omega}, \theta - 2\pi)$. Note that although both slew maneuvers take the spacecraft to the same desired final orientation, each proceeds along different paths in $\mathcal{C}$. □

C.2 Paden-Kahan Subproblems

In this section we present geometric algorithms to solve two simple inverse kinematics problems, known as the Paden-Kahan subproblems. The algorithms presented below are customized for unit vectors that emanate from a common origin. The general algorithm for both subproblems presented below appears in [16].

C.2.1 First Paden-Kahan Subproblem

The first Paden-Kahan subproblem provides the angular displacement needed to rotate a starting point into a final point about a given axis. The subproblem is illustrated in Figure C.1.

Given: Two unit vectors $\vec{u}$ and $\vec{v}$, and a rotation axis $\vec{\omega}$ (also a unit vector). Assume that all vectors start at a common origin.

Find: The rotation angle θ that will rotate $\vec{u}$ about $\vec{\omega}$ into $\vec{v}$.

Solution: With regard to a common reference frame, let $\mathbf{u}$ and $\mathbf{v}$ be the column vector representation of $\vec{u}$ and $\vec{v}$, respectively. Also let $\boldsymbol{\omega}$ be the column vector representation of $\vec{\omega}$, and let $\hat{\omega}$ be the skew symmetric matrix formed from the elements of $\boldsymbol{\omega}$. We aim to find θ such that

$$\exp(\hat{\omega}\theta) \cdot \mathbf{u} = \mathbf{v}. \tag{C.4}$$

1. Define $\mathbf{u}'$ and $\mathbf{v}'$ to be the projections of $\vec{u}$ and $\vec{v}$ onto a plane perpendicular to $\vec{\omega}$. Thus,

$$\mathbf{u}' = \mathbf{u} - \boldsymbol{\omega}\boldsymbol{\omega}^T\mathbf{u} \tag{C.5}$$

$$\mathbf{v}' = \mathbf{v} - \boldsymbol{\omega}\boldsymbol{\omega}^T\mathbf{v}. \tag{C.6}$$

2. Verify that the problem has solution(s) by confirming

$$\boldsymbol{\omega}^T\mathbf{u} = \boldsymbol{\omega}^T\mathbf{v} \tag{C.7}$$

$$\|\mathbf{u}'\| = \|\mathbf{v}'\|. \tag{C.8}$$

   If either of these conditions fails, then it is impossible to rotate $\vec{u}$ into $\vec{v}$ using the axis $\vec{\omega}$.

3. If $\mathbf{u}' = 0$, then $\vec{u}$ and $\vec{v}$ both lie on $\vec{\omega}$. There are infinite number of solutions, since

$$\boldsymbol{\omega} = \mathbf{u} = \mathbf{v}.$$

   Any displacement θ will solve the problem.

4. Else, determine the *counter-clockwise* angular displacement about $\vec{\omega}$ using

$$\theta = \text{atan2}\left(\boldsymbol{\omega}^T(\mathbf{u}' \times \mathbf{v}'), \mathbf{u}'^T\mathbf{v}'\right). \tag{C.9}$$

□

To apply this procedure to the rotation of an aimsight $\vec{e}_\text{i}$ into a target-vector $\vec{e}_\text{f}$ about an axis $\vec{\omega}$, we set $\vec{u} = \vec{e}_\text{i}$ and $\vec{v} = \vec{e}_\text{f}$. With θ obtained from the procedure, the slew maneuver that rotates $\vec{e}_\text{i}$ into $\vec{e}_\text{f}$ counter-clockwise about $\vec{\omega}$ is $M_\text{CCW} = M(\vec{\omega}, \theta)$. Of course, the clockwise slew maneuver is $M_\text{CW} = M(\vec{\omega}, \theta - 2\pi)$.

C.2.2 Second Paden-Kahan Subproblem

In inverse kinematics, this subproblem is used to rotate a starting point into a finishing point using two subsequent rotations about given axes [16]. In this report, however, we use the second Paden-Kahan subproblem to solve for the intersection of two circles on the unit sphere $\mathcal{S}$. The subproblem is illustrated (without the sphere) in Figure C.2.

Given: Unit vectors $\vec{p}$ and $\vec{q}$, and unit axes $\vec{\omega}_1$ and $\vec{\omega}_2$. Assume that all vectors start at a common origin.

Find: The critical angular displacements for which $\vec{p}$, when rotated about axis $\vec{\omega}_1$, just penetrates the cone formed by rotating $\vec{q}$ about $\vec{\omega}_2$.

Solution: Let $\mathbf{p}$ be the column vector representation of $\vec{p}$ and let $\mathbf{q}$ be the column vector representation of $\vec{q}$. Similarly, let ω_1 and ω_2 be the column vector representations of $\vec{\omega}_1$ and $\vec{\omega}_2$. Let

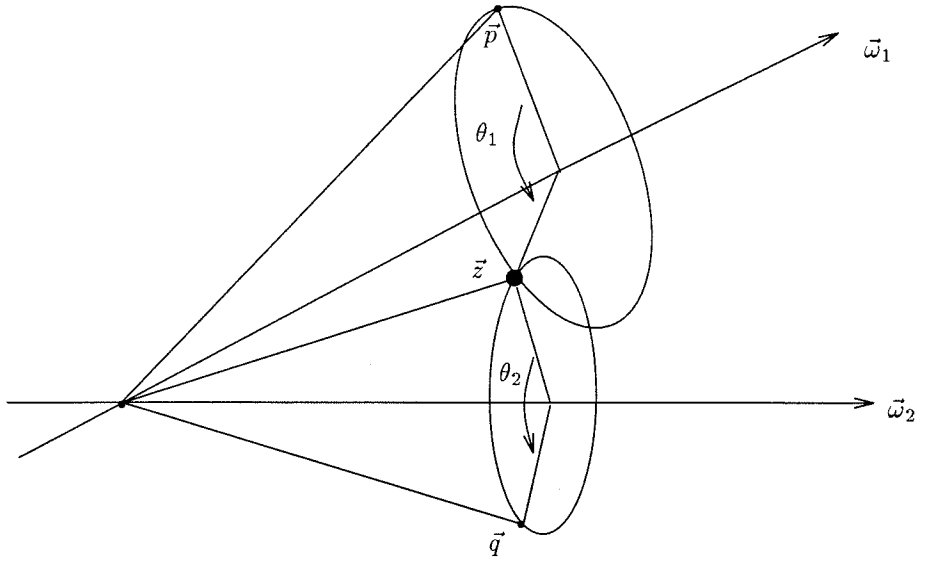

Figure C.2: Second Paden-Kahan subproblem. The intersection of the two circles is found by rotating $\vec{p}$ and $\vec{q}$ about $\vec{\omega}_1$ and $\vec{\omega}_2$, respectively, until the two vectors intersect.

the circle traced by rotating $\vec{p}$ about $\vec{\omega}_1$ be called a p-circle, and let the circle traced by rotating $\vec{q}$ about $\vec{\omega}_2$ be called a q-circle.

We note that there may be zero, one, two, or infinitely many intersection points, depending on the relative orientation and sizes of the p-circle and the q-circle. Let n denote the number of solutions.

1. Define

$$\vec{c} := \vec{\omega}_2 \times \vec{\omega}_1.$$

   Let $\mathbf{c}$ be the column vectorization of $\vec{c}$.

2. If $\mathbf{c} = \mathbf{0}$, then the vectors $\vec{\omega}_1$ and $\vec{\omega}_2$ are either aligned or anti-aligned. The p-circle and the q-circle either do not intersect or overlap completely.

   (a) If $\vec{\omega}_1 \cdot \vec{\omega}_2 = 1$ (aligned), then set n according to

$$n = \begin{cases} 0, & \vec{p} \cdot \vec{\omega}_1 \neq \vec{q} \cdot \vec{\omega}_2 \quad \text{(disjoint)}; \\ \infty, & \vec{p} \cdot \vec{\omega}_1 = \vec{q} \cdot \vec{\omega}_2 \quad \text{(overlapping)}. \end{cases}$$

   (b) If $\vec{\omega}_1 \cdot \vec{\omega}_2 = -1$ (anti-aligned), then set n according to

$$n = \begin{cases} 0, & \vec{p} \cdot \vec{\omega}_1 \neq -\vec{q} \cdot \vec{\omega}_2 \quad \text{(disjoint)}; \\ \infty, & \vec{p} \cdot \vec{\omega}_1 = -\vec{q} \cdot \vec{\omega}_2 \quad \text{(overlapping)}. \end{cases}$$

The algorithm has determined that there are no critical angular displacements ($n = 0$) or that *all* angular displacements about $\vec{\omega}_1$ are critical ($n = \infty$.). The algorithm exits.

3. Else, there are at most two intersection points, depending on whether the circles are disjoint, tangent, or intersecting. Assume a point $\vec{z}$ exists that is common to both circles (either a tangency point or an intersection point). Thus, denoting with $\mathbf{z}$ the column vectorization of $\vec{z}$, we have

$$e^{\widehat{\omega}_1\theta_1}\mathbf{p} = \mathbf{z} = e^{\widehat{\omega}_2\theta_2}\mathbf{q} \tag{C.10}$$

for some angles θ_1 and θ_2 about axes $\vec{\omega}_1$ and $\vec{\omega}_2$.

From the linear independence of $\boldsymbol{\omega}_1$, $\boldsymbol{\omega}_2$, and $\mathbf{c}$, we express $\mathbf{z}$ in components as

$$\mathbf{z} = \mu\boldsymbol{\omega}_1 + \nu\boldsymbol{\omega}_2 + \lambda\mathbf{c}. \tag{C.11}$$

4. With a little development [16], we can set

$$\mu = \frac{(\boldsymbol{\omega}_2{}^T\boldsymbol{\omega}_1)\boldsymbol{\omega}_2{}^T\mathbf{q} - \boldsymbol{\omega}_1{}^T\mathbf{p}}{(\boldsymbol{\omega}_2{}^T\boldsymbol{\omega}_1)^2 - 1}, \tag{C.12}$$

$$\nu = \frac{(\boldsymbol{\omega}_2{}^T\boldsymbol{\omega}_1)\boldsymbol{\omega}_1{}^T\mathbf{p} - \boldsymbol{\omega}_2{}^T\mathbf{q}}{(\boldsymbol{\omega}_2{}^T\boldsymbol{\omega}_1)^2 - 1}. \tag{C.13}$$

5. As shown in [16], we set

$$\lambda^2 = \frac{\|\mathbf{p}\|^2 - \mu^2 - \nu^2 - 2\mu\nu\boldsymbol{\omega}_1{}^T\boldsymbol{\omega}_2}{\|\mathbf{c}\|^2}. \tag{C.14}$$

This equation has either zero, one, or two distinct real solutions. We set n to the number of distinct real solutions.

6. We compute the critical angular displacements according to the number of real solutions n.

   (a) For $n = 0$, there are no critical angular displacements: the p-circle and q-circle do not intersect.

   (b) For $n = 1$, there is one critical angular displacement η. (The circles are tangent.) We find η using the first Paden-Kahan subproblem, rotating $\vec{u}$ about $\vec{\omega}_1$ into $\vec{z}$. The target-vector $\vec{z}$ is computed via (C.11), using the repeated root λ from (C.14).

   (c) For $n = 2$, there are two critical angular displacements η_1 and η_2. (The circles intersect.) We use the first Paden-Kahan subproblem twice: to rotate $\vec{u}$ first into $\vec{z}_1$, and then again into $\vec{z}_2$. The target-vectors $\vec{z}_1$ and $\vec{z}_2$ are computed via (C.11), using the two roots λ_1 and λ_2 from (C.14). □

This procedure is used in the 1-slew aiming planner to determine the critical angular displacements about a rotation vector $\vec{\omega}$ for which the instrument $\vec{b}$ just penetrates its corresponding hazard cone defined by the threat vector $\vec{t}$ and sensitivity angle α, as illustrated in Figure 3.2. To use the procedure, we set $\vec{p} = \vec{b}$, $\vec{\omega}_1 = \vec{\omega}$, $\vec{\omega}_2 = \vec{t}$, and we select $\vec{q}$ as any point on the h-circle.

Appendix D

Source Code

D.1 Obtaining the Source Code

Source code for the motion planners described in this report can be obtained via anonymous ftp from `avalon.caltech.edu`, in the directory `/home/tonyv`. The name of the file to download is `so3_motion.tar.gz`, which is a compressed archive made with the Unix `tar` command. The archive can also be obtained via the World Wide Web at `ftp://avalon.caltech.edu/home/tonyv`.

To extract the source code, download the archive into the directory where you want the code, and run the following commands:

```
gunzip so3_motion.tar.gz
tar xvf so3_motion.tar
```

These commands will create several subdirectories with the routines contained inside. The subdirectories are listed below:

`utils`	general utility routines that are used in `so3_motion` but might also be useful for other applications.
`support`	common support routines that are geared mainly towards `so3_motion` applications.
`plotters`	simple plotting routines that aid in presenting the results.
`attxfer1`	routines for solving the 1-slew attitude transfer problem and routines for applying various metrics to particular slew maneuvers (for later use by the optimizers).
`aim1`	routines for generating and optimizing solutions to the 1-slew aiming problem.
`aim2`	routines for generating and optimizing solutions to the 2-slew aiming problem.
`stereo`	routines that aid in visualizing the results in the stereographic plane.
`examples`	MATLAB scripts and data files for the examples presented in this report.

D.2 Using the Programs

Before running MATLAB, be sure that the directories containing the routines are available in MATLAB's search path. A simple way to do this is to add the following commands to your `~/matlab/startup.m` file, where `$SO3_HOME` is the directory into which the archive was extracted.

```
path(path,'$SO3_HOME/utils')
path(path,'$SO3_HOME/support')
path(path,'$SO3_HOME/plotters')
path(path,'$SO3_HOME/attxfer1')
path(path,'$SO3_HOME/aim1')
path(path,'$SO3_HOME/aim2')
path(path,'$SO3_HOME/stereo')
path(path,'$SO3_HOME/examples')
```

Within each directory there is a `readme.txt` file that describes the functions. Additionally, the header portion of each file contains descriptive information that is accessible with the MATLAB `help` command.

D.3 Creating the Examples

The following commands can be used to generate the plots for the examples shown in this report.

Example 3.1

Run `main1cmp.m`, and enter `31` when prompted for the hazard set identification. The script will automatically display the results graphically. The spacecraft final attitudes for the MARG and ANGSEP routines are given in the matrices `F1a_marg` and `F1a_ang`, respectively. The optimal slew parameters are returned in the variable pairs `(wmarg, thmarg)` and `(wang, thang)`. The slew axes are given in spacecraft body coordinates at the start of the slew. To convert the spacecraft vectors in the initial spacecraft frame to inertial vectors, pre-multiply by the initial attitude matrix:

```
F0a * wmarg
```

To convert spacecraft vectors in the final attitude to inertial coordinates, use the final attitude matrix:

```
F1a_marg * e0s0
```

To generate the stereographic projection of the MARG maneuver, enter

```
sb(F0a,e0s0,efa,wmarg,thmarg,H,eye(3),phi_samples,1)
```

at the MATLAB prompt. For the ANGSEP maneuver, use

```
sb(F0a,e0s0,efa,wang,thang,H,eye(3),phi_samples,1)
```

instead (`sb` is found in the `stereo` subdirectory).

Example 3.2

This example is generated in the same manner, but enter `32` for the hazard set identifier instead.

Example 4.1

For the MARG results, run the script `main2co.m`. Enter the desired resolution when prompted, and select hazard set identifier `41`. For the ANGSEP results, run `main2cb_cf.m` instead. Be warned that the routines may take a long time to execute, especially at the higher resolutions. The slew maneuver parameters for the 2-slew sequence are returned in the variable pairs `(w21, th21)` and `(w22, th22)`. Again note that both slew axis, `w21` and `w22`, are given in spacecraft body coordinates.

When the routine completes execution, run the script `showbest` to display the 2-slew maneuver. Use the MATLAB command `view(2)` to generate the topdown views shown in Chapter 4. Displaying the maneuvers as a connected curve in the stereographic plane requires some manipulation of the stereographic reference frame; the following commands perform the necessary transformation and will properly display the results:

```
figure;
sb(F0a,e0s0,efa,w21,th21,H,eye(3),phi_samples,1);
sb(F1a,e0s0,efa,w22,th22,H,F1a',phi_samples,1);
```

Note that the tranpose is taken on the seventh parameter of the second `sb` command.

Example 4.2

This example is generated in the same manner, but enter `42` for the hazard set identifier instead.

Bibliography

[1] Ralph Goddard, "Autonomy DDF Deliverables," Inter-office Memorandum IOM-343-94-253, July 5, 1994, Jet Propulsion Laboratory, California Institute of Technology.

[2] Ralph Goddard, Private Communication, December 1995.

[3] Michael D. Griffin, James R. French, *Space Vehicle Design,* American Institute of Aeronautics and Astronautics, Inc., Washington DC, 1991.

[4] Ching-Fang Lin, Tasso Politopoulos, Tie-Jun Yu, Fred Hadaegh, "Autonomous Spacecraft Control Systems," *Proceedings of the American Control Conference,* Seattle, Washington, June 1995, pp. 510–514.

[5] Fred Hadaegh, Edward Mettler, "Autonomous Spacecraft Guidance and Control," *Proceedings of the AIAA Guidance, Navigation, and Control Conference,* San Diego, California, July 1996, AIAA-96-3924.

[6] Peter C. Hughes, *Spacecraft Attitude Dynamics,* John Wiley & Sons, New York, 1986.

[7] Paul E. Jacobs, *Planning Robot Motion with Dynamic Constraints,* Ph.D. dissertation, University of California at Berkeley, 1989.

[8] Erwin Kreyszig, *Advanced Engineering Mathematics,* John Wiley & Sons, New York, 1967.

[9] Jean-Claude Latombe, *Robot Motion Planning,* Kluwer Academic Publishers, Boston, 1991.

[10] Jean-Paul Laumond, Paul E. Jacobs, Michel Taïx, Richard M. Murray, "A Motion Planner for Nonholonomic Robots," *IEEE Transactions of Robotics and Automation,* vol. 10, no. 5, October 1994, pp. 577–593.

[11] Robert E. Lindberg, "Two Impulse Large Angle Satellite Attitude Transfers," Univ. of Virginia, School of Engineering and Applied Science, Charlottesville, Virginia, USA, May, 1976.

[12] Martin W. Lo, Private Communication, August 1, 1996.

[13] Lockheed Press Release. Lockheed Missiles and Space Co., April 17, 1996.

[14] Colin R. McInnes, "Large Angle Slew Maneuvers with Autonomous Sun Vector Avoidance," *Journal of Guidance, Control, and Dynamics,* vol. 17, no. 4, 1994, pp. 875–977.

[15] Ismael Lopez and Colin R. McInnes, "Autonomous Rendezvous Using Artificial Potential Function Guidance," *Journal of Guidance, Control, and Dynamics,* vol. 18, no. 2, 1995, pp. 237–241.

[16] Richard M. Murray, Zexiang Li, S. Shankar Sastry, *A Mathematical Introduction to Robotic Manipulation*, CRC Press, Ann Arbor, 1994.

[17] Sandra L. Scrivener and Roger C. Thompson, "Survey of Time-Optimal Attitude Maneuvers," *Journal of Guidance, Control, and Dynamics,* vol. 17, no. 2, 1994, pp. 225–233.

[18] Hans Seywald, Renjith R. Kumar, Samir S. Deshpande, and Michael L. Heck, "Minimum Fuel Spacecraft Reorientation," *Journal of Guidance, Control, and Dynamics,* vol. 17, no. 1, 1994, pp. 21–29.

[19] Malcolm D. Shuster, "A Survey of Attitude Representations," *The Journal of the Astronautical Sciences,* vol. 41, no. 4, October-December 1994, pp. 439–517.

[20] Willem H. Steyn, "Near-Minimum-Time Eigenaxis Rotation Maneuvers Using Reaction Wheels," *Journal of Guidance, Control, and Dynamics,* vol. 18, no. 5, 1995, pp. 1184–1189.

[21] Panagiotis Tsiotras and James M. Longuski, "A New Parameterization of the Attitude Kinematics," *The Journal of the Astronautical Sciences,* vol. 43, no. 3, July–September 1995, pp. 243–262.

[22] James R. Wertz, ed., *Spacecraft Attitude Determination and Control*, Kluwer Academic Publishers, Boston, 1995.